Preface

We would like to present, with great pleasure, the inaugural volume-3, Issue-9, September 2017, of a scholarly journal, *International Journal of Engineering Research & Science*. This journal is part of the AD Publications series *in the field of Engineering, Mathematics, Physics, Chemistry and science Research Development*, and is devoted to the gamut of Engineering and Science issues, from theoretical aspects to application-dependent studies and the validation of emerging technologies.

This journal was envisioned and founded to represent the growing needs of Engineering and Science as an emerging and increasingly vital field, now widely recognized as an integral part of scientific and technical investigations. Its mission is to become a voice of the Engineering and Science community, addressing researchers and practitioners in below areas

Chemical Engineering	
Biomolecular Engineering	Materials Engineering
Molecular Engineering	Process Engineering
Corrosion Engineering	
Civil Engineering	
Environmental Engineering	Geotechnical Engineering
Structural Engineering	Mining Engineering
Transport Engineering	Water resources Engineering
Electrical Engineering	
Power System Engineering	Optical Engineering
Mechanical Engineering	
Acoustical Engineering	Manufacturing Engineering
Optomechanical Engineering	Thermal Engineering
Power plant Engineering	Energy Engineering
Sports Engineering	Vehicle Engineering
Software Engineering	
Computer-aided Engineering	Cryptographic Engineering
Teletraffic Engineering	Web Engineering
System Engineering	
Mathematics	
Arithmetic	Algebra
Number theory	Field theory and polynomials
Analysis	Combinatorics
Geometry and topology	Topology
Probability and Statistics	Computational Science
Physical Science	Operational Research
Physics	
Nuclear and particle physics	Atomic, molecular, and optical physics
Condensed matter physics	Astrophysics
Applied Physics	Modern physics
Philosophy	Core theories

Chemistry	
Analytical chemistry	Biochemistry
Inorganic chemistry	Materials chemistry
Neurochemistry	Nuclear chemistry
Organic chemistry	Physical chemistry
Other Engineering Areas	
Aerospace Engineering	Agricultural Engineering
Applied Engineering	Biomedical Engineering
Biological Engineering	Building services Engineering
Energy Engineering	Railway Engineering
Industrial Engineering	Mechatronics Engineering
Management Engineering	Military Engineering
Petroleum Engineering	Nuclear Engineering
Textile Engineering	Nano Engineering
Algorithm and Computational Complexity	Artificial Intelligence
Electronics & Communication Engineering	Image Processing
Information Retrieval	Low Power VLSI Design
Neural Networks	Plastic Engineering

Each article in this issue provides an example of a concrete industrial application or a case study of the presented methodology to amplify the impact of the contribution. We are very thankful to everybody within that community who supported the idea of creating a new Research with IJOER. We are certain that this issue will be followed by many others, reporting new developments in the Engineering and Science field. This issue would not have been possible without the great support of the Reviewer, Editorial Board members and also with our Advisory Board Members, and we would like to express our sincere thanks to all of them. We would also like to express our gratitude to the editorial staff of AD Publications, who supported us at every stage of the project. It is our hope that this fine collection of articles will be a valuable resource for *IJOER* readers and will stimulate further research into the vibrant area of Engineering and Science Research.

Mukesh Arora

(Chief Editor)

Dr. S.R.Boselin Prabhu

Ph.D, Wireless Sensor Networks, M.E. Network Engineering, Excellent Professional Achievement Award Winner from Society of Professional Engineers Biography Included in Marquis Who's Who in the World (Academic Year 2015 and 2016). Currently Serving as Assistant Professor in the department of ECE in SVS College of Engineering, Coimbatore.

Dr. Maheshwar Shrestha

Postdoctoral Research Fellow in DEPT. OF ELE ENGG & COMP SCI, SDSU, Brookings, SD Ph.D, M.Sc. in Electrical Engineering from SOUTH DAKOTA STATE UNIVERSITY, Brookings, SD.

Zairi Ismael Rizman

Senior Lecturer, Faculty of Electrical Engineering, Universiti Teknologi MARA (UiTM) (Terengganu) Malaysia Master (Science) in Microelectronics (2005), Universiti Kebangsaan Malaysia (UKM), Malaysia. Bachelor (Hons.) and Diploma in Electrical Engineering (Communication) (2002), UiTM Shah Alam, Malaysia

Dr. D. Amaranatha Reddy

Ph.D.(Postdocteral Fellow,Pusan National University, South Korea), M.Sc., B.Sc. : Physics.

Dr. Dibya Prakash Rai

Post Doctoral Fellow (PDF), M.Sc.,B.Sc., Working as Assistant Professor in Department of Physics in Pachhuncga University College, Mizoram, India.

Dr. Pankaj Kumar Pal

Ph.D R/S, ECE Deptt., IIT-Roorkee.

Dr. P. Thangam

BE(Computer Hardware & Software), ME(CSE), PhD in Information & Communication Engineering, currently serving as Associate Professor in the Department of Computer Science and Engineering of Coimbatore Institute of Engineering and Technology.

Dr. Pradeep K. Sharma

PhD., M.Phil, M.Sc, B.Sc, in Physics, MBA in System Management, Presently working as Provost and Associate Professor & Head of Department for Physics in University of Engineering & Management, Jaipur.

Dr. R. Devi Priya

Ph.D (CSE),Anna University Chennai in 2013, M.E, B.E (CSE) from Kongu Engineering College, currently working in the Department of Computer Science and Engineering in Kongu Engineering College, Tamil Nadu, India.

Dr. Sandeep

Post-doctoral fellow, Principal Investigator, Young Scientist Scheme Project (DST-SERB), Department of Physics, Mizoram University, Aizawl Mizoram, India- 796001.

Mr. Abilash

MTech in VLSI, BTech in Electronics & Telecommunication engineering through A.M.I.E.T.E from Central Electronics Engineering Research Institute (C.E.E.R.I) Pilani, Industrial Electronics from ATI-EPI Hyderabad, IEEE course in Mechatronics, CSHAM from Birla Institute Of Professional Studies.

Mr. Varun Shukla

M.Tech in ECE from RGPV (Awarded with silver Medal By President of India), Assistant Professor, Dept. of ECE, PSIT, Kanpur.

Mr. Shrikant Harle

Presently working as a Assistant Professor in Civil Engineering field of Prof. Ram Meghe College of Engineering and Management, Amravati. He was Senior Design Engineer (Larsen & Toubro Limited, India).

Table of Contents

About Modeling and Simulation of Heat Exchange Convective Surfaces of the Steam Generator

Adelaida Mihaela Duinea

Department of Electrical, Energetic and Aerospace Engineering, Faculty of Electrical Engineering, University of Craiova, Craiova, Romania

Abstract — *Among the priority issues that the modern society has to be solved, include also the energy and environmental issues. The notion of control (process control) has expanded in recent years, encompassing new areas such as automatic control of quality, the data processing with decisional purpose for one strategic leadership, ensuring uninterrupted of the system maintainability and thus, security and viability of the entire ensemble. In this context are part and the simplified simulation methods of the energetic installations from the power plants. The paper expose, in the first part, the importance of the steam generator in the operation of power plants, presents the energy processes complexity, emphasizing the importance of their management and automation to increase energy efficiency of each link in the chain. Then, taking as its starting point the real operational aspects, the mathematical modeling, the simulation and automatic control of steam generator, the paper proposes the development of a mathematical model in absolute units and the simulation the operation of a convective heat exchange surface of the steam generator in steady and dynamic regime.*

Keywords — ***Mathematical model, modeling, power plant, simulation, steam generator.***

I.   INTRODUCTION

The paper presents a study for the application about the steam generators in terms of modeling and simulation of their operation in steady and dynamic regime in power plants. Treat modeling itself of steam generator: it is based on physical model of each heat exchange surfaces, simplifying assumptions adopted, equations for conservation of mass, energy and momentum and the heat transfer equations. Also is presented the model in relative units imposed by the literature - highlighting the entire set of mathematical equations the processes occurring in the installation, the coefficients given in the literature, and the disadvantages involved in its use. Then, as an alternative, is proposed the steam generator model in absolute units: processing of the basic equations, are highlighted development its advantages - eliminating the recalculation sequence of parameters at each step, eliminating the linearization around the stabilized operating point, nonlinear characteristics are included in the model, determining the coefficients of thermal heat exchange between agents and the exchange surfaces in real-time, and the disadvantages involved in its use. The theoretical model proposed, in absolute units, implemented in Matlab-Simulink, leads to the simulations of the operating in dynamic regime for all components of steam generator. The model provides information about the influence of each parameter - input and output (pressure, temperature, and flow for water supply, combustion gases) on monitored parameters, namely pressure and temperature live steam. The results from the simulation are compared with values measured for parameters in real operation. The aim was to provide information allowing analysis of the model of each heat exchange surfaces on the one hand and on the other hand time for calculation to be within the real time operation. The steam generator model can be completed with the modules of the turbine-generator group with their installations and internal services and of the electrical part of power plant. All these models of the stationary and dynamic regimes can be implemented in computer systems and leads to the creation of a system for the management and control in electrical and thermal energy supply.

II.   THE IMPORTANCE OF STEAM GENERATORS IN POWER PLANT OPERATION

Considering the great technical and economic importance for energy, the dynamics of the specific processes of the most important energy aggregates - steam generator and steam turbine - has been the subject of numerous studies and research, starting with the dynamic analysis of a steam generator with natural circulation and continuing with the analysis of its optimal and suboptimal control, or of the plant assembly. The vast majority of models is designed specifically for control or proposes new techniques to solve. Therefore, global models are conveniently reduced to allow for dynamic analysis of the plant assembly with significant, generally accepted simplifications. For this purpose, the theory of linear control, which describes the state of the boiler using linear differential equations with constant coefficients, is sufficient, [2], [4].

Steam generators (boilers) are water vaporization systems that use the heat generated by the combustion of a fuel or an industrial process (heat recovery boilers). In boilers used in power plants, the steam from the vaporization process is overheated at a temperature higher than the saturation temperature of saturated steam to raise its enthalpy. It distinguishes two main circuits: water-steam and air-combustion gases. The steam-water circuit of the generator consists of pipe systems immersed in the flue gas ducts. From a functional point of view, the following heat transfer surfaces of this circuit are distinguished: Economizer - increases the temperature of the supply water to a value close to the saturation value, the heat transfer between the water and the flue gases is convective; Vaporizer - it ensures the passage of water from the liquid phase to the saturated steam, the heat transfer being carried out predominantly by radiation; The Primary Superheater - realizes the overheating of the saturated steam up to the temperature level desirable, heat transfer convective - radiation and Intermediate Heater - occurs in conventional steam boilers and provides an increase in steam temperature already released in the turbine high pressure body. The manner in which the heat transfer is effected on the one hand and the level of temperature required by the water-steam agent, on the other hand, requires the way in which these heat exchange surfaces are located inside the channels of combustion gases, [2], [4].

Inside the vaporizer tubes phase change takes place, the heat transfer coefficients have large values. In these circumstances it is necessary to place the heat exchange surfaces into the furnace where the outside of the tubes, the heat transfer coefficients are also large - achieving heat transfer by radiation is predominant. For the primary, intermediate superheater, and economizer case, the heat transfer coefficients can be obtained inside the pipes are slightly lower than for vaporizer, the three areas are located in the convective generator zone. High power boilers energy groups, 510 or 1035 t/h are Benson type boilers with Π-shaped building or tower. The boiler primarily presentation intended purpose of the study, namely the modeling of operating modes. Each power unit of 315MW is equipped with two steam boilers of 510 t/h identical type Benson, forced to pass single variable evaporation point, built in the form of Π.

III.   CONVECTIVE HEAT EXCHANGE SURFACE PRESENTATION

In the dynamic modeling and control of steam generator are used mainly three types of one-dimensional models for the analysis of fuel combustion stability at low loads, the dynamic analysis of air-gas path and predetermining spatial distribution of water-vapor properties - models for studying the control pressure, temperature, level, dynamic load variation. The models are mathematically expressed by a set of equations from differential equations to partial differential equations; their nature is depending on the modeled process complexity and the purpose of their use. Modeling and simulation of heat exchangers is an essential problem of any simulation program and especially of steam generators, detailing the following general concepts, [11]: segmentation, disconnection, the biphasic mixture and thermal transfer. The location and complexity of the processes in steam boilers steam boilers had required that the process can be structured in technological modules.

Thus the economizer, a surface of the convective heat exchange, is mounted in the end of the heating surface of the steam generator, resulting in a saving of fuel corresponding to the heat recovery. Economizer heating surface is usually made from steel pipe or, more commonly, cast iron pipe with wings in the form of double coil, transversely spaced apart, forming economizer package supported by the support tube and connected to cylindrical collectors - inlet and outlet respectively. The economizer is placed on top of the convective circulation before the outlet gases to the air super heaters. Water passes through the economizer flue gas counter. The physical model of the economizer is shown in Fig. 1.
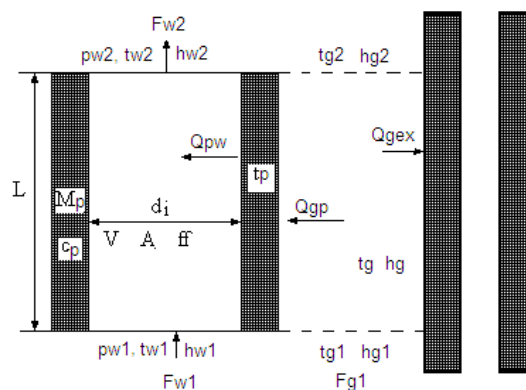
FIG.1. THE PHYSICAL MODEL OF THE ECONOMIZER

where: F_{w1}, F_{w2} are the mass flow of water input-output, kg/s; F_{g1}, F_{g2} are the mass flows of flue gas input-output, kg/s; Q_{gp} –

the heat transmitted from flue gas to pipes, W; Q_{pw} – the heat transmitted from sheet to water, W; t_{w1}, t_{w2} – the temperature of the water input-output, ^{o}C; t_{g1}, t_{g2} the temperature of the flue gas input-output, ^{o}C; t_{g} – temperature of the flue gases, ^{o}C; t_{p} – average temperature pipes, ^{o}C; p_{w1}, p_{w2} – the economizer inlet, respectively outlet water pressure, bar; h_{w1}, h_{w2}, h_{g1}, h_{g2} – the enthalpy of the water inlet-outlet or flue gas, kJ/kg^{o}C; M_{p} – the metal mass, kg; V – the total volume free, m^{3}; A- water flow area,m^{2}; f_{f} – friction coefficient; d_{i} – inside diameter of the pipe, m.

The physical processes describing the economizer operation are: single-phase flow through pipes; heat transfer from flue gases to pipes; heat accumulation in the pipe material; heat transfer from the economizer pipes to the heating water.

The simplifying hypotheses adopted in the mathematical model are, [11]: the economizer is without boiling; the variables of the model satisfy the physical principles; the economizer is considered to be made of a single package; the model is with concentrated parameters and contains only time, not spatial derivations; gravitational and acceleration losses are not important; heat transfer is predominantly by convection.

With the hypotheses presented, the mathematical model is described by the:

The impulse conservation equation is reducing to:

$$p_{w2} = p_{w1} - \beta F_{w1}^{2} \tag{1}$$

The heat transfer equation, predominantly by convection, from the gases to the economizer pipes:

$$Q_{gp} = k_{gp} S \left(t_{g} - t_{p} \right) \tag{2}$$

with k_{gp} – the convective heat transfer coefficient from the gases to the economizer pipes, W/mK; S – the heat exchange surface, m^{2}; t_{g} – the average flue gases temperature, ^{o}C; t_{p} – the average temperature of the pipes, ^{o}C.

The heat transfer equation, predominantly by convection, from the economizer pipes to the water:

$$Q_{pw} = k_{pw} S \left(t_{p} - t_{w} \right) \tag{3}$$

with k_{pw} – the convective heat transfer coefficient from the economizer pipes to the water, W/mK; S – the heat exchange surface, m^{2}; t_{s} – the average water temperature, ^{o}C.

Convective heat transfer coefficients are determined using the criteria equations given in the literature:

$$k_{gp} = 0,2 \cdot \frac{\lambda}{d_{e}} \left(\frac{w \cdot d_{e}}{v} \right)^{0,65} \cdot \mathrm{Pr}^{0,33} \cdot C_{z} \cdot C_{s} \tag{4}$$

$$k_{pa} = 0,021 \cdot \frac{\lambda}{d_{i}} \left(\frac{w \cdot d_{i}}{v} \right)^{0,8} \cdot \mathrm{Pr}^{0,43} \cdot C_{z} \cdot C_{s} \tag{5}$$

Relationships in which thermodynamic properties are calculated in real time using MATLAB functions for the fluid achieved value by the pressure and temperature.

The mass conservation equation:

For the water

$$\frac{d}{d\tau} \left(V_{w} \rho_{w} \right) = F_{w1} - F_{w2} \tag{6}$$

and for the gases:

$$\frac{d}{d\tau}\left(V_g \rho_g\right) = F_{g1} - F_{g2} \tag{7}$$

The equation of heat accumulation in the economizer pipes:

$$M_p c_p \frac{d}{d\tau}\left(t_p\right) = Q_{gp} - Q_{pw} \tag{8}$$

The energy conservation equation, taking into account the mass conservation

For the water:

$$V_w \rho_w \frac{d}{d\tau}\left(h_w\right) = Q_{pw} + F_{w1} h_{w1} - F_{w2} h_{w2} \quad \Rightarrow \quad V_w \rho_w c_w \frac{d}{d\tau}\left(t_w\right) = k_{pw} S\left(t_p - t_w\right) + F_{w1} c_{w1} t_{w1} - F_{w2} c_{w2} t_{w2} \tag{9}$$

and for the gases:

$$V_g \rho_g \frac{d}{d\tau}\left(h_g\right) = F_{g1} h_{g1} - F_{g2} h_{g2} - Q_{gp} \quad \Rightarrow \quad V_g \rho_g c_g \frac{d}{d\tau}\left(t_g\right) = F_{g1} c_{g1} t_{g1} - F_{g2} c_{g2} t_{g2} - k_{gt} S\left(t_g - t_p\right) \tag{10}$$

The system of equations to determine unknown operational sizes, in relative units, is the same as the superheater, the corresponding coefficients being given by the literature, [8], [9].

In absolute units, the unknown sizes are the expression, [7]:

For the water pressure at the exit of the economizer:

$$p_{w2} = p_{w1} + \left\{ \frac{1}{10^5} \left[-\frac{9.86 \cdot g}{v_w} - F_w^2 \frac{1}{A} v_w \left(\frac{f_f \cdot L}{d_i} \right) \cdot 0.25 \right] \right\} \tag{11}$$

For the average water temperature:

$$t_w = \int \left[Q_{pw} + h_{w1} F_{w1} - h_{w2} F_{w2} \right] \frac{1}{V_w \rho_w c_{pw}} d\tau \tag{12}$$

For the water temperature at the exit of the economizer:

$$t_{w2} = 2t_w - t_{w1} \tag{13}$$

For the average gases temperature:

$$t_g = \int \left[h_{g1} F_{g1} - h_{g2} F_{g2} - Q_{gt} \right] \frac{1}{V_g \rho_g c_{pg}} d\tau \tag{14}$$

For the gases temperature at the exit of the economizer:

$$t_{g2} = 2t_g - t_{g1} \tag{15}$$

IV. SIMULATING OF THE ECONOMIZER

As stated in the presentation of mathematical model equations of heat transfer models used in relative units, data from the literature were replaced by equations of heat transmission by convection. For both the convective heat transfer coefficient of combustion gas in the pipes and water pipes were prepared from the calculation block diagrams, Fig. 2.
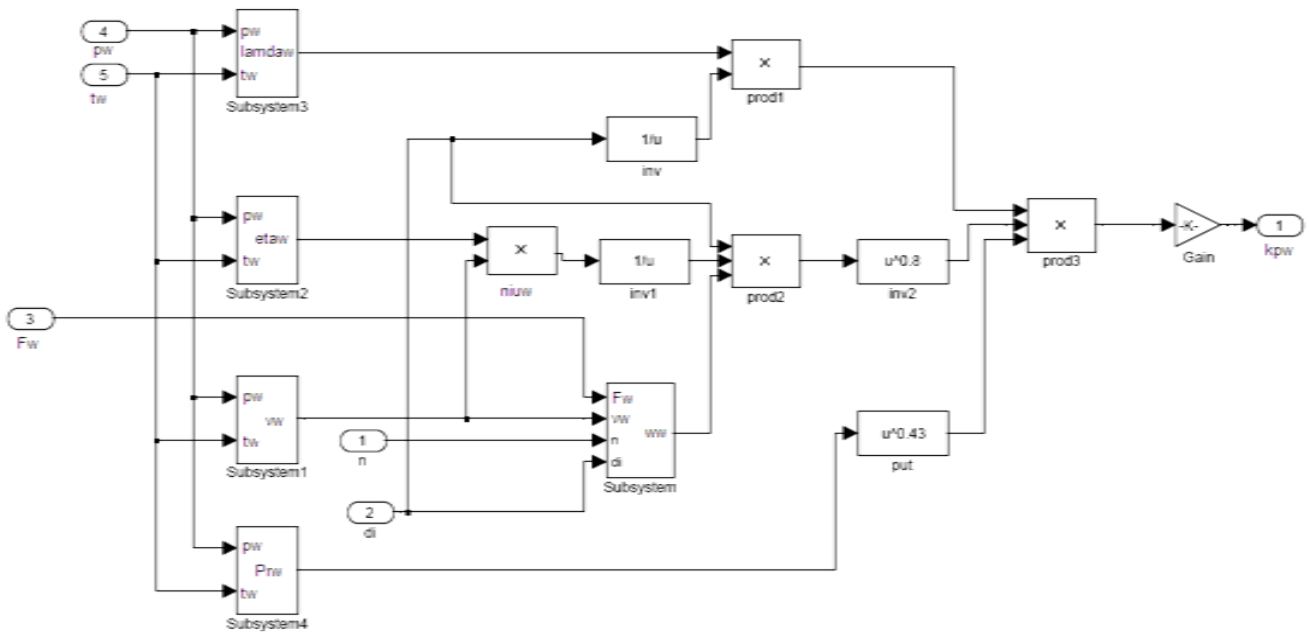
FIG.2. DIAGRAM CALCULATION OF THE CONVECTIVE HEAT EXCHANGE COEFFICIENT

MATLAB functions were created for Prandtl number, friction coefficient, thermal conductivity, kinematics viscosity and specific volume of water being determined by the pressure and temperature of the fluid attained, Fig 3.
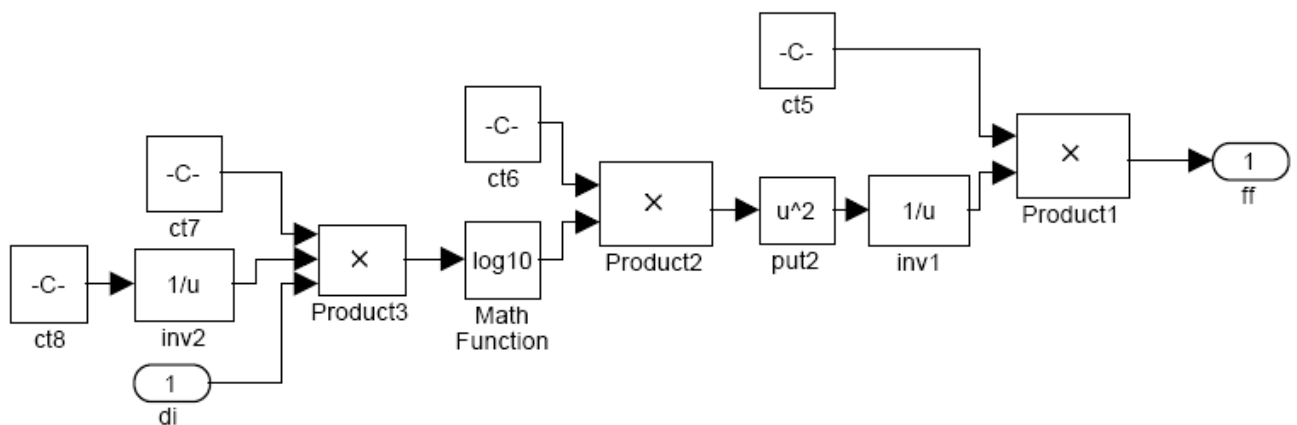
FIG.3. DIAGRAM CALCULATION OF THE FRICTION COEFFICIENT

From the point of view of the simulation of the operation of this heat exchange surface was analyzed at unitary variations of the input sizes on the outlet water pressure and the required water flow.
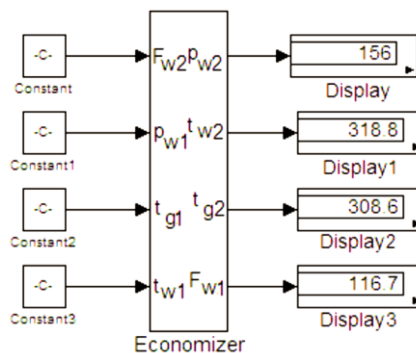
FIG.4. BLOCK DIAGRAM – SIMULATING OF THE ECONOMIZER OPERATION
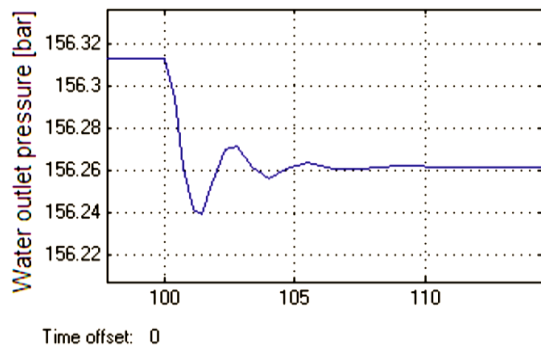
FIG.5. WATER PRESSURE VARIATION AT THE EXIT OF THE ECONOMIZER WITH THE ENTRANCE TEMPERATURE
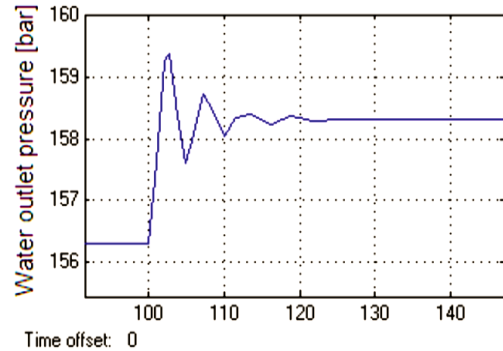
FIG.6. WATER PRESSURE VARIATION AT THE EXIT OF THE ECONOMIZER WITH THE ENTRANCE PRESSURE
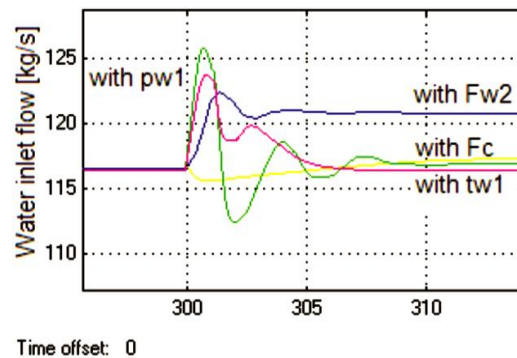
FIG.7. WATER FLOW VARIATION AT THE EXIT OF THE ECONOMISER

Analyzing the dynamic behavior of the steam generator economizer, step variations of the sizes - water temperature entering the economizer, economical input water pressure, combustion gas inlet temperature - it is found that the balance is achieved by damped oscillations. Output water pressure is greatly influenced by inlet pressure.

V. CONCLUSION

The model in absolute units is the basis for simulating the operation of the dynamic steam generator, [7]. He presents the major advantage of eliminating the sequence of recalculation of parameters at each step - in the models in relative units the whole set of coefficients is determined and entered into the model according to the parameters achieved in a previous reference regime; eliminates linearization around the stabilized operating point, nonlinear features being included in the model; it finds its own non-linear function points and updates parameter values; allows the determination of heat exchange coefficients between thermal agents and real-time exchange surfaces, their values obtained by computing within the limits recommended by the literature; removes the empirically determined coefficients, including the calculated exchange coefficients, from the heat exchanges exchanged between the thermal agents; it is characterized, with all its advantages presented above, as a slower model - relative to the one in relative units - due to the iterative calculation. The model in absolute units can be the basis for an intelligent system for simulation in real time operation of a steam generator. It is recommended to develop on other energy equipment. This supposes mathematical models in absolute units for the turbine and the electric generator, simulations of their static and dynamic regimes operation.

REFERENCES

[1] Ahluvalia, K.S; Domenichini, R. Dynamic modeling of a combined cycle plant, Trans.ASME Journal of Engineering for Gas Turbines and Power, 1990, vol 112.

[2] Badea, A.; Necula, H.; Stan, M.; Ionescu, L.; Blaga, P.; Darie, G. Equipment and Thermal Installations, Editura Tehnică, Bucharest, RO, 2003, Technical Publishing House.

[3] Duinea, A. M. Analysis, modeling and simulation of the heat exchange surfaces functioning in the steam generators, Craiova, RO, 2015, Sitech Publishing House.

[4] Duinea, A.; Mircea, I. Heat and mass transfer, Craiova, RO, 2006, Publisher Universitaria.

[5] Duinea, A. M.; Ciontu M.; Bratu C. (2016) Some considerations about the hierarchy of the technical solutions for the modernization of power plants. International Journal of Energy.

[6]   Duinea, A. M.; Mircea, P. M. Issues regarding the furnace operation of the steam generator in dynamic regime Journal of sustainable energy, 2015, vol V, pp 31-34.

[7]   Duinea, A. Contributions for computerized management of energy facilities operation PhD Thesis, Craiova, RO, 2009.

[8]   Lăzăroiu, Gh.; Pănoiu, N.; Dănilă, N. Adaptive adjustment of the steam temperature, Energy Journal, 1997, no. 8.

[9]   Hazi, G. Optimization techniques in energetic engineering, Chişinău, MO, 2004, Technical Publishing House.

[10] Lăzăroiu, Gh. Programming systems from modeling and simulation, Bucharest, RO, 2005; Publishing Politehnica Press.

[11] Lăzăroiu, Gh. Modeling and simulation of dynamic operation of power plants, Bucharest, RO, 2000; Printech Publishing House.

A Correlative Analysis of Machining Parameters with Surface Roughness for Ferrous and Non- Ferrous Alloy Materials

Asim M Saddiqe[1], Murali R V[2]

[1]Level 4 B. Engg CAME student, Caledonian College of Engineering, Oman
[2]Faculty, Department of Mechanical and Industrial Engineering, Caledonian College of Engineering, Oman

***Abstract*—** *Average Surface Roughness (R_a) is one of the most frequently used texture parameters to define the quality of turned components. The roughness values of a turned surface much depends on cutting parameters such as cutting speed, feed rate and depth of cut. Optimization of these parameters is very important in relation to surface roughness as they reveal the best suitable conditions for the turning operation. In this project, a correlative study of machining parameters and the surface roughness for ferrous (stainless steel 304) and non–ferrous alloy (Aluminium) material is carried out. Response Surface Methodology (RSM) and Analysis of Variance (ANOVA) techniques are employed in this analysis to explain the influence of different cutting parameters on surface roughness values. The combination of optimum experimental parameters can be found by machining these ferrous and non-ferrous materials in CNC turning center and finding the least surface roughness parameters. ANOVA analysis, integrated with Design Expert software, is used to determine effective ratios of the parameters and subsequently the relationships between input parameters and their responses relationship are established. The minimum surface roughness results in reference to spindle rpm, feed rate, and depth of cut are determined and estimation of the optimal surface roughness values (Ra) for least surface roughness are the results obtained in the study. In case of stainless steel 304, optimal values of cutting speed, feed and depth of cut against the least surface roughness value of 1.33 microns are found to be 220 m. min^{-1}, 0.2 mm. rev^{-1} and 0.3 mm respectively. In case of Aluminium, optimal values of cutting speed, feed and depth of cut against the least surface roughness value of 2.8 microns are 200 m. min^{-1}, 0.2 mm. rev^{-1} and 1.15 mm respectively. These results reaffirm that RSM and ANOVA techniques are useful and efficient in achieving optimal set of machining parameters for select ferrous and non-ferrous materials in correlating the surface finish values.*

Keywords*— *Response Surface Methodology, Analysis of Variance, Computer Numerical Control, Surface Roughness, Machining Parameters.

I.   INTRODUCTION

Surface roughness is defined as the shorter frequency of real surfaces relative to the troughs. When machined parts are looked at carefully, their surfaces are found to embody a complex shape made of a series of peaks and troughs of varying heights, depths, and spacing. Surface roughness is greatly affected by the microscopic asperity of the surface of each part. Surface roughness for a machined component depends on the following factors:

- cutting speed selected
- depth of cut set
- feed rate set
- spindle speed set
- type of coolant used
- type of cutting tool used
- Type of material being machined etc

In recent times, industrial manufacturing process has become more advanced and they are trying to produce the products at lesser cost and enhanced quality. Surface roughness is the most important factor which can increase the quality of machine components. Influence of each factor aforementioned on surface roughness can be experimentally predicted by using Response Surface Methodology (RSM) method supported by Analysis of Variance (ANOVA) technique. This experimental work is carried out on a CNC turning center in Caledonian College of Engineering. The experimental results help to predict the most optimal cutting parameters to achieve the least surface roughness values so that reliability, quality and longevity of the product are ensured at minimum product cost. This paper aims at analyzing and investigating the different machining parameters such as cutting speed, feed rate and depth of cut and their effect on surface roughness values for different ferrous alloy and non-ferrous alloys using RSM and ANOVA techniques and to make a comparative study on the same. Investigation results in proposing a new scope of improvement for industrial applications. This is a thrust area for new researchers to work

on and produce some productive results which will benefit the production industries by choosing correct set of machining parameters.

II.   BACKGROUND STUDIES

In production industries, manufacturing process plays a vital role in achieving maximum productivity and quality of products. This manufacturing process can be of two type secondary and primary process. Secondary process contains machining while primary manufacturing contains Forging, Welding, and Casting etc. For calculating the total production time for a particular product, actual machining time and materials removal rate (MRR) are important variables and these values determine the average surface roughness (R_a) values. Mild steel (EN8) and Aluminum are the work materials used in this study. Mild steel materials are frequently used for making shafts, connecting rods, bolts, hydraulic rams, screws and many machining parts. Its hardness ranges from 201-255HBand its major elements of composition are as follows: Carbon (0.36-0.44%), Silicon (0.1-0.4%), Phosphorus (0.05%) Manganese (0.60-1.00%) and Sulphur (0.05%) (Ganesh, et al., 2014).

Machine tool technology is very important for all sectors of economy as it produces all tools which generate production. Experimental Investigation on the mild steel has been carried out for turning operation in a lathe machine and it is concluded that RSM technique is giving better results than the Taguchi technique. Surface roughness plays an important role in determining the quality of products which in turn implies that the cutting tool wear and material removal rate also have an effect on the quality of the product as demonstrated subsequently by Subhajit & Mukherjee (2014).

In another study by Qureshi et al. (2015), P20 steel is used for optimization process for moulds and the cutting tool is TiN coated tungsten carbide. The methodology used for this work is Taguchi method. Taguchi method studies the parameter space in limited experiments by using orthogonal arrays. For measuring surface roughness Mitutoyo Surftest SJ-201P a surface roughness tester is used. The parameters which are analyzed are Spindle Speed (m/min), Feed rate (mm/rev), Depth of Cut (mm), and Ra (μm).

This study on AISI P20 steel carried out and it gives away the following outcomes:

- For high speed CNC turning, the recommended optimum parameters for surface roughness are combinations of 0.610, 0.240 and 0.4943.

- It can be determined that for the optimum results the combination of and a middle value of depth of cut 0.1mm, low level feed of (0.1mm/rev) and the high level of cutting speed (200m/min) are best. In the study Taguchi method is used optimize of AISI P20 steel in high speed CNC turning conditions. The optimization is carried out through experiments by using different parameters like speed, feed, and depth of cut (Qureshi et al., 2015).

Rao et al., (2014) demonstrated that in doing experiments with Niobium alloy C-103, the response surface analysis technique contains (i) Box-Wilson Central Composite Design (CCD) method and (ii) Box-Behnken Design (BBD). Both methodologies need a quadratic relationship between the responses and experimental factor. In the present attempt, CCD is chosen and straight turning process is considered on CNC lathe machine. ANOVA is also used to control the working ranges of parameters which show response curves. The parameters which are analyzed are Spindle Speed (rpm), Feed (mm/rev), Depth of Cut (mm) and Surface Roughness (μm).This study has shown that in turning operation for Niobium alloy, the values of parameters obtained are depth of cut = 0.37mm, feed = 0.15 mm/rev and cutting speed =84.32m/min in order to minimize the cutting force. The optimization is carried out through experiments by using different parameters like speed, feed, and depth of cut. It is concluded that the greatest effect on surface roughness is cutting force which is realized through depth of cut. If the depth of cut is increasing then cutting force will also increase.

In this paper, several impactful factors effecting surface roughness values of the component are considered for optimization process. This process is suitably developed by implementing RSM/ANOVA techniques to achieve a set of optimal values for achieving least surface roughness values which is very important from the industrial point of view.

III.   MATERIALS & METHODS

A typical ferrous (stainless steel 304 grade) and non-ferrous material (Aluminum) are selected for the purpose of study. Stainless steel is the combination of different metals making it with very handful properties. Type 304 is the most extensively used austenitic stainless steel, because of its composition in which 18% chromium and 8% Nickel. It has good strength and strong resistant to corrosion and has good welding and forming properties as well as has good draw ability. It can be made into different shapes without annealing. Key mechanical and physical properties are presented in Table 1 while chemical composition is presented in Table 2 for reference.

TABLE 1
KEY PROPERTIES OF 304 STEEL

PROPERTY	VALUE
Density	4500 kg/m^3
Specific Heat	0.50 kJ/kg-K
Thermal Conductivity	16.2 W/m-k
Modulus of Elasticity	193 GPa
Melting Point Range	1399 °C -1454°C
Ultimate Tensile Strength	510-620 MPa

TABLE 2
CHEMICAL COMPOSITION OF 304 STEEL

ELEMENT	TYPE 304 (%)
Carbon	0.08 max.
Manganese	2.00 max.
Phosphorus	0.045 max.
Sulfur	0.03 max.
Silicon	0.75 max.
Chromium	18.00-20.00
Nickel	8.00-12.00
Nitrogen	0.10 max.
Iron	Balance

Type 304 stainless steel is used in the food industry. This is suitable for distilling, milk processing as well as in storage tanks, fermentation vats, yeast pans, and pipelines. Due to its corrosion resistance ability it is used in cooking appliances, coffee pots, refrigerators, tabletops, sinks and stoves. They have also have application in the in the dyeing industry, water filtration systems, marine nuts, screws and bolts, mining equipment, heat exchangers, chemical containers, and architecture etc.

On the other hand, Aluminum is a light weight, silvery white, recyclable, strong and excellent corrosion resistant metal. It has a high thermal conductivity, is non-toxic, has low density, and can be easily cast, machined and formed. It is also non-sparking and non-magnetic. Aluminum is used in large number of products which includes airplane parts, beer kegs, window frames, kitchen utensils, foils, cans. Key mechanical and physical properties are presented in Table 3 for reference.

CNC machine which is used for this experiment is ACE Designers, Fanuc oi-Mate-TD. Key specifications of the CNC Lathe are listed below:

- Flat Nose ø110mm Spindle
- 8 station Bi-Directional Turret (BTP-50)
- Tail stock with External Rotating Center.
- Spindle Motor Power: 5.5 KW
- Spindle Speed: 50-5000 RPM
- Between Center Length: 200 mm
- Maximum Machining Diameter: 190 mm
- Standard Chuck size: 135 mm

Mitutoyo Surftest SJ-301 is a device which is used for measuring average surface roughness of the test materials. International standards like JIS-B-061-1982, JIS-B-0601-1994, ANSI, ISO, and DIN are set while measuring the surface texture parameters. Cemented carbide tool is used for machining the materials as it has tantalum carbide (TaC), titanium carbide (TiC) or tungsten carbide (WC) as the aggregate. Here in this study tungsten carbide aggregate is used (code TNMG 160408NN LT 10).

TABLE 3
KEY PROPERTIES OF ALUMINIUM

PROPERTY	VALUE
Density	2.70 g cm^{-3}
Specific Heat	897 J/kg-K
Thermal conductivity	205 W/m K
Young's modulus	70.3 GPa
Melting Point	660°C

Therefore, in this attempt, RSM and ANOVA techniques are employed to explain the influence of different cutting parameters on surface roughness values. The combination of optimum experimental parameters can be found by machining these ferrous and non-ferrous materials in CNC turning center and finding the least surface roughness parameters. ANOVA analysis, integrated with Design Expert software, is used to determine effective ratios of the parameters and subsequently the relationships between input parameters and their responses relationship are established. The minimum surface roughness results in reference to spindle rpm, feed rate, and depth of cut are determined and estimation of the optimal surface roughness values (Ra) for least surface roughness are the results obtained in the study.

IV. DESIGN OF EXPERIMENTS

Design of experiments (DOE) is an efficient method to obtain the relationships between input and output in a particular process. Input is the effecting factors while output is the response of that process. It is very useful to find cause and affect relationships. In order to optimize the output this information is required to manage process inputs. Various components of DoE are listed in here.

Factors: It is the input of the process. Factors or the parameters which are affecting the process. Levels: It is the maximum and lower limit which is giving to the process. For a two level design the levels will be high and low Response: Response is the output of the experiments which gives the desired effect. An important stage of RS model generation by RSM is the planning of experiments. The parameters which are used for the experiments are cutting speed (Vc-m/min), feed (f- mm/rev), and depth of cut (d-mm) with two levels label as high and low level as depicted in Table 4.

TABLE 4
MACHINING PARAMETERS
(Stainless steel 304)

Name	Type	Low	High
Cutting speed (m. min^{-1})	Factor	170	270
Feed (mm. rev^{-1})	Factor	0.2	0.4
Depth of cut (mm)	Factor	0.3	2

In this investigation, 17 experiments for each type of materials were conducted considering 3 cutting parameters. The generated values of the experiment performed for Stainless Steel and Aluminium are presented in tables 4 through 7 as follows.

TABLE 5
VALUES GENERATED BY ANOVA
(Stainless steel 304)

Std	Run	Factor 1 A:Cutting speed m/min	Factor 2 B:Feed mm/rev	Factor 3 C:Depth of cut mm	Response Response surface roughness microns
6	1	270	0.3	0.3	2.19
4	2	270	0.4	1.15	3.65
11	3	220	0.2	2	1.89
15	4	220	0.3	1.15	2.27
16	5	220	0.3	1.15	2.41
8	6	270	0.3	2	2.27
12	7	220	0.4	2	3.14
10	8	220	0.4	0.3	3.38
13	9	220	0.3	1.15	2.41
2	10	270	0.2	1.15	1.41
9	11	220	0.2	0.3	1.33
17	12	220	0.3	1.15	2.36
7	13	170	0.3	2	2.35
1	14	170	0.2	1.15	1.9
3	15	170	0.4	1.15	3.07
14	16	220	0.3	1.15	2.19
5	17	170	0.3	0.3	2.16
6	1	270	0.3	0.3	2.19
4	2	270	0.4	1.15	3.65
11	3	220	0.2	2	1.89

TABLE 6
MACHINING PARAMETERS
(Aluminium)

Name	Type	Low	High
Cutting speed (m. min⁻¹)	Factor	170	270
Feed (mm. rev⁻¹)	Factor	0.2	0.4
Depth of cut (mm)	Factor	0.3	2
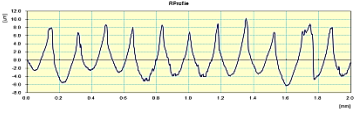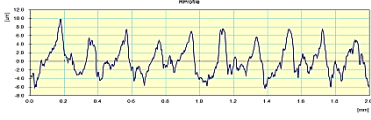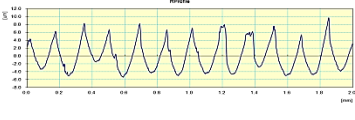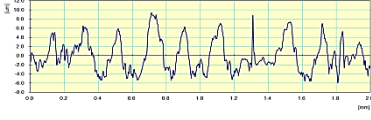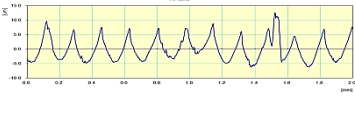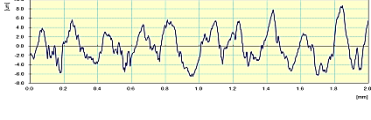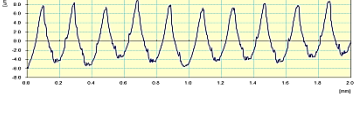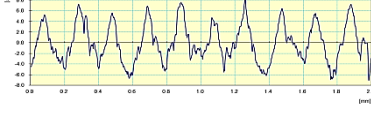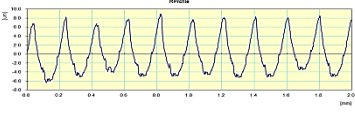
TABLE 7
VALUES GENERATED BY ANOVA
(Aluminium)

Std	Run	Factor 1	Factor 2	Factor 3	Response
		A:Cutting speed	B:Feed	C: Depth of cut	Response surface roughness
		m/min	mm/rev	mm	microns
6	1	270	0.3	0.3	2.19
4	2	270	0.4	1.15	3.65
11	3	220	0.2	2	1.89
15	4	220	0.3	1.15	2.27
16	5	220	0.3	1.15	2.41
8	6	270	0.3	2	2.27
12	7	220	0.4	2	3.14
10	8	220	0.4	0.3	3.38
13	9	220	0.3	1.15	2.41
2	10	270	0.2	1.15	1.41
9	11	220	0.2	0.3	1.33
17	12	220	0.3	1.15	2.36
7	13	170	0.3	2	2.35
1	14	170	0.2	1.15	1.9
3	15	170	0.4	1.15	3.07
14	16	220	0.3	1.15	2.19
5	17	170	0.3	0.3	2.16
6	1	270	0.3	0.3	2.19
4	2	270	0.4	1.15	3.65
11	3	220	0.2	2	1.89

Stainless steel and Aluminum specimens for turning operation are of diameter of 30mm and of length 100 mm.

V.   RESULTS AND DISCUSSION

Surface roughness plays an important in the designing and manufacturing, if there is an improvement in surface finish values, and then the cost of manufacturing will decrease. Therefore our aim is to decrease the surface roughness values at an optimal set of machining parameters. Surface roughness is measured for select materials by using Mitutoyo SJ-301 for three different places of the material and an average has been taken into consideration. The roughness experiment results show that the minimum roughness from the stainless steel 304 machined parts is 1.33 microns while the minimum surface roughness in the Aluminium machined parts is 2.73 microns.

	Exp 7 Run1 Ra=3.16		Exp 4 Run 2 Ra=2.66
	Exp 7 Run2 Ra=3.05		Exp 4 Run 3 Ra=2.85
	Exp 7 Run3 Ra=3.23		Exp 5 Run 1 Ra=2.72
	Exp 8 Run1 Ra=3.31		Exp 5 Run 2 Ra=2.88
	Exp 8 Run2 Ra=3.52	**FIGURE 2 ROUGHNESS PROFILE – ALUMINIUM**	
FIGURE 1 ROUGHNESS PROFILE – SS 304			

VI.   CONCLUSION

This study presents the findings of an experimental investigation into the effect of turning parameters like cutting speed, feed rate and depth of cut by turning ferrous (stainless steel 304) and non- ferrous material (Aluminium) in the CNC turning center and then checked the surface roughness values with Mitutoyo SJ-301 instrument. The effects of parameters and their correlation with the surface roughness and the optimal values have been analysed.

In case of stainless steel 304, optimal values of cutting speed, feed and depth of cut against the least surface roughness value of 1.33 microns are found to be 220 m. min^{-1}, 0.2 mm. rev^{-1} and 0.3 mm respectively. In case of Aluminium, optimal values of cutting speed, feed and depth of cut against the least surface roughness value of 2.8 microns are 200 m. min^{-1}, 0.2 mm rev^{-1} and 1.15 mm respectively.

These results reaffirm that RSM and ANOVA techniques are capable of achieving optimal set of machining parameters for select ferrous and non-ferrous materials machining and to effectively correlate the surface finish values obtained. Therefore, it is concluded that for stainless steel 304 feed and depth of cut are major influencing factors while for Aluminium, the feed rate is the major influencing factor in order to get minimum surface finish values. The study and associated results/outcomes of the analysis would add value to the current literature available in this research domain.

Effect of machining parameters on the tribology of the machined components can be a vast area to study and investigate. In this attempt, the effects of cutting parameters such as speed, feed and depth of cut are considered and their correlation with the surface roughness are analysed and presented. Although the current approach which is used to find the optimal parameters is Response surface method and ANOVA. The optimal results are varying for surface finish and therefore there should be improved unique values for the model to get even better surface finish values in the future work. Furthermore investigation and analysis can be extended to include other mechanical properties such as fatigue and torsion etc in order to enhance the level of investigation into this effect. Finally, a number of different materials such as alloys (ferrous and non-ferrous) can be subject to this kind of study in order to draw a wider analysis and conclusion by taking this work as a reference work. This can open up new fields of research for young researchers to go beyond in this field and can benefit the industry.

REFERENCES

[1] Ganesh, N., et al., 2014. Optimization of cutting parameters in turning of EN 8 steel using response surface method and genetic algorithm. *International Journal of Mechanical Engineering and Robotics Research*. 3(2).

[2] Qureshi, A., et al., 2015. Optimization of Cutting parameters for Surface roughness in CNC turning of P20 steel. *International Journal of Scientific & Engineering Research*. 6(12).

[3] Phogat, A., et al., 2013. Optimization of cutting parameters for turning operations based on response surface methodology. *International Journal of Enhanced Research in Science Technology & Engineering*. 2(7). p. 83-89.

[4] Rao, S.K., et al., 2014. Optimization of Cutting parameters for cutting force on Turning of Niobium alloy C-103 by using Response Surface Methodology. *International Journal of Innovative Science, Engineering & Technology*. 1(4).

[5] Subhajit, D, & Mukherjee, S., 2014. Optimization of cutting parameters for improving surface roughness in turning operation using taguchi method and anova, *International Journal of Research in Engineering and Technology*. 3 (6).

Appropriate algorithm method for Petrophysical properties to construct 3D modeling for Mishrif formation in Amara oil field

Jawad K. Radhy AlBahadily[1], Medhat E. Nasser[2]

Department of geology, college of science, Baghdad University, Baghdad, Iraq

Abstract— *Geostatistical modeling technicality hasutilized to build the geological models before scaling-up. Possible images of the area under investigation have provided from these methods that honor the well data and have the same variability computed from the original data. Property modeling is the process of filling the cells of the grid with discrete (facies) or continuous (petrophysics) properties. When interpolation between data points, propagate property values along the grid layers have executed. The main branch in the modeling algorithms obtainable is between Deterministic and Stochastic methods in Petrel. Both kinds of algorithms are available in the Facies and Petrophysical modeling processes.The process of well log up scaling is required to post values in each cell of the 3D grid where each of the wells is situated; to achieve these averages well properties are used to populate each of the cells. Three Dimension modeling has built depending to 12 wells for Mishrif formation in Amara oil field. All wells have PHIE and Water Saturation logs, which exported from interactive petrophysics software. Thereafter, scale up well logs has carried out for these wells. To building the model, there are different methods of distribution of petrophysical properties. Eight methods have executed in order to propagate property values through construct Porosity and Water Saturation Models. Depending on the results, there are not data from the modeling corresponding exactly to the true data from the log interpretation for the same well, but it approximate from the true data in different percentage .Sequential Gaussian Simulation suitable algorithm method to build the 3D modeling for Mishrif formation.*

Keywords— *Deterministic algorithms, Mishrif Formation, Petrophysical properties, Reservoir modeling, stochastic algorithm.*

I.   INTRODUCTION

Geostatistical modeling technicality is widely used to build the geological models before scaling-up. Possible images of the area under investigation have provided from these methods that honor the well data and have the same variability computed from the original data. When few data are available or when data obtained from the wells are insufficient to have to characterize the petrophysical conduct and the heterogeneities of the field, further constraints are needed to gain a more factual geological model. For instance, seismic data or stratigraphic models can supply average reservoir information with an excellent area covering, but with a poor vertical resolution[1].

The procedure of preparing the input data into property modeling, it involves applying transformations on input data, identifying trends for continuous data, vertical proportion, and probability for discrete data. This is then utilized in the facies and petrophysical modeling to include that the same trends occur in the result.The Data Analysis utility lets analyze data interactively to gain a better understanding of the trends within your data. Also, benefit from an understanding of the relationships across all your data types[2].

II.   BASIC CONCEPTS

Property modeling is the process of filling the cells of the grid with discrete (facies) or continuous (petrophysics) properties[3]. Petrel assumes that the layer geometry provided to the grid follows the geological layering in the model area. Thus, are these processes dependant on the geometry of the existing grid. When interpolation between data points, propagate property values along the grid layers will be executed by Petrel.The main branch in the modeling algorithms obtainable is between Deterministic and Stochastic methods in Petrel. Both kinds of algorithms are available in the Facies and Petrophysical modeling processes.

With the same input, data will constantly grant the same outcome through Deterministic algorithms. These algorithms will generally run much quicker and are very transparent - it is easy to see why a particular cell has been given a particular value. The disadvantage is that models with little input data will automatically be smooth even though evidence and experience may

suggest that this is not likely. Getting a good idea of the uncertainty of a model away from the input data points is often difficult in such models.

Stochastic algorithms use a random seed in addition to the input data, so while consecutive runs will give similar results with the same input data, the details of the result will be various. Sequential Gaussian Simulation included in Stochastic algorithms have more complex and therefore take much longer to run, but they do honor more aspects of the input data, the variability of the input data specifically. This means that local lows and highs will appear in the results which are not steered by the input data and whose location is simply an artifact of the random seed utilized. The result will have a distribution more typical of the real case, although the specific variation is unlikely to match. This can be useful, particularly when taking the model further to simulation as the variability of a property is likely to be just as important as its average value. The disadvantage is that some important aspects of the model can be random and it is important to perform a proper uncertainty analysis with several realizations of the same property model with diverse random seeds [2].

The aim of property modeling is to distribute properties between the wells such that it realistically preserves the reservoir heterogeneity and matches the well data [3].

III.   METHODOLOGY

3.1   Data Import

Many data should be provided to Petrel software in order to construct a 3D model. Import data describes the data import procedure and the various data formats supported and organize the imported wells in sub folders. Well data were imported in three steps:

3.1.1   Well Heads

Well heads of twelve boreholes of Amara Oil Field, the well header information has been imported into Petrel, (figure1). There are 15 default system attributes available in the attribute list [2]: The well name, UWI : the unique well identifier, Well symbol, Surface X coordinate, Surface Y coordinate, Kelly Bushing (KB) value, TD (TVD): the vertical depth value, TD (MD) : the measured depth value of the last point in the well, Top depth (MD) and Bottom depth (MD).

3.1.2   Well tops

Well tops of the reservoir units of Mishrif Formation have been also imported as well as the total depth of each well, which represents the markers for each unit, shows in figure (2).
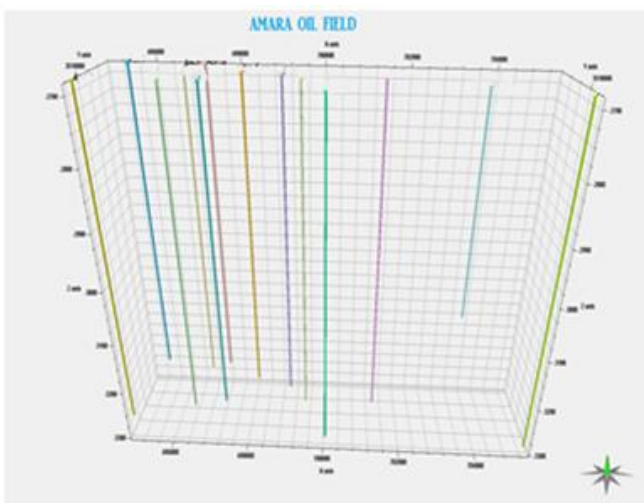
FIGURE 1: WELLS OF THE STUDY AREA   **FIGURE 2: WELL TOPS OF THE STUDY AREA**
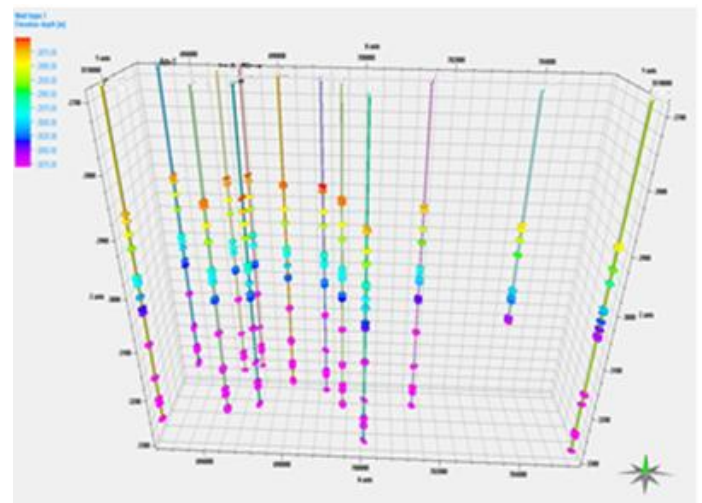
3.1.3   WellLogs

This type of data included importing well logs (PHIE and SW logs) for each of the twelve studied wells that were exported from IP software of each well. Wells logs have shown in figure (3).
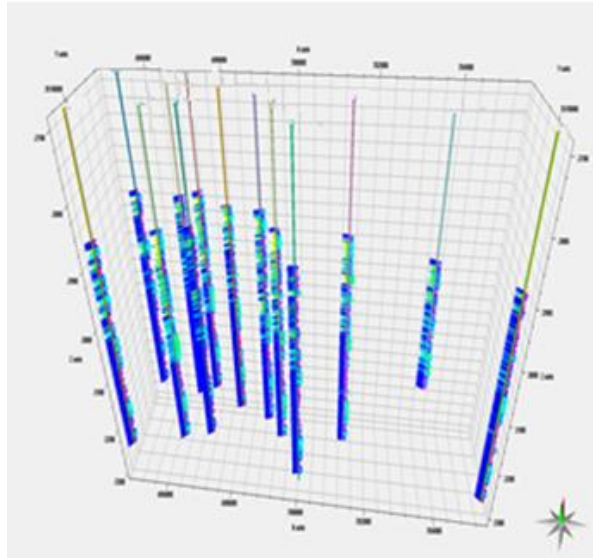
FIGURE 3: WELLS LOGS OF THE STUDY AREA WITH PHIE AND SW

3.2 Structural Modeling

A 3D structural model is made of geological interfaces such as horizons and faults honoring available observation data. These surfaces should fit the data within an acceptable range, depending on data precision and resolution[4].

A structure contour map is one of the most important tools for three-dimensional structural interpretation because it represents the full three-dimensional form of a map horizon. The mapping techniques to be discussed are equally applicable to surface and subsurface interpretation[5].

Structural maps were built depending on the well tops for all Amara wells as well as the available structural map for the top of Mishrif Formation from 2D seismic. Contour maps have been built to each zone of the formations figure (4) Structure Modeling of Mishrif Formation.
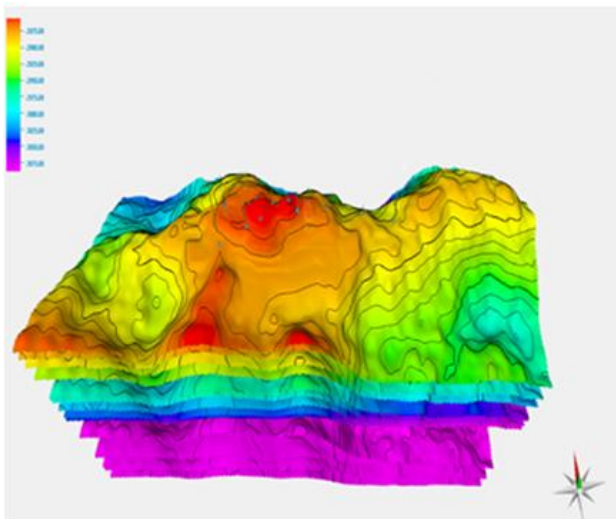
FIGURE 4: STRUCTURE MODELINF OF MISHRIF FORMATION
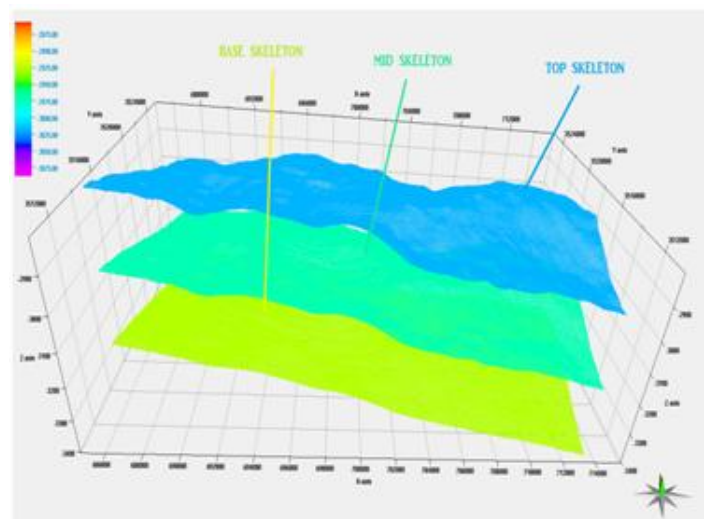
FIGURE 5: THE SKELETONS OF MISHRIF FORMATION IN AMARA OIL FIELD

3.2.1 Pillar Gridding

As a first step in building the framework of the 3D grid model, Pillar Gridding must be used in order to build the framework of the 3D grid. Pillar Gridding is the process of making the skeleton framework. The skeleton is a grid consisting of a Top, the Mid and Base skeleton grid as seen in the figure (5), each attached to the Top, the Mid and the Base points of the key pillars [6].

3.2.2   Make horizons

This process usually defines the main depositional units of the 3D grid. make horizon process inserts the inputs surfaces into the 3D grid.The inputs can be surfaces from seismic or well tops, line interpretations from seismic, or any other point or line data defining the surface.The make horizon process places all horizons defined directly from structure data into the 3D grid.The normally includes unconformity surfaces and primary horizons within sequences.The 3D grid these horizons are placed into consists only of pillars defined in the pillar Gridding process.The pillars define the corners of the cells that will ultimately be created in the 3D grid. Values are interpolated at each pillar based on nearby input data for the horizon.The interpolated values defined the surface in the 3D grid. The first step is to make horizons that honor the grid increment. The result after the Pillar Gridding process is a 3D grid consisting of a set of pillars connecting the Base, Mid, and Top Skeletons. The grid cell size is defined by the spacing between the pillars at a given vertical position[7]. Figure (6) represents horizons of the main units of Mishrif Formation.
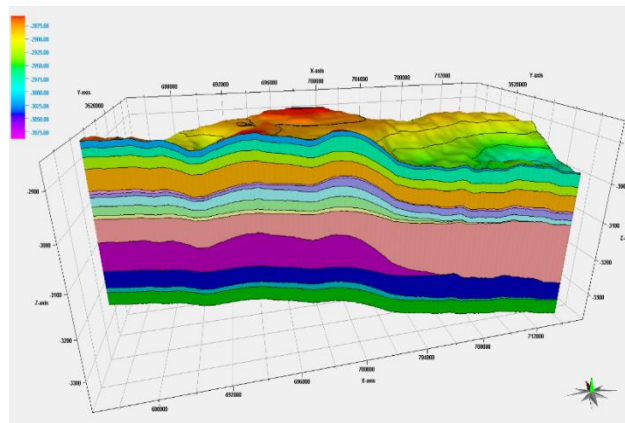
FIGURE 6: SECTION SHOWS MAIN HORIZONS OF MISHRIF FORMATION

3.2.3   Layering

The final step in building the structural framework is to define the thickness and orientation of the layers between horizons of the 3D Grid. These layers, in conjunction with the pillars, define the cells of the 3D Grid that are assigned attributes during property modeling. The Layering process will only make a finer resolution of the grid and no input data is used for this process. The vertical resolution of the gridcan define by setting the cell thickness, defining a number of cells or using a fraction code. When specifying the cell thickness, the zone division can either follow the base or the top of the zone.

The layers should be defined based on the properties to be modeled. Usually, the layer thickness should be the thickness of the thinnest facies to be modeled. However, the number of cells increases when the layer thickness decreases, [6]. Each reservoir unit in Mishrif formation has been divided into many layers depending on facies and petrophysical properties as illustrated in figure (7). MA is divided into 5 layers, MB11 has been divided into 6 layers, MB12 unit has been divided into 3 layers, MB11 has been divided into 6 layers, MB13 unit has been divided into 3 layers, MB11 has been divided into 6 layers, MB21 unit has been divided into 5 layers , MC1 unit has been divided into 3 layers, and MC2 unit has been divided into 3 layers.
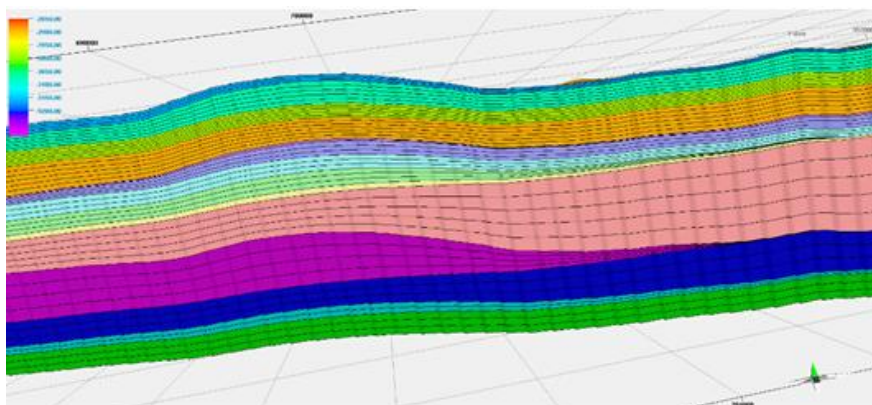
FIGURE 7: THE LAYERING IN THE MISHRIF FORMATION

3.3   Scale up Well logs

The process of well log up scaling is required to post values in each cell of the 3D grid where each of the wells is situated; to achieve these average well properties are used to populate each of the cells. To choose the setting parameters for the upscaling in terms of the averaging method, log treatment as lines or points and method of upscaling are applied. In terms of the setting properties the logs are treated as lines or points; the setting using points means that the logs are treated as points and only the point values would be used in making this averages. Line averages mean that the logs are treated as lines such that line values outside upscaled cells can also be used interpolated averages in between log points. The upscaling methods are dived into simple, through cell and Neighbour cells.

The upscale well logs with different averaging methods require the process of data analysis as a basis to control the property of the models.

The simple method is used to give property values to cells as much as the wells penetrate the cells, no matter how tiny the cells are in dimension. The Through cell method gives a value to a cell only when opposite cell walls are penetrated by the cells; this is to ensure that only a tiny section of the well path does not provide only the reasonable confidence to post values to the cell as in the case of the simple method. The last method is the Neighbor cells which is similar to the simple method where all cells are posted with values as far as the well penetrate them, the variant is that cells adjacent one another in the same layer would be averaged. (Ahanor, 2012). The simple method has used in carrying out the upscaling process as applied in the Amara Oil Field field shows in figures (8) and (9).
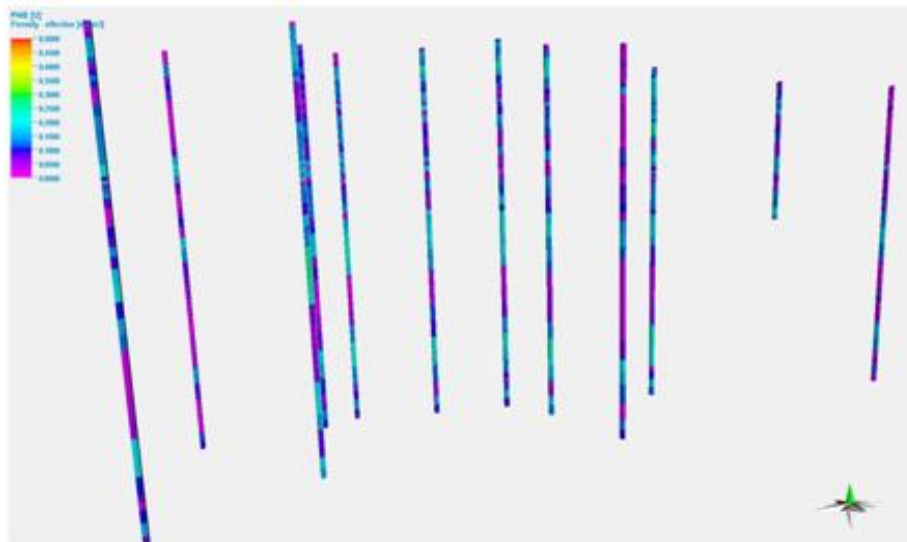
FIGURE 8: SCALE UP OF PHIE FOR MISHRIF FORMATION
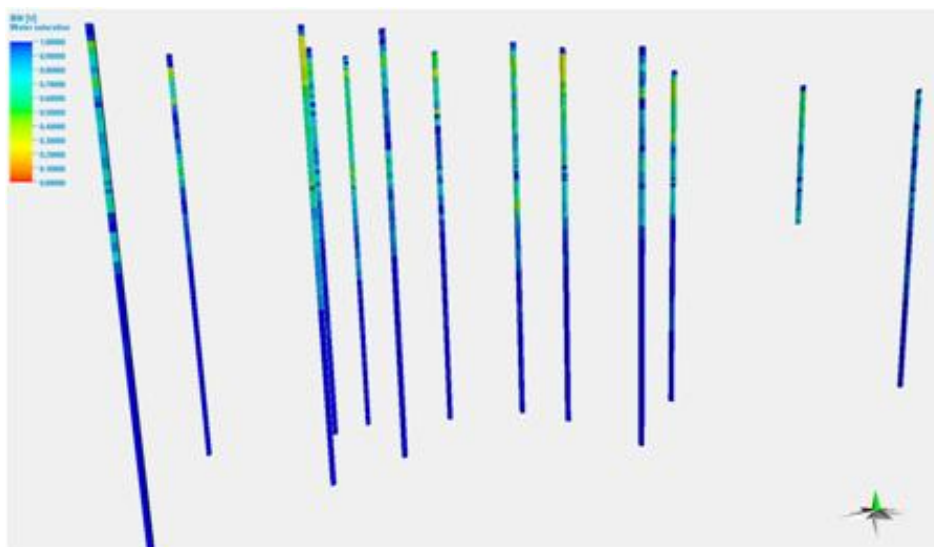
FIGURE 9: SCALE UP OF WATER SATURATION FOR MISHRIF FORMATION

3.4 Petrophysical Model

The aim of a geological reservoir model is to provide a complete set of continuous reservoir parameters (i.e. porosity and water saturation) for each cell of the 3D grid. Many different techniques can be used to generate these parameters [8].

3.4.1 Porosity Model

Porosity model was built depending on the results of porosity logs (density and neutron) which have been corrected and interpreted in the IP software .

As porosity modeling is concerned, no seismic attributes that may be used as a predictor have been identified. Therefore, the 3D distribution of the porosity is based on the vertical well profiles.The well data are transformed (normal score) so they are approximately Gaussian distributed. The Gaussian model is characterized by various statistical parameters, which reflect the spatial variability of the porosity[8].

The variogram parameters indicate to what degree the measured porosity values in a position can impact the unobserved porosity values in a position nearby. First, a sequential screening algorithm simulates one realization of an unconditional Gaussian field. The grid cells that correspond to well trajectories are each assigned to a value corresponding to the measured upscaled well logs. The cells with the values for the well trajectories are ''merged'' with the unconditional Gaussian field. This is done by standard kriging techniques and results in a conditional Gaussian field that honors the well logs, standard deviations, and variograms specified [8].

3.4.2 Water Saturation Model

Water Saturation is calculated based on distributions related to porosity ranges. The full range of porosity has been divided into five arbitrary classes in which associated Water Saturation values from logs were statistically analyzed. It turned out that within each porosity class, related Water Saturation data fit a log normal distribution. These distributions condition perfectly the modeling of the Water Saturation for each porosity class. This fast and simple method allows the generation of a consistent water saturation distribution that respects a realistic degree of correlation between porosity and saturation. With this simple technique, the distribution of the saturation is performed in one step for all the reservoir cells that are located above the Oil-Water Contact (OWC).

The definition of this hydrocarbon contact is complicated due to the small density contrast between the oil and the water, the occurrence of a flushed zone, the heterogeneous character of the reservoir, and poor well borehole conditions that negatively impact on the acquisition of reliable geological data. The definition of the OWC is therefore possible by a complete and simultaneous analysis of different types of data: conventional logs, resonance magnetic logs, wireline tester pretests, drill stem tests, and cores [8].

The same geostatistical method of porosity model was used in the water saturation model. After the scale up of water saturation that exported from IP software the water saturation model was built for each reservoir unit of the Mishrif Formation in the Amara Field.

IV.   RESULTS AND DISCUSSIONS

Three Dimension modeling has built depending to 12 wells for Mishrif formation in Amara oil field. All wells have PHIE and Water Saturation logs, which exported from interactive petrophysics (IP v3.6) software. Thereafter, scale up well logs has carried out for this wells.

To building the model there are different methods of distribution of petrophysical properties. These methods involve (l. Gaussian random function simulation 2. sequential Gaussian simulation 3. kriging 4. kriging interpolation 5. kriging (Gslib) 6. functional 7. moving average 8. closest). Eight methods have executed in order topropagate property values through construct Porosity and Water Saturation Models.

Then insert new well to the models and create PHIE and Water Saturation logs from the Porosity and Water Saturation models where the new well penetrated the models in points that have values of PHIE and Water Saturation, therefore, the new well has PHIE and water saturation logs for each method. With variety methods of distribution of petrophysical properties, consequently, differents in results.

Which method reflect approximately the realistic distribution of the properties.Appropriate algorithm method to build the 3D modeling for Mishrif formation has chosen through comparison between the porosity and water saturation logs of new well

exported from the models and the porosity and water saturation logs from interactive petrophysics software (after made scale up well logs).

The results of the eight methods have shown in the following figures that have named in PHIE(U) and SW(U) refers to the results from modeling and PHIE13(U) and SW13(U) refers to the results from log interpretation.
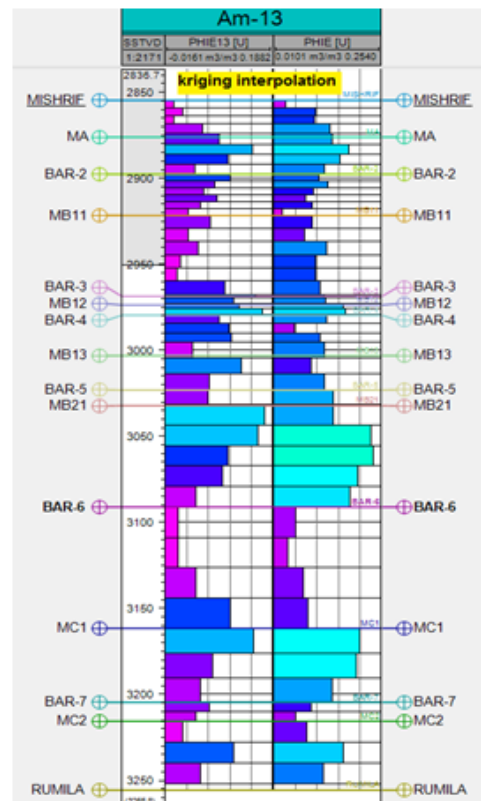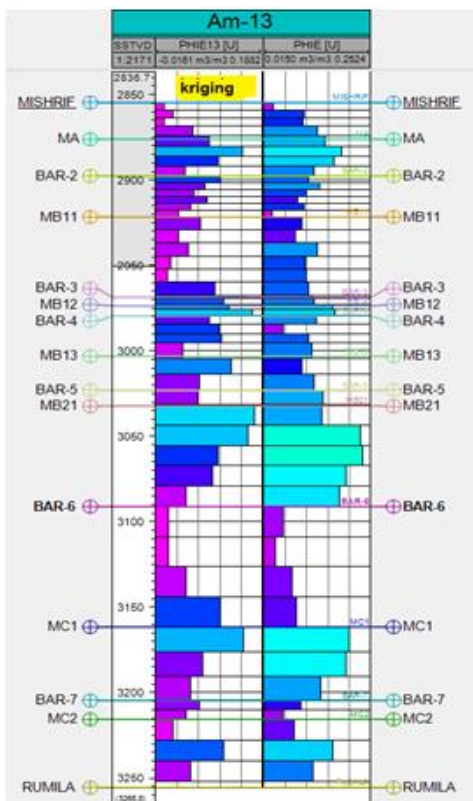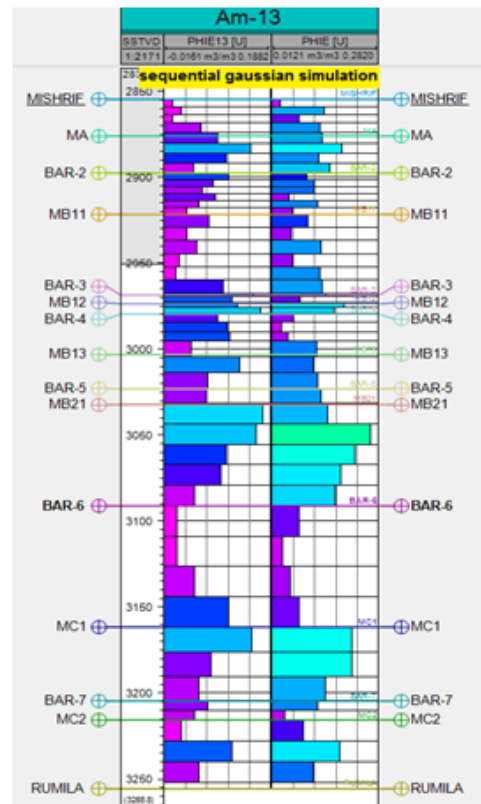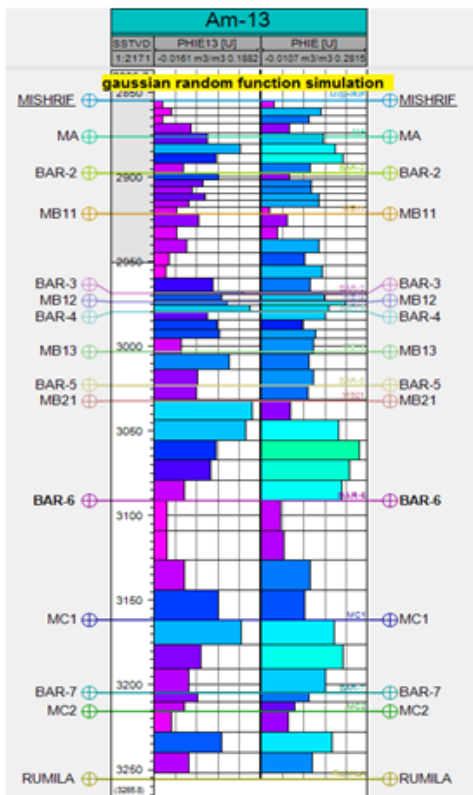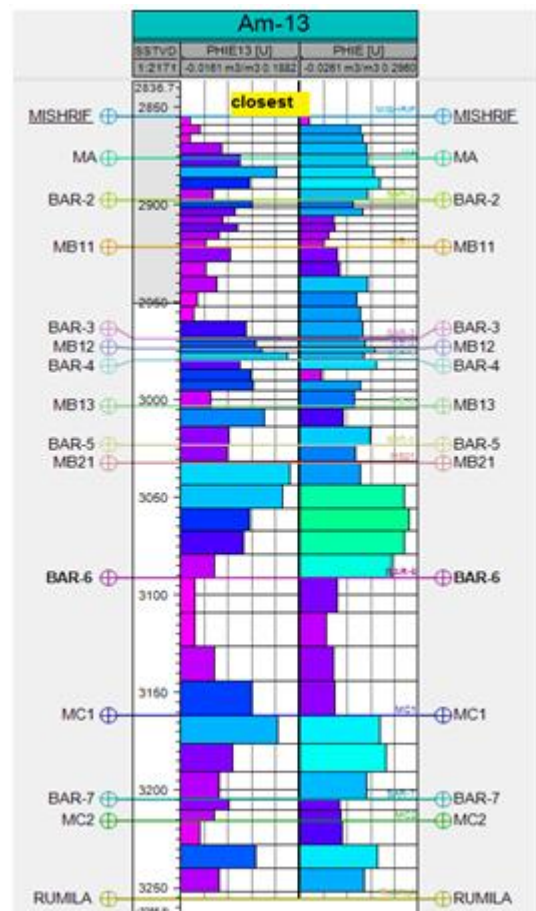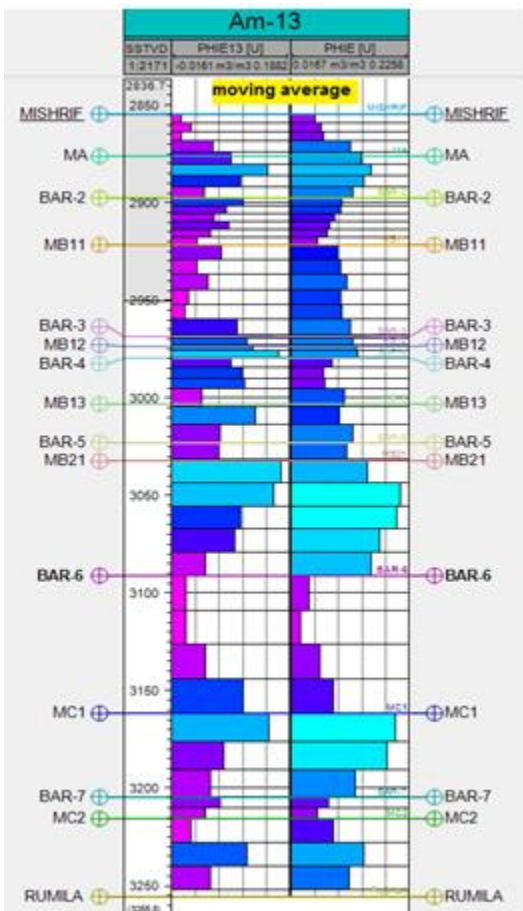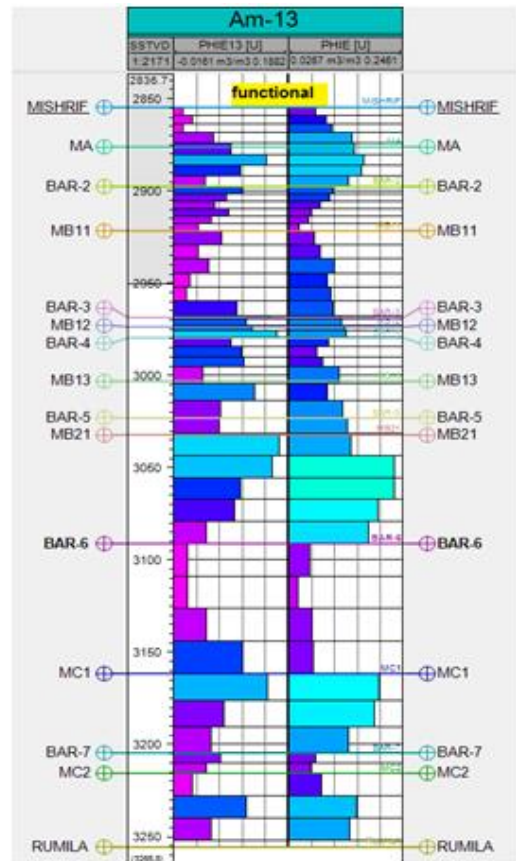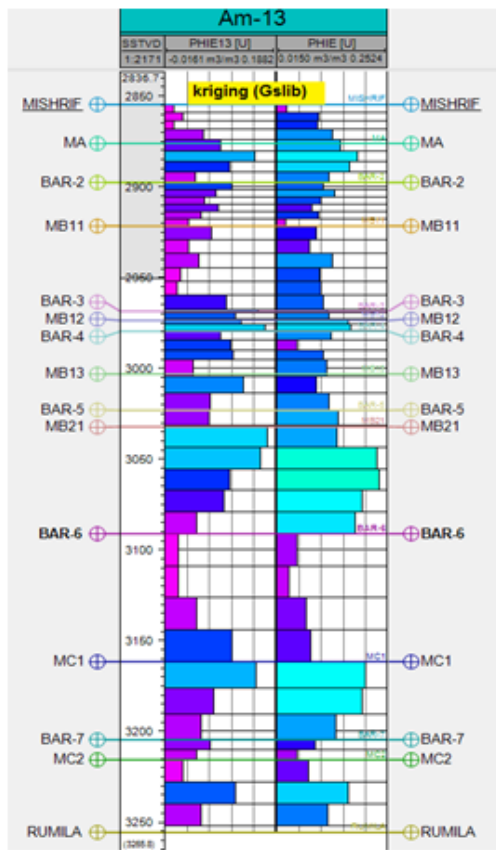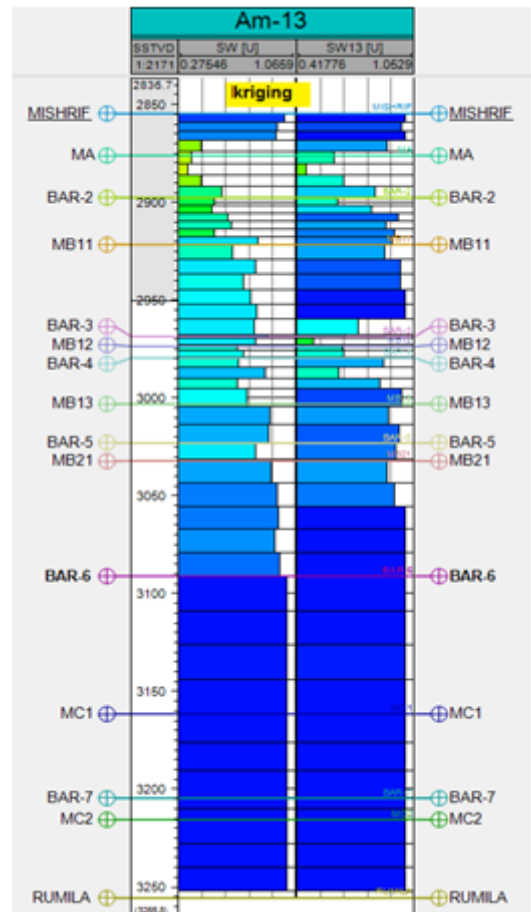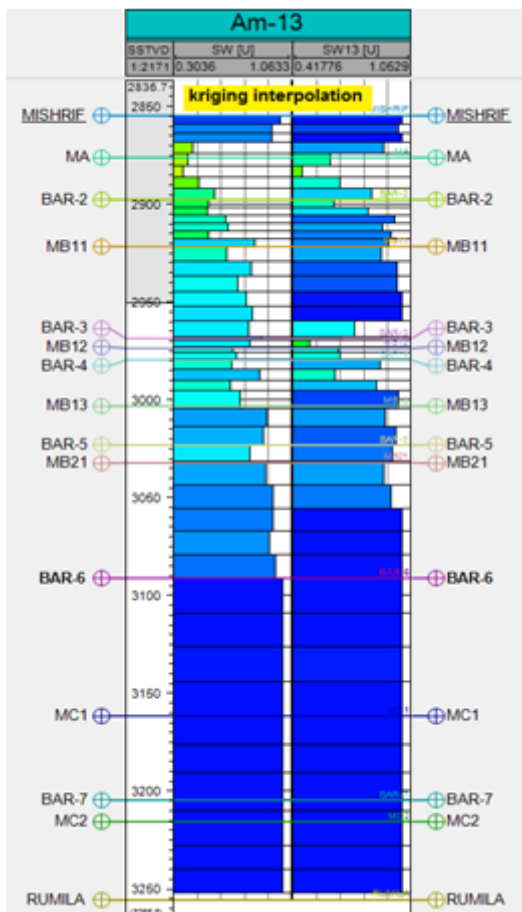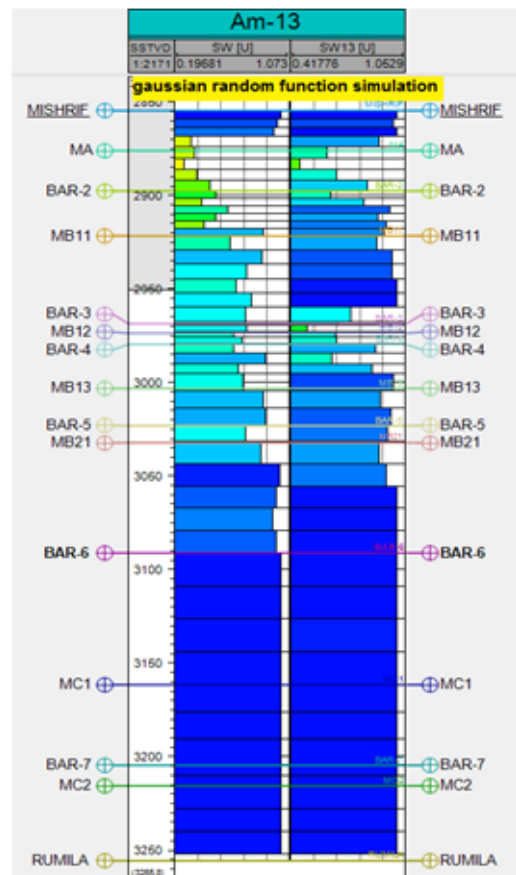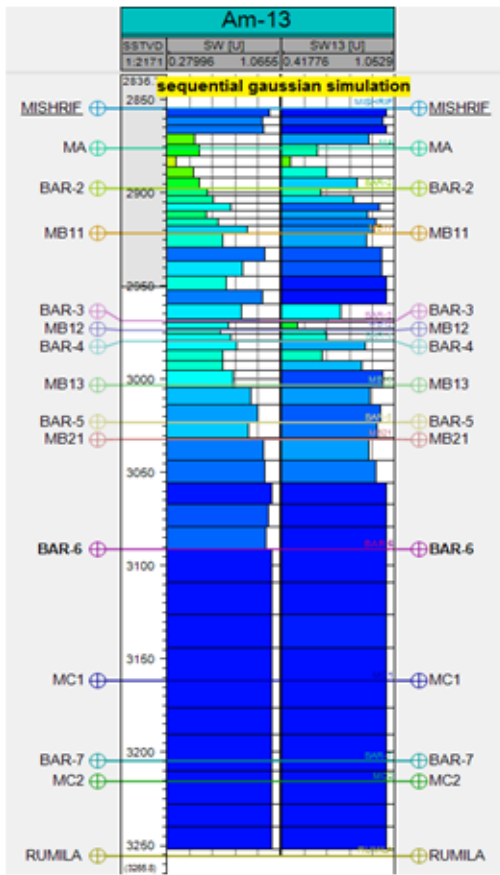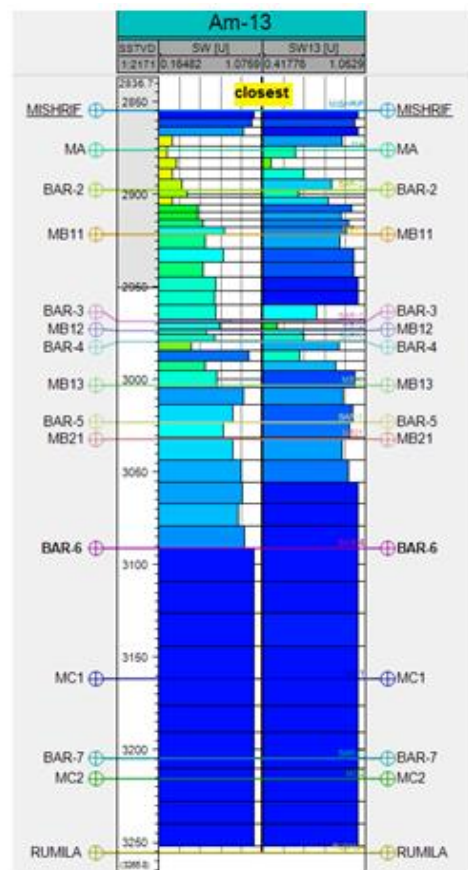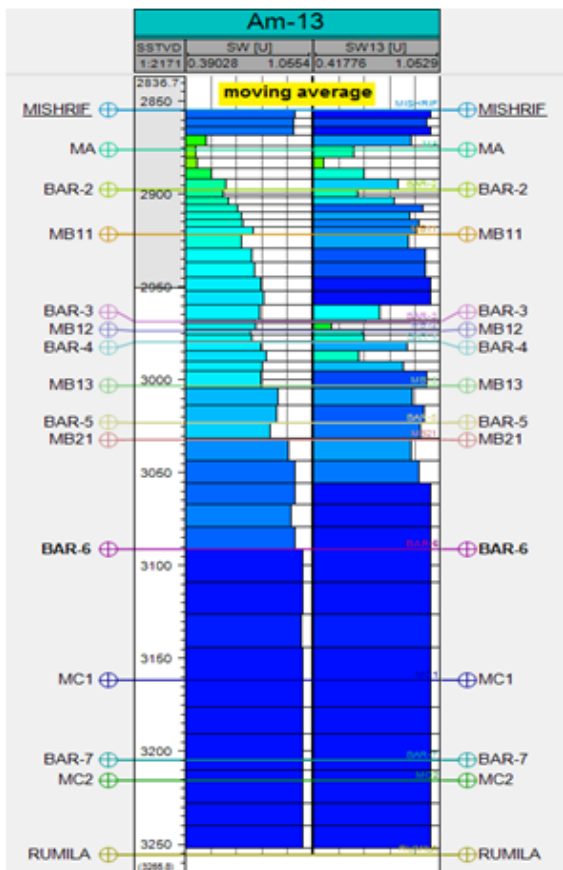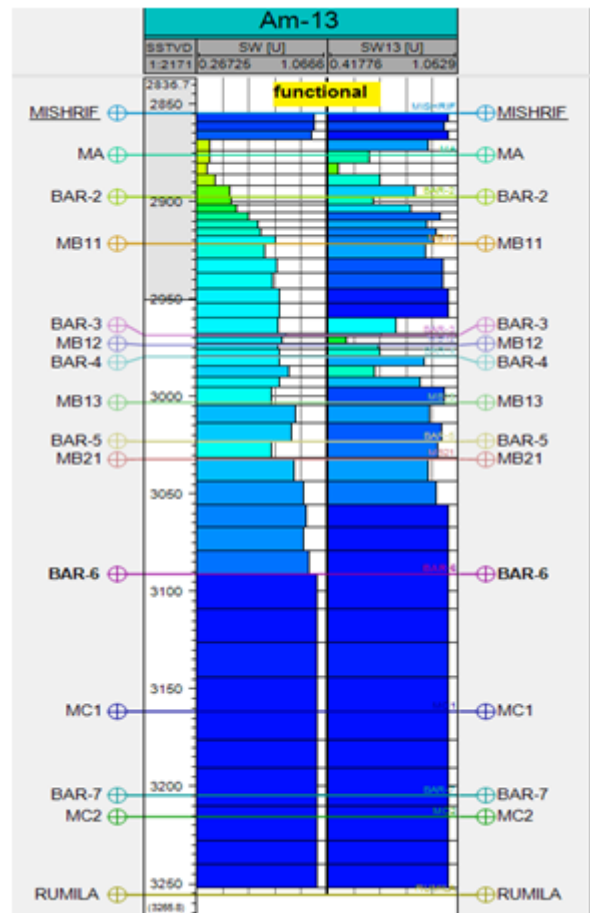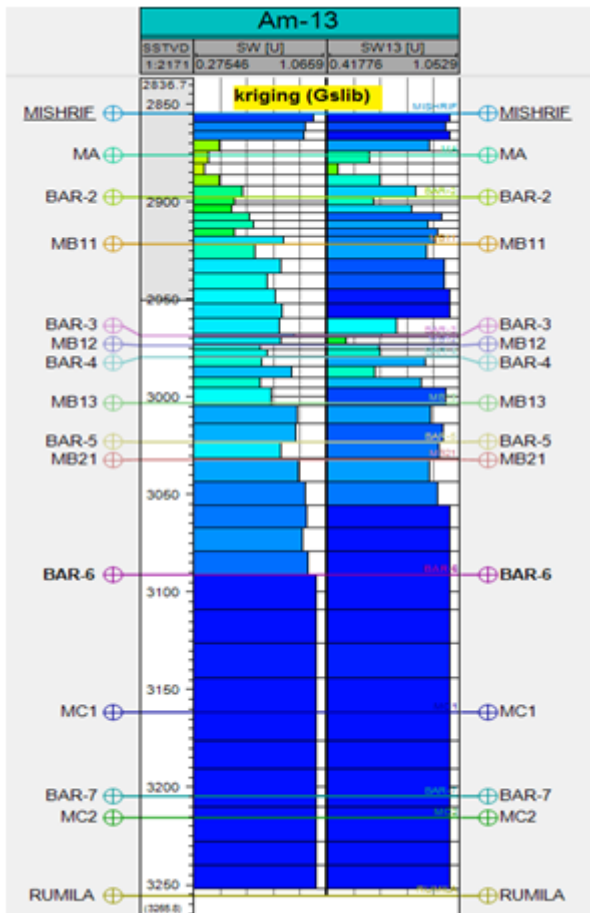
V.   CONCLUSION AND RECOMMENDATION

Depending on the results, there are not data from the modeling corresponding exactly to the true data from the log interpretation for the same well, but it approximate from the true data in different percentage .The quality of the results strongly reliance on the type of the method. Sequential Gaussian Simulation suitable algorithm method to build the 3D modeling for Mishrif formation.

REFERENCES

[1]   B. Doligez, H. Beucher, F. Geffroy, eta R. Eschard, «Integrated Reservoir Characterization: Improvement in Heterogeneity stochastic Modeling by integration of additional external constraints», *AAPG*, or. 333–342, 1999.

[2]   Schlumberger, *Petrel Seismic to Simulation Software*, libk. 1. Schlumberger, 2010.

[3]   O.-C. Adaeze eta A. U.P, «FACIES MODELLING AND PETROPHSICAL PROPERTIES OF X-FIELD, ONSHORE, NIGER DELTA, NIGERIA», *Int. J. Sci. Invent. Today*, libk. 5, zenb. 2, or. 136–151, 2016.

[4]   G. Caumon, P. Collon-Drouaillet, C. Le Carlier De Veslud, S. Viseur, eta J. Sausse, «Surface-based 3D modeling of geological structures», *Math. Geosci.*, libk. 41, zenb. 8, or. 927–945, 2009.

[5]   J. Richard H. Groshong, *3-D Structural Geology A*. 2006.

[6]   Schlumberger, *Petrel Introduction Course*. 2007.

[7]   Schlumberger, *Reservoir Engineering Course Petrel 2010*. Houston, 2010.

[8]   B. Johnny *et al.*, «Definition of a 3D integrated Geological Model in a Complex and Extensive Heavy Oil Field, Oficina Formation, Faja de Orinoco, Venezuela», *AAPG Annu. Meet.*, zenb. Figure 2, 2003.

Investigation of the Remote Detector Experiments on the Gorbunov Effect

Kapranov B.I.[1], Avdochenko B.I.[2], Sutorikhin V.A.[3]

[1]Ph. D., Professor, TPU, Tomsk
[2]Ph. D., Professor, TUSUR, Tomsk
[3]Chief specialist LLC "Remote Indicators of Active Defects", Tomsk

Abstract— *Investigations of the effect Gorbunova possible to determine the localization of the defect contactless microwave sensor from a distance of 70-180 mm. the possibility of indexing latent defect by comparing results before and after heating.*

Keywords— *Microwave imaging method non-destructive testing of metals, the «Gorbunov» effect reactivation of samples, the indication of defects in the metal.*

I.   INTRODUCTION

The problem of determination of defects in metal structures in a contactless manner through the use of a microwave sensor is relevant since as was developed a miniature, semiconductor devices, like the generator of Gunn diodes. Existing methods of inspection are divided into active (ultrasonic sensing) and passive (acoustic emission). Both methods have their advantages and disadvantages. Our group of researchers has managed to combine both methods. Develop and test remote indicator of active defects (RIAD). If the definition of apparent defects at the stage of structural failure there are two ordering methods, we study the initial stage of destruction, disorders in crystal lattices, studies of mechanical tensions inside of metals with the determination of the initial stage of destruction is just beginning. The use of the method of determination of internal defects with the help of MW until recently been controversial because of the known limitations, it was believed that this method may not reveal defects within the metal, inside of the welded joints [1]. Practice has proved that this restriction is removed when using the phenomenon discovered by our group, under the guidance of Professor V. I. Gorbunov[2]. The essence of the Gorbunov effect, discovered in 1995, lies in the fact that in the interaction of weak ultrasound (less than 20 W/cm2), with dangerous defects in the metal formed during the acts of acoustic emission, is the appearance of a variable electrical surface conductivity. The interaction of the ultrasound with the defect ranging from ten minutes to hundreds of hours. The use of microwave oscillations in interaction with variable surface conductivity becomes one of the new, combining active and passive methods of nondestructive testing.

II.   EXPERIMENT AND STUDY

The definition of the initial stage of destruction of metal structures is an important and challenging task. The destruction begins with disturbances in the crystal lattices inside metal with a substantial mechanical strength of the structures. To detect changes of the crystal lattices apply the complex methods used in laboratory research. The use of the method of determination of internal defects with the aid of microwave radiation, proposed by the group of Professor Gorbunov [2], is a promising direction in the diagnosis of early destruction and becomes one of the priority methods of non-destructive imaging.

The possibility of identifying defects in the lifting of loads with structures decreases with time, however, the initial stage of destruction is retained, and with increasing loads of possible catastrophic situation. To increase the activity defects in old structures used in reactivation of the structures by heating and rapid cooling [3], however, the heating and rapid cooling is often impossible or unacceptable, for example, in pipelines with asphalt or filled with oil. Also study other possibilities of reactivation, without heating and cooling. It has been suggested that the activity of defects can be restored by gamma radiation. The authors reviewed the possibilities of applying the microwave method in terms of the impact on the area of the defect in the metal x-ray radiation.

Laboratory models of remote indicator of active defects took place with the use of several types of control devices. First used the spectrum analyzer SK4-59 with a sensitivity of -110 dB/MHz, designed to control output signals of continuous operation. When using pulsed mode of operation ultrasonic generators for mechanical excitation of samples (frequencies of 40-400 KHz, amplitude 60 V - 200 V, a duty ratio of 50-200, a repetition rate of 1-2 KHz) was unable to obtain a clear image due to the lack of phase synchronization.

Then as a registered device used a digital oscilloscope firms «AKTAKOM» (ASK-3106) with analysis bandwidth up to 1000 MHz, external clock signals from the ultrasonic generator. The image of the reflected signal had a clear shape, it was possible to observe the useful signal a reactivation of the samples by heating and rapid cooling. The amplitude of the useful signal is much greater than the amplitude of noise components (the beam width in the absence of a useful signal). The result is displayed in a graphic file.
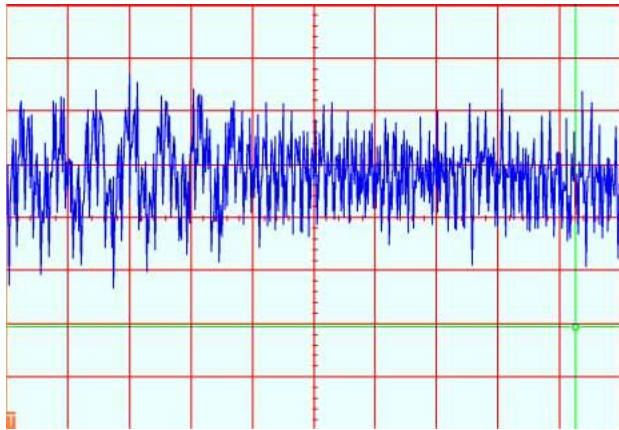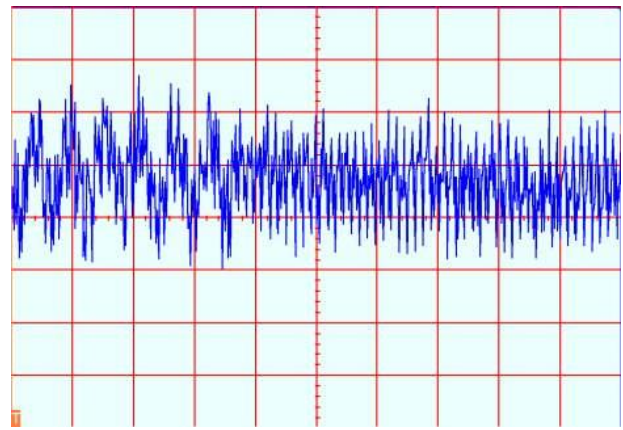
a – THE STEEL SAMPLE   **b – ALUMINUM SAMPLE**

FIG.1. WAVEFORMS DURING THE OPERATION OF GAMMA RADIATION.
The scale along X =20µs.Scale Y=20 mV.

For comparison of the ability to restore the activity of the samples using gamma-radiation was used, x-ray tube with a tungsten anode, the capacity of which increased smoothly with increasing operating voltage. The image of the defects was recorded on recycled tape.

Pictures of sample of St4 steel and aluminum, given below, Fig. 2 and 3.
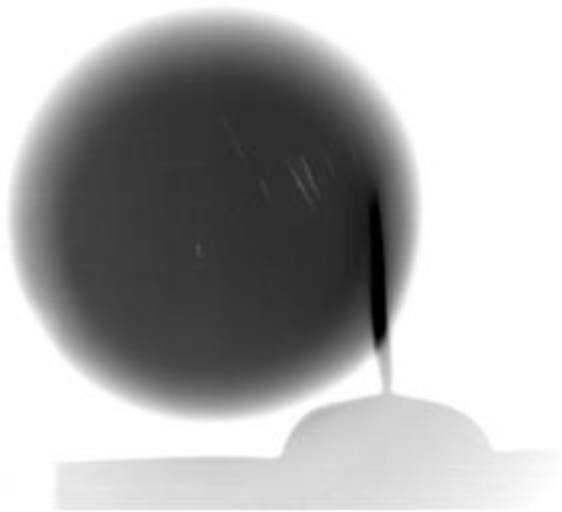
FIG.2 RADIOGRAPH OF A STEEL SAMPLE St4
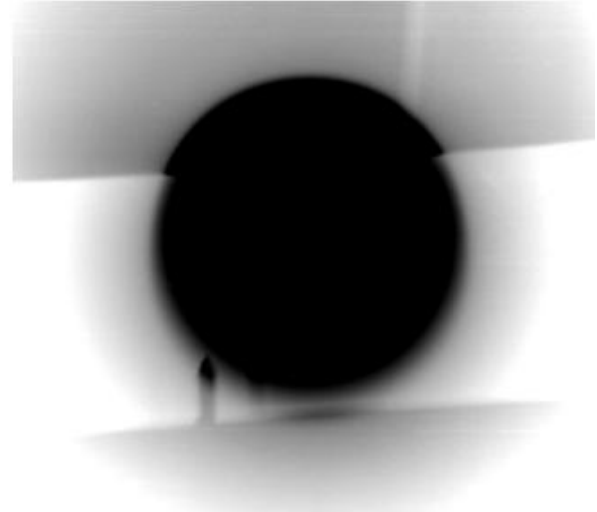
FIG.3 RADIOGRAPH OF THE ALUMINUM SAMPLE .AT BOTTOM LEFT, SHOWS THE BEGINNING OF CRACKS, THE WIDTH OF BAR 40 mm, LENGTH 250 mm, THICKNESS (DEPTH OF DRAWING) OF 20 mm., DARK SPOT IN THE CENTER OF THE MAIN BEAM

At the bottom on the right there is a grey outline of the neck of the specimen with a crack, the crack length 40-43 mm, width 3.1 mm, the end of the crack close to the middle of the sample. A dark spot in the center of the main beam.

Configuration of the microwave equipment was conducted prior to the inclusion of the generator of gamma rays. Then remotely activated the x-ray machine, used smooth increase in power with voltage regulation between 40 to 120 KV, exposure time 15 sec. A specimen with a crack were excited by ultrasound with a frequency of 48 KHz and an amplitude of

60V. The reflected microwave signal frequency of 10 GHz were recorded with the phase detector remote indicator of active defects [2]. On the oscilloscope screen observed the voltage at the output of the microwave sensor. The level of the noise signal at the phase detector output was 20 mV. Useful signal from a steel sample exceeds the noise by 5-6 dB, from aluminum sample, the ratio signal/noise was 3-4 dB. The measurement error of 1-1. 5 dB. The signal was measured before, during and after irradiation of the sample.

III.   RESULT AND CONCLUSION

The useful signal recorded by the oscilloscope, the form of which is shown in Fig. 1 does not change its value in all ranges of capacity with on and off of the gamma radiation source. As a result of experiments failed to record the presence or absence of reaction of the samples to gamma radiation at different power and directions of radiation on the crack and on the part of the sample exposed to the microwave field frequency of 10 GHz.

REFERENCES

[1] Control the limit of elastic deformation of the microwave method. V. I. Gorbunov, V. A. Sutorikhin,/ Nondestructive Testing. No. 7, 1999 P. 75-80.

[2] Microwave Nondestructive Testing Method V. I. Gorbunov & V. A. Sutorikhin Applied Physics Research, Vol. 4, No. 1; February **2012**. P. 206-210

[3] DopIer Radar in Crack Testing Vladimir Sutorichin , Sergei Brichkov British Journal of Applied Science & Technology, 4(23), **2014**, p. 3315-3321

Dimensional analysis application when calculating heat losses

Romana Dobáková[1], Natália Jasminská[2], Tomáš Brestovič[3], Mária Čarnogurská[4], Marián Lázár[5]

Department of Power Engineering, Faculty of Mechanical Engineering, Technical University of Košice,
042 00 Košice, Slovak Republic

Abstract—*The article describes the procedure for the determination of heat loss through a mathematical model, which was processed through a dimensional analysis. The output of this model is a simple relationship where, based on the locating constant and the regression coefficient, it is possible to determine the loss of the piping system. Subsequently, this method was applied to calculate the heat loss of a pre-insulating pipe buried underground.*

Keywords—*heat loss, heat network, model, dimensional analysis.*

I. INTRODUCTION

Currently, the determination of heat losses is most often achieved through the so-called balancing method, based on the experimental detection of temperature drops into and out of the network. In order to determine the total heat loss of a given section based on the balance method, it is necessary to know the temperature of the heat transfer medium at the beginning and end of the examined section with sufficient precision (at least to two decimal places for short sections) and the instantaneous mass flow rate of the water.

The determination of heat loss through this method is only suitable for very long sections of heat distribution, where the error in measuring the temperature difference does not cause a significant error in the following determination of heat losses. To measure the temperature difference of the heat transfer medium of the short sections, a top measuring technique is required, which cannot be permanently installed in each network, especially when the combined distribution system is several dozen kilometers long.

II. MATHEMATICAL MODEL OF HEAT LOSS

A dimensional analysis was used to design a new model to obtain information on the interconnection of relevant variables affecting heat loss through the creation of dimensionless arrays.

The advantage of a dimensional analysis is that it is possible to obtain a small number (two or three) from a large number of physical variables, on which the phenomenon depends, of a small number of non-dimensional arrays. The second advantage is that the acquired functional dependence has a universal validity for all other heat distribution meeting geometric and heat similarity with the examined distribution.

The basis of the mathematical model is a dimensional analysis, based on the principle of the dimensional homogeneity of the equations.

A dimensional analysis requires a preliminary analysis of the nature of the phenomenon. It serves to find the variables from a set of parameter variables affecting the examined phenomenon, and to compile a set of the minimum number of dimensionless arrays comprised from them.

When applying a dimensional analysis, the most important phase is the correct selection of transmuted variables that can affect the phenomenon.

During the research, we investigated the interrelationship of the involved transmuted variables, each of which can be dependent on others. The majority of all variables (except one) can be independently controlled. This one transmuted variable thus becomes a dependent variable. When selecting dependent variables, we often introduce a variable in the assembled relationship, which is not transmuted in the examined conditions, but comprise a dimensionless number in combination with the transmuted variables[2].

Including more than one transmuted variable in an examined relationship is a mistake as serious as omitting any of the involved variables affecting the examined phenomenon. On the contrary, it is not a problem to introduce variables into a relationship that does not have any effect on the phenomenon because it will arise from another solution. In order to correctly

select the involved transmuted variables, it is necessary to create a certain idea of the examined phenomenon beforehand and to consider which independent variables must be taken into account in the description of the action. It results that from the examined phenomenon we must learn from experience or analogy why it can be influenced by a certain transmuted physical variable.

Two methods [2] are used to describe the phenomenon based on a dimensional analysis:

- The Rayleigh Method,

- The Buckingham Method, the so-called   - theorem, which is used more frequently.

III.   CREATION OF THE HEAT LOSS MODEL

To As mentioned above, the mathematical model for calculating the total heat loss (heat output) is based on a dimensional analysis and its mathematical interpretation is influenced by the correct choice of relevant variables by which the phenomenon is assumed to be significantly influenced.

Among the relevant variables affecting the heat losses of heat networks, based on the experience of the heat network operator and the professional literature, the quantities characterizing heat losses are easily measurable in practice. For the following quantities

- temperature of the heat transfer medium T_i (K)
- the ambient temperature T_e (K)
- the heat conductivity of the insulation λ_{iz} $(W \cdot m^{-1} \cdot K^{-1})$
- the heat conductivity of the soil λ_{zem} $(W \cdot m^{-1} \cdot K^{-1})$
- the depth of the pipe buried in the ground H (m)
- the mass flow water rate in the pipe Q_m $(m \cdot s^{-1})$
- specific heat loss (linear heat flow density) q_l $(W \cdot m^{-1})$
- theinsulation's outside diameter d_3 (m)

The length dimension is repeated among the selected relevant variables. Only one physical variable of the same size group can be included in the solution. On this basis, it is possible to directly construct a dimensionless array called a simplex, whose shape is as follows:

$$\pi_1 = \frac{d_3}{H}, \qquad \text{or} \qquad \pi_1 = \frac{H}{d_3} \qquad (1)$$

Based on the above, the complete physical equation expressing the dependence of relevant variables is the function of just the selected relevant variables and has the following form:

$$\varphi(q_l, T_i, H, \lambda_{zem}, Q_m) = 0. \qquad (2)$$

Based on the dimensional diversity of the relevant variables, these will be displayed in groups, i.e.

$$\pi_i = q_l^{x_1} \cdot T_i^{x_2} \cdot H^{x_3} \cdot \lambda_{zem}^{x_4} \cdot Q_m^{x_5}. \qquad (3)$$

The dimension matrix A has $n = 5$ columns and $m = 4$ rows for the base units and is in the form of:

$$
\begin{array}{c}
\quad q_l \ \ T_i \quad H \quad \lambda_{zem} \ Q_m \\
\begin{array}{c} kg \\ m \\ s \\ K \end{array}
\left\|
\begin{array}{ccccc}
1 & 0 & 0 & 1 & 1 \\
1 & 0 & 1 & 1 & 0 \\
-3 & 0 & 0 & -3 & -1 \\
0 & 1 & 0 & -1 & 0
\end{array}
\right\| .
\end{array}
\qquad (4)
$$

With the value of matrix $h = 4$ and the number of relevant variables $n = 5$ it is possible to create the total of $i = n - h$, i.e. 1 dimensionless array π. The unknown variables cannot be uniquely determined because the number of unknown $x_i > m$. Therefore, the rectangular matrix is divided into two parts in terms of the dimensional analysis. The first part of the matrix will be square with the number of h columns and h rows (matrix P, see below), with the columns of the matrix selected so that the determinant is nonzero ($\Delta_P \neq 0$). It corresponds to the distribution of the x_i vector. The form of the square matrix **P** and the vector of the unknown variables x_i, indicated as **R**, is written in the simplified form:

$$\mathbf{P} \cdot \mathbf{R} = (-1) \cdot \mathbf{Q} \cdot \mathbf{S}, \tag{5}$$

where   Q   - vector array with the number $h = 1$ and the number of rows $n = 4$,

        S   - vector of unknown variable with the number of $h = 1$ columns and the number of rows $n = 1$.

Equation (5) expressed through (3) and (4) can be represented in a broken-down form through the relationship

$$\begin{Vmatrix} 0 & 0 & 1 & 1 \\ 0 & 1 & 1 & 0 \\ 0 & 0 & -3 & -1 \\ 1 & 0 & -1 & 0 \end{Vmatrix} \cdot \begin{Vmatrix} x_2 \\ x_3 \\ x_4 \\ x_5 \end{Vmatrix} = (-1) \cdot \begin{Vmatrix} 1 \\ 1 \\ -3 \\ 0 \end{Vmatrix} \cdot \begin{Vmatrix} x_1 \end{Vmatrix} \tag{6}$$

The determinant of the matrix P is determined e.g. based on the Laplace development. We performed the choice of the excess unknown x_1, while both choices must be linearly independent. The matrix of choices has the form:

$$\begin{matrix} & x_1 \\ & \begin{Vmatrix} 1 \\ 0 \end{Vmatrix} \begin{matrix} 1^{st}\ choice \\ 2^{nd}\ choice \end{matrix} \end{matrix} \tag{7}$$

By multiplying the matrices according to (5), there applies

$$\left\| \mathbf{P} \right\|_{4 \times 4} \cdot \left\| \mathbf{R} \right\|_{4 \times 1} = \left\| \mathbf{C} \right\|_{4 \times 1}, \tag{8}$$

$$\left\| \mathbf{Q} \right\|_{4 \times 2} \cdot \left\| \mathbf{S} \right\|_{2 \times 1} = \left\| \mathbf{F} \right\|_{4 \times 1}. \tag{9}$$

Later it applies that

$$\left\| C \right\|_{4 \times 1} = (-1) \cdot \left\| F \right\|_{4 \times 1}. \tag{10}$$

Since the type of matrices in expression (10) is the same, for the matrix elements from the equation (6) in the application of this relationship must apply:

$$x_4 + x_5 = -x_1$$

$$x_3 + x_4 = -x_1$$

$$-3x_4 - x_5 = 3x_1$$

$$x_2 - x_4 = 0$$

By solving this set of linear equations we attain an independent vector as output

$$\begin{matrix} x_1 x_2 & x_3 & x_4 & x_5 \\ \pi_2 \begin{vmatrix} 1 & -1 & 0 & -1 & 0 \end{vmatrix} \end{matrix} \tag{11}$$

This solution corresponds to the dimensionless array in the form:

$$\pi_2 = \frac{q_l}{T_i \cdot \lambda_{zem}} \tag{12}$$

According to the rules of the dimensional analysis from relationship (11), it follows that the physical variable, which answers the unknown x_3 and x_5, does not affect heat loss, since its value is zero, meaning that it has arisen from the solution.

The dimensionless form of the heat loss function can be written in the form:

$$\Psi\ (\pi_1,\ \pi_2) = 0 \tag{13}$$

The dimensionless array π_2 contains the variable q_l , therefore this array can be expressed as a function of independent array π_1 in the form:

$$\pi_2 = \varphi\ (\pi_1) \tag{14}$$

The actual progress of the function of these two dimensionless arrays can be described e.g. power function in the form:

$$\pi_2 = A\ .\ \pi_1^{\ B}\ , \tag{15}$$

which in terms of further solution is suitably transformed into logarithmic coordinates to linear dependence

$$\log \pi_2 = \log A + B \cdot \log\ \pi_1 \tag{16}$$

By adding physical variables to dimensionless arrays in relationship (15), we reach the expression to determine the value of the total heat loss in the form:

$$\frac{q_l}{T_i\ .\ \lambda_{zem}}\ =\ A\ \cdot \left(\frac{d_3}{H}\right)^B \tag{17}$$

or $\qquad q_l = A.T_i.\ \lambda_{zem}.\ d_3^{\ B}.\ H^{-B}$ $\quad$ (W·m^{-1}) $\tag{18}$

The relationship (18) is universally applicable to all types of heat systems, both aboveground and underground, both inlet and return. To determine the specific value of a measured heat loss q_l according to relationship (18), for any type of the above-mentioned heat networks, it is necessary to respect the change in locating constant A and the regression coefficient B. It is possible for you to gain the type of network only on the basis of an experiment.

The characteristics of the heat network under detailed investigation are as follows: the network is underground, the nominal diameter DN125, the outside pipe diameter $d_2 = 133$ mm, the wall thickness of the pipe $s = 3.6$ mm, the insulation thickness $s_{iz} = 33.5$ mm, the length of the examined network $L = 78$ m, the mean value of the heat conductivity coefficient of the insulation (as a function of the water temperature in the inlet pipe) $\lambda_{iz}= 0.041$ W·m^{-1}·K^{-1}, the mean value of the heat conductivity coefficient of the insulation) $\lambda_{iz} = 0.040$ W·m^{-1}·K^{-1}, the mean value of the heat conductivity coefficient of soil $\lambda_z = 1.35$ W·m^{-1}·K^{-1}, the mean value of the heat transfer coefficient from the surface of the earth to the external environment $\alpha_0 = 3$ W·m^{-2}·K^{-1}, the depth of the buried pipe $H = 1.06$ m.

The temperature of the water entering the inlet pipe ranged from 55 to 70 °C. Water temperature rising from the return pipe is from 50 to 60 °C. The average value of the ambient temperature t_e in the considered month was considered -1.5 °C (271.65 K).

The calculation of the locating constant A and the regression coefficient B in relationship (15) is performed on the basis of the smallest squares method. The second possibility to gain them is demonstrating the dependence of dimensionless π_2 and π_1 in the logarithmic coordinates directly. After selecting a regression line type and displaying the regression equation, it is possible to directly obtain information on the value of the locating constant and regression coefficient. The dependence of the dimensionless arrays π_2 and π_1 was obtained from a specific heat network conducted underground in channel less stored for the month January 2016 (Fig. 1 and 2)

It is the most suitable to determine A and B from the values obtained from the measurements of all the specified physical variables during the one year, especially for the inlet and for the return pipes. This will ensure the impact of a wide range of ambient temperature and the temperature of the heat transfer medium in the A and B values in functional dependence (15)
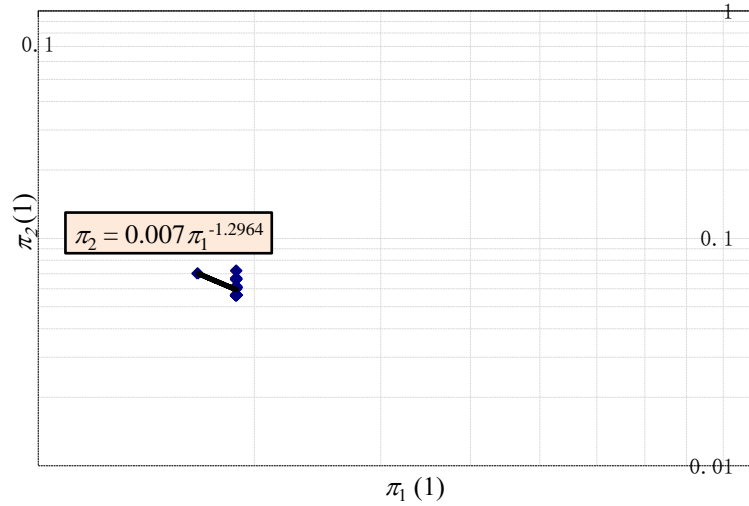
FIGURE 1: The calculation of the locating constant and the regression coefficient for the inlet pipe
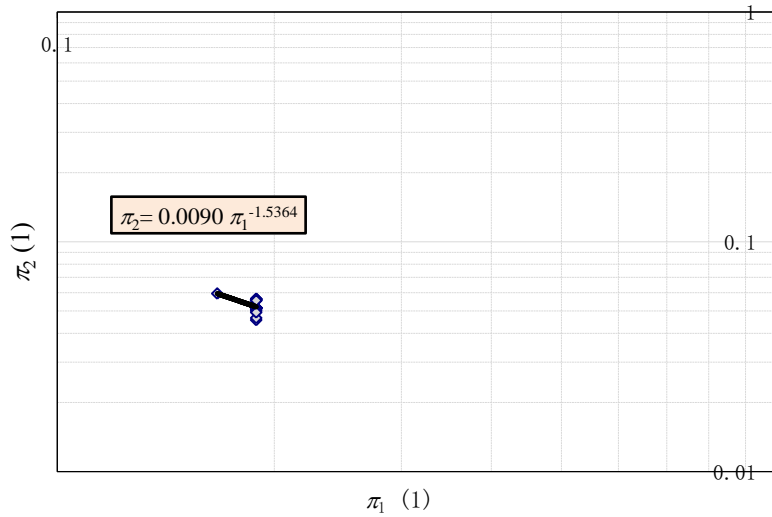
FIGURE 2: The calculation of the locating constant and the regression coefficient for the return pipe

Using Visual Basic, the locating constant, the regression coefficient and the relative heat loss according to (18) are calculated for the air temperature t_e from –20 to +30 ℃ and the temperature of the heat transfer medium t_i from 45 to 70 ℃. Their progress is in Fig. 3 and 4.
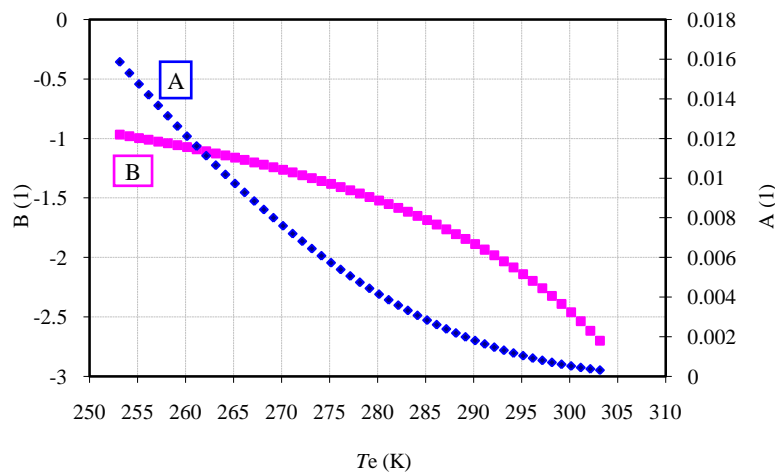
FIGURE 3: The progress of locating constant A and regression coefficient Bfor an ambient temperature range from –20 to + 30 ºC for the inlet pipe.
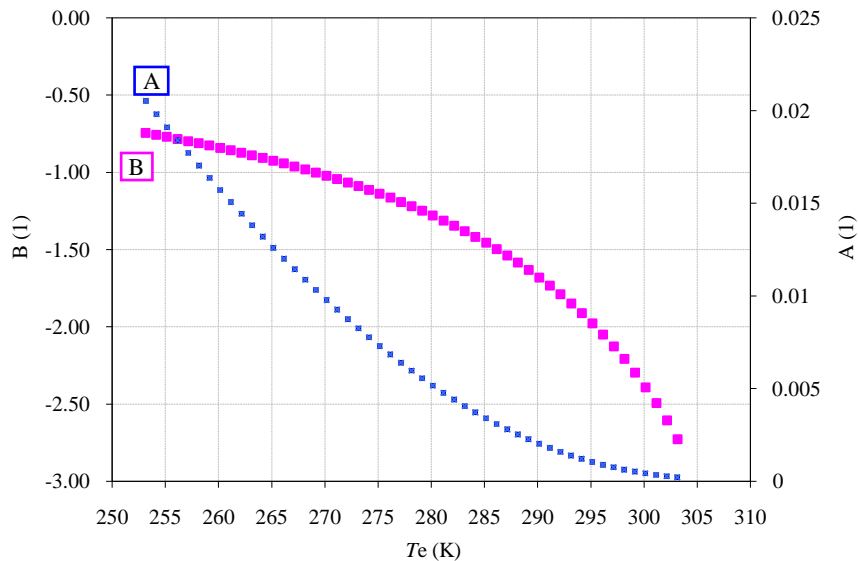
FIGURE 4: The progress of locating constant A and regression coefficient B for an ambient temperature range from –20 to + 30 ºC for the return pipe.

IV. CONCLUSION

The newly developed model for determining heat loss does not impose significant demands on the measurement of individual variables, it allows quick results on heat loss, it is reliable and offers some comfort. Putting it into actual practice would, from the point of view of both the manufacturer and the distributor of heat, does not signify any increase in finances and at the same time would make it possible to clearly determine the value of the total or specific heat loss of the network.

This model finds its justification mainly when examining loss on short pipe sections where recording of a drop in water temperature through regular thermometers is impossible or where little accurate information is obtained.

ACKNOWLEDGEMENTS

REFERENCES

[1] M.Čarnogurská, D. Knež, R. Fedurcová, "Matematický model tepelnýchstrát v nadzemnýchrozvodnýchsústavách," Setkáníkateder hydromechaniky a termomechaniky, Blansko, 2005

[2] M. Čarnogurská, "Zakladymatematického a fyzikálnehomodelovania v mechaniketekutín a termodynamike,"Viela, Košice, 2000.

[3] M. Rédr, M. Prihoda, "Základytepelnejtechniky," Praha, SNTL, 1991.

[4] J.B. Jones, G.A. Hawkins, "Engineering Termodynamics,"John Wiley, New York, 1986.

[5] W. Rohsenow, J.P. Hartnett, Y.I Cho,"Handbook of Heat Transfer," McGraw-Hill, 1998.

Design of a Hydrogen Compressor Powered by Accumulated Heat and Generated in Metal Hydrides

Natália Jasminská[1], Tomáš Brestovič[2], Ľubica Bednárová[3], Marián Lázár[4], Romana Dobáková[5]

Department of Power Engineering, Faculty of Mechanical Engineering, Technical University of Košice, 042 00 Košice, Slovak Republic

Abstract—The proposed article describes a compressor design for using the heat generated in the hydrogen absorption process into the metal alloy during compression. The absorption of hydrogen into the alloy occurs after the desired pressure has been achieved, whereby the catalytic effect of the used metals to dissociate the hydrogen molecule and the subsequent diffusion of the hydrogen atoms into the intermetallic space of the lattice occur. The absorption process is accompanied by a gradual increase in pressure up to the total saturation value of the metal. The equilibrium pressure at which the absorption occurs is highly dependent on the temperature of the alloy. The difference in the equilibrium pressures of MH materials at an acceptable temperature change has led to efforts of creating a hydrogen compressor that would use MH heating and refrigeration heat cycle.

Keywords—hydrogen, alloy, compressor, compression, absorption.

I.   INTRODUCTION

In nature hydrogen does not naturally occur in an unbound molecular form. It is most often produced through the partial oxidation of natural gas, steam reforming and electrolysis of water.

If it is not in use immediately after production, it is necessary to store it. Most storage methods, in view of the low hydrogen density, require the use of a compressor that increases the pressure to the desired level.

The hydrogen compressor is currently used to increase hydrogen pressure mainly through mechanical means. Rotary turbines are used at high volumetric flow rates, and at low flow rates there are mainly used piston compressors, or pressure multipliers utilizing hydraulic mechanisms. There was an attempt to test compressors using proton exchange membranes and simple compressors with metal hydride alloy.

The compressor powered by accumulated heat and generated in metal hydrides operates in a closed thermodynamic cycle, where hydrogen is stored at low temperatures with the catalytic effect of metals. Then the hydrogen molecules are dissociated and atomic diffusion into the intermetallic structure of the alloy occur. Once the alloy is saturated with hydrogen, it is necessary to bring in heat from an external source, thus increasing the pressure by shifting the working point to a higher isothermal curve. At higher temperatures, it is possible to desorb hydrogen from the alloy and reduce the storage capacity to the original state. It is possible to shift the subsequent lowering of the temperature to the starting point [1-4].

II.   THE BASIC CHARACTERISTICS OF A HYDROGEN COMPRESSOR

The compressor for compressing hydrogen, which is driven by the interaction of hydride formation in a metal or intermetallic compound with hydrogen to the metal hydride, is considered to be a promising application for the hydrogen energy system. The advantage of a hydrogen compressor rests in its simplicity in the design, compactness, safety, reliability, absence of moving parts and the possibility of consuming waste heat instead of electricity.

$$M(s) + \frac{x}{2}H_2(g) \xleftrightarrow{\text{absorption / desorption}} MH_x(s) + Q \tag{1}$$

where: M-metals or alloys, with a solid phase, g - gas phase, Q- temperature generated during absorption (J).

The process of forming the metal hydride by absorbing hydrogen into the metal alloy is accompanied by heat release Q. In desorption process, that is, during decomposition, the alloy consumes approximately the same amount of heat.

The absorption and desorption process is strongly dependent on the proper characteristic of the reaction (1), including its thermodynamic and kinetic characteristics, including the very important heat and mass transfer. Important aspects also include the composition, structure and morphology of the solid phase connected to the process. These properties are mainly related to the basic aspects of the studied metal hydride materials.

The use of metallic hydrides for the thermal compression of hydrogen is based on the equilibrium pressure peq, the equilibrium pressure change and the temperature described by the van Hoff equation [5, 6]:

$$\ln p_{eq} = \frac{\Delta H}{RT} - \frac{\Delta S}{R}$$ (2)

Where ΔH - the enthalpy change (J·mol^{-1}), ΔS- change of entropy connected with the absorption or desorption in a metal hydride (J·mol^{-1}·K^{-1}).

The compressor starts performing thedesorption of hydrogen if the equilibrium pressure of the hydride exceeds the set pressure value. In this case, the storage pressure is constant with the set pressure value. The operating principle of the single-level hydrogen compressor is illustrated in Fig. 1.
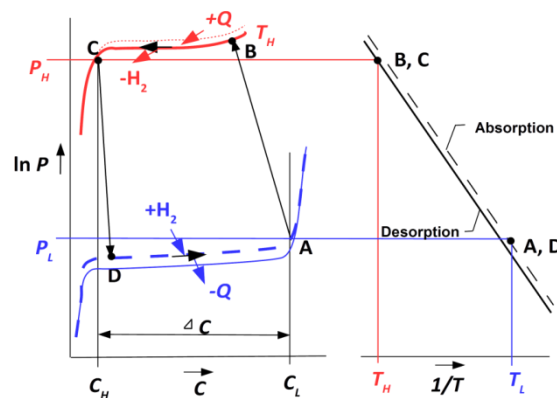
FIGURE 1: The operating principle of the single-level MHx hydrogen compressor [6]

As shown in Fig. 1, the operation of the single-level compressor consists of 4 processes:

DA – hydrogen absorption in low temperature (TL) and low pressure (PL),
AB – adequate heating and compression when changing from TL to TH temperature,
BC – the desorption of compressed hydrogen at the TH temperature and elevated PH pressure,
CD – adequate cooling from TH to TL.

According to the equation (2) the pressure increases exponentially with the increasing temperature and large pressure values can be obtained through slight temperature changes. On the basis of the metal hydride the compressor can be designed to cover a wide range of operating pressure ratios using suitable alloys.

To achieve high pressure, the individual units of the hydride can be connected in a series, each unit containing a different kind of alloy and consequently increasing pressures. The most important properties of a suitable alloy for hydrogen compression are: good hydrogen absorption – desorption rate, smaller enthalpy change, rapid reaction kinetics and good structural stability during cycles. High pressure gradient metal hydrides are suitable for the compressor depending on the temperature change, especially in a low temperature area. The efficiency of the single-level hydrogen compressor is given by the relation [6]:

$$\eta = \frac{m \cdot \left(R \cdot T_{H} \cdot \ln p_{H} - R \cdot T_{L} \cdot \ln p_{L} \right)}{m \cdot c_{p} \cdot \left(T_{H} - T_{L} \right) + \Delta H}$$ (3)

where: η is the efficiency of (-),m - the weight of the metal hydride (kg), c_{p}- the specific heat capacity of the metal hydride (J·kg^{-1}·K^{-1}), p_{L}- equilibrium pressure at the absorption temperature T_{L}(Pa), p_{H} - equilibrium pressure at the

desorptiontemperature T_H (Pa), ΔH - the enthalpy change of the metal hydride (kJ·mol^{-1}), R - universal gas constant (J·mol^{-1}·K^{-1}).

The hydrogen absorption and desorption kinetics are significantly influenced by the thermal conductivity and porosity of various metal hydrides. The hydrogen is first absorbed into the metal hydride at a low pressure and temperature [7, 8]. The hydrogen remains in the hydride unless exposed to an increased temperature or pressure drop. In the case that the temperature increase is sufficient and the pressure of the high-pressure vessel is less than the pressure in the MH tank, the hydrogen leaves the MH tank at pressures ranging from 3 to 10 times the original fed pressure. Multi-level metal hydride hydrogen compressors use a combination of different types of metal hydrides to increase the overall compression ratio. A two-level metal hydride compressor is shown in Fig. 2 [9].
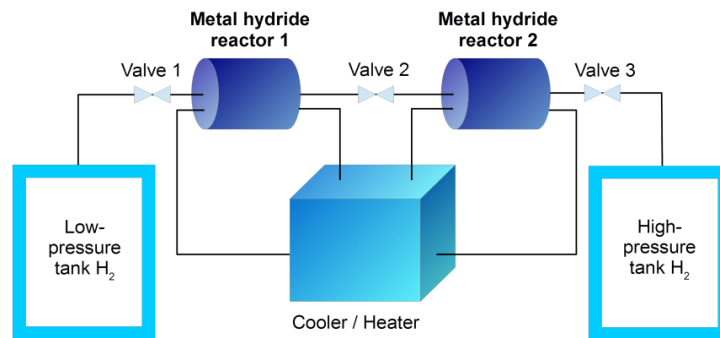
FIGURE 2: A diagram of a two-level metal hydride compressor

The concept of a multi-level compressor is based on the compression of a single level. It has been shown that by increasing the input pressures, the compression ratio remains almost constant. Using a two-level system, it is possible to increase the final pressure in the system using the second compression cycle [9].

III.   PROPOSAL FOR A HYDROGEN COMPRESSOR

With compressors using metal hydride alloys there is a significant transport and heat management mechanism. The absorption of hydrogen into the metal alloy results in the release of heat, which proportionally increases the equilibrium gas pressure. The absorption of hydrogen at a relatively lower temperature, ensured by cooling, occurs at a lower pressure.

After the absorption and subsequent heat transfer, a significant increase in hydrogen pressure occurs, with a compression ratio of more than 3, with a temperature increase by several tenths of degrees. Increasing the kinetics process is achieved through the proper design of the pressure vessel and the intensification of the heat inlet and outlet. A new, original proposed solution to ensure continuous operation is the tandem connection of the metal hydride tanks with the heat-exchange provided with a heat pump (Fig. 3).
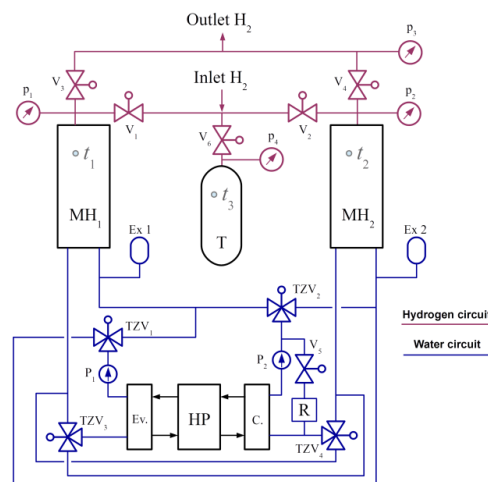
FIGURE 3: Tandem hydrogen compressor block diagram

The essence of the development is to connect the heat pump (HP) and tandem arrangement of the metal hydride tanks (MH$_1$ and MH$_2$) to continuous hydrogen compression by using the thermal cycle. The heat pump removes the heat from the storage tank where the hydrogen is absorbed and transported into a tank where the hydrogen is already absorbed to increase the pressure. After compressing and releasing the hydrogen into the end pressure vessel, a reverse heat transfer process occurs between the tanks to ensure the continuous operation of the compressor. The advantage of the solution is the continuous and safe compression of the hydrogen flow volumes. Safety is ensured by preventing the contact of system's moving parts with the compressed hydrogen. A pressure vessel (T) that temporarily stores hydrogen on the low pressure side serves to ensure continuous operation even during the adsorption/desorption cycle. To remove excess heat on the side of the condenser (C.), an additional cooler (R) serves.

The preparation and composition of the metal hydride alloy is the key to its storage properties. The working pressure of the compressor level is dependent on the composition of the alloy. It is also necessary to define the degradation of the metal hydride alloy in the use of hydrogen with the oxygen admixture produced during the electrolysis of water.

IV.   SELECTION OF A SUITABLE TYPE OF A METAL HYDRIDE FOR HYDROGEN COMPRESSOR

The selection of the hydrogen compressor tanks is influenced by several parameters such as: tank capacity, alloy absorption capacity, minimum filling time, maximum discharge period, maximum pressure range, temperature range and the composition of the alloy that fills the tank. The HBond 500 metal hydride tank was used to design the hydrogen compressor. The nominal capacity of the metal hydride tank is 0.5 m^3 H$_2$. The tank is produced from stainless steel and is equipped with an internal heat exchanger, an internal filter and a quick connector for connecting hydrogen.

The HBond 500 can be filled with hydrides with different thermodynamic properties. The test pressure is 30 bar. The used container is filled with basic type AB5 alloy with alloy composition La$_{0.85}$Ce$_{0.15}$Ni$_5$.

The maximum pressure in filling the tank is 15 bar. The maximum inlet hydrogen temperature can reach 40 °C. The hydrogen tank is provided with an internal heat exchanger as shown in Fig. 4.
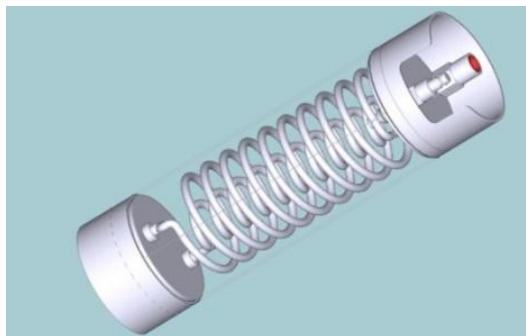
FIGURE 4: H Bond 500 Tank

The rate of hydrogen desorption is dependent on the temperature of the metal hydride. The maximum tank discharge rate is 8.33 Nl.min^{-1}. The reaction heat is 1 MJ·m^{-3} of the desorbed hydrogen and this heat must be supplied through a water circuit.

The metal alloy contained in the tanks was tested in the Material Science Institute at Helsinki Technical University, where no degradation of the absorption capacity was observed even after 1000 cycles. The minimum purity of hydrogen is 99.9%. Since the metal hydride does not release any other impurities, the purity of the hydrogen at the outlet is the same or even better than the inlet.

The storage system is equipped with all the tools and valves necessary for its proper function throughout the entire system.

Experimental measurements for the setting of pressure and temperature dependence for the creation of P-T characteristics were performed on the alloy La$_{0.85}$Ce$_{0.15}$Ni$_5$. The obtained data will serve the primary thermodynamic design of the hydrogen compressor.

Fig. 5 is a *p-T* diagram depicting the pressure dependence on the concentration of stored hydrogen in isothermal conditions. The measurement of the pressure-to-temperature dependence was performed at a constant concentration of hydrogen (0.9 wt.%). The measurement of the absorption capacities of metal hydride alloys and pressure gradients will be performed continuously with the formation of new types of alloys.
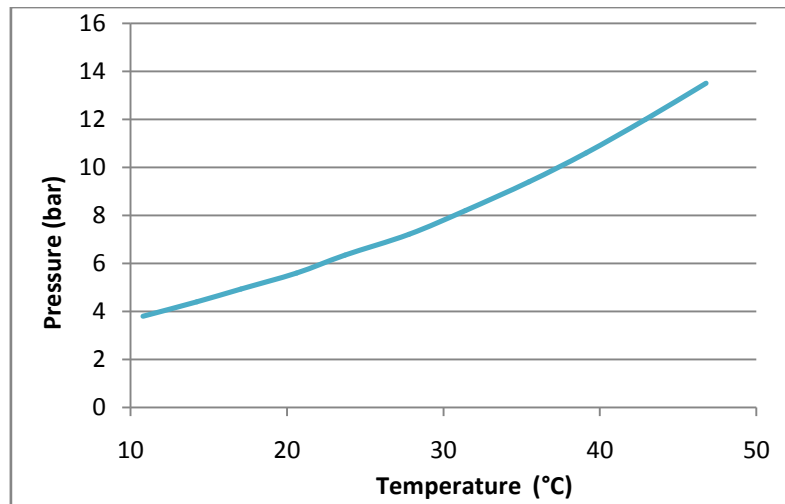
FIGURE 5: P-T characteristic of alloy La$_{0.85}$Ce$_{0.15}$Ni$_5$ at 0.9 wt% of the stored hydrogen

V.　CONCLUSION

The article described the basic concept of the development of a hydrogen compressor using metal hydride materials with the tandem connection of tanks. A heat pump is designed for heat transfer, which minimizes the energy demand of hydrogen compression.

The development of a hydrogen compressor has great potential for innovative social and economic needs in the development and application of hydrogen technologies in the automotive industry and transport, mainly in the context of Slovak and European innovation strategy.

The economic benefit of the submitted work is limited by the implementation of the hydrogen economy, mainly in the automotive industry in Slovakia. The hydrogen compressor prototype is a unique solution in relation to safety of operation, since hydrogen does not come in contact with moving or compressing elements during compression or with the rotating parts of the system.

ACKNOWLEDGEMENTS

REFERENCES

[1] S. Mellouli, F. Askri, H. Dhaou, A. Jemni, S. Ben Nasrallah, "A study of the thermal behavior of a deformable metal-hydride bed," International journal of hydrogen energy, pages 1711-1724. November 2006.

[2] S. Mellouli, F. Askri, H. Dhaou, A. Jemni, S. Ben Nasrallah, "Hydrogen storage in metal hydride tanks equipped with metal foam heat exchanger". International journal of hydrogen energy, pages 9393 - 9401. October 2009.

[3] B.SIKINTUNA, F.LAMARI-DARKRIM, M. HIRSCHER, "Metal hydride materials for solid hydrogen storage: A Review," International journal of hydrogen energy, pages 1121 - 1140. November 2006.

[4] Z.Cao, L. Ouyang,H.Wang, J. Liu, D.Sun, Q.Zhang, M.Zhu, "Advanced high-pressure metal hydride fabricated via TieCreMn alloys for hybrid tank," International journal of hydrogen energy, pages 2717 – 2728. December 2014

[5] M.V.Lototsky,V.A.Yartys,B.G.Pollet,Jr.R.C,Boweman,"Metal hydride hydrogen compressors: A review.," International journal of hydrogen energy, pages: 5818 – 5851. January 2014.

[6] G.Popeneciu, V.Almasan, Coldea, D. I. Lupu,I.Misan, O.Ardelean, "Investigation on a tree-stage hydrogen thermal compressor based on metal hydrides," Journal of Physics: Conference Series 182, 012053. 2009.

[7] A. Sarkar,R.Benerjee, "Net energy analysis of hydrogen storage option," International journal of hydrogen energy, pages: 867-877. 2005.

[8] R.Schulz, J.Huot,G.Liang, S.Boily,G.Lalande, MC. Denis,etal.,"Recent development in the applications of nanocrystalline materials to hydrogen technologies," Mater SciEng A 1999;267:240

[9] M.Hirscher, M.Becher, "Hydrogen storage in carbon nanotubes," J Nanosci Nanotech 2003; 3(1–2):3–17.

Load on a wind turbine blade and its stress condition

Mária Čarnogurská[1], Marián Lázár[2], Romana Dobáková[3], Jiří Marek[4]

[1,2,3]Department of Power Engineering, Faculty of Mechanical Engineering, Technical University of Košice, 042 00 Košice, Slovak Republic,

[4]VŠB – Technical University of Ostrava, Faculty of Metallurgy and Materials Engineering, Ostrava –Poruba, Czech Republic.

Abstract *– The article provides an analysis of the stress and deformation conditions of NACA blade at wind speed of 3-12 m/s and in a parking position (over 20 m/s). The wind speed of 9 m/s and Poisson's glass-epoxy laminate with a value of 0.43 initiates yaw of the blade tip from the axis of rotation by 651 mm. Von Mises stress reaches a value of 75.58 MPa. Visualization of airflow around the blade demonstrates that flow separation occurs at the point of blade mounting in the hub and the speed is higher than airflow speed around the blade tip.*

Keywords *– the finite element method, visualization of air-flow, stress of the blade.*

I.   INTRODUCTION

Wind power installations are used to convert kinetic energy of wind into electricity. This conversion can be performed in various ways, however, so-called Betz limit with a power coefficient of 0.593 cannot be surpassed. When the value of the coefficient is greater than 0.5, aerodynamic efficiency rises up to 85%. Precisely manufactured blades, e.g. NACA type blades, must be utilised in order to achieve such efficiency. This type of blades represents the most effective method how to generate the pressure difference required in a wind turbine rotor. Blades of this type can also reach a considerable proportion of the aerodynamic lift c_y to aerodynamic drag coefficient c_x. The values of both coefficients are affected by the angle of attack α, which determines pressure distribution on the blade as well as its stress state.

II.   DETERMINATION OF AERODYNAMIC FORCE

Blade stress is a product of resultant aerodynamic force R (Fig. 1) and there are two methods of its calculation. Either by axial and tangential force or by means of drag and lift force. Axial force *T* can be determined by Equation (1) for a selected number of cross sections of the blade along its length (Fig. 2):

$$dT_i = (1/8)\cdot dc_{T_i}.\rho \cdot \pi \cdot D^2 \cdot \upsilon_o^2 \tag{1}$$

where *D* – rotor diameter (m), υ_o-wind speed, ρ - air density, c_T – axial force coefficient.
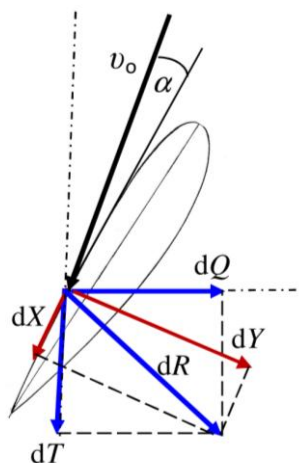
FIGURE 1: Forces on a blade element
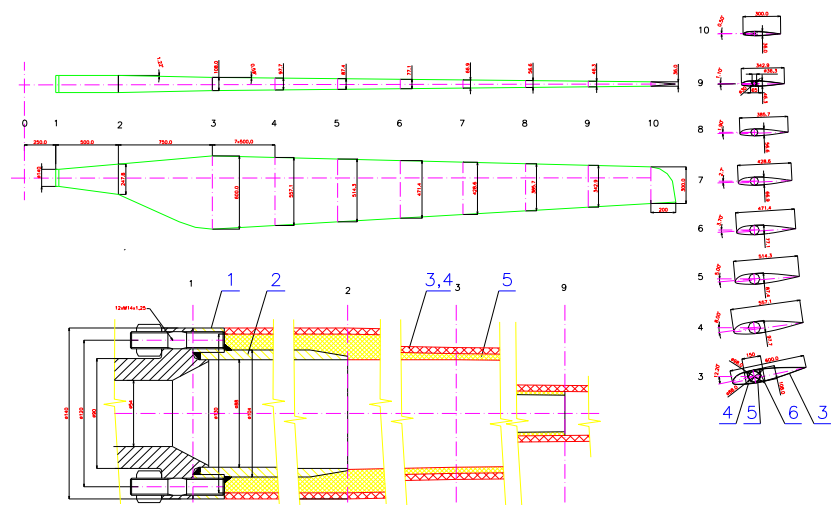
FIGURE 2: The geometry of a wind turbine rotor blade

Equation (2) can be used to determine elemental tangential force dQ for all investigated distances r_i from the axis of rotation employing known torque coefficient c_M:

$$dQ_i = \frac{dM_{ki}}{r_i} \tag{2}$$

$$\text{where} \quad M_k = (1/16) \cdot c_M \cdot \rho \cdot \pi \cdot D^3 \cdot \upsilon_o^2 \tag{3}$$

Axial force coefficient c_T and torque coefficient c_M depend on the blade pitch angle and their courses are given in [2]. Elementary aerodynamic force dR_i can be then determined for the distances r_i from the axis of rotation as defined by equation (4):

$$dR_i = \sqrt{dT_i^2 + dQ_i^2} \tag{4}$$

The static effect of airflow on stress conditions was examined by the resultant aerodynamic force R, determined by integrating of elemental axial forces and tangential forces along the entire length of the blade. Calculation of aerodynamic forces by means of drag force and lift force is based on relationship (5) to (7). Drag force can be determined as follows:

$$X = \frac{1}{2} \cdot \rho \cdot c_x \cdot S_t \cdot \upsilon_o^2 \tag{5}$$

where S_t is an airfoil area - given as a product of the airfoil chord length and the height of a blade, $\rho -$ air density, $c_x -$ drag coefficient, $\upsilon_o -$ air velocity. Lift force, which acts perpendicularly on the air speed, is a function of the lift coefficient c_y:

$$Y = \frac{1}{2} \cdot \rho \cdot c_y \cdot S_t \cdot \upsilon_o^2 \tag{6}$$

Relationship (6) indicates the resultant aerodynamic force R as follows:

$$R = \sqrt{X^2 + Y^2} \tag{7}$$

III.   RESULTS OF THE STUDY OF FORCE CONDITIONS ON THE BLADE

The rotor remains in the basic operational position at wind speeds from 3 to 9m/s. Therefore, the load condition of the blade was analysed at maximum wind speed of 9 m/s. The calculation of stress condition was performed employing the FEM method (Finite Elements Method). Airflow around the blade is also visualised in this state.

The analysed blade has a length of 5000 mm. A geometric model of the blade for the structural analysis of a stress condition and deformation of the blade with the effect of wind of the speed of 9 m/s was developed by SOLID elements with a quadratic base function.

The calculation model of the blade contains 6610 elements in total. The boundary condition was defined by wind pressure acting onto the blade in a normal direction and the effect of centrifugal force and gravitational acceleration. Material properties were included separately for the metal cantilever beam and the coat of the blade as well as its internal epoxy-fiberglass reinforcement. The cantilever beam is made of material 12 021.1 (yield strength Re = 235 MPa). When safety factor n=1.5, allowable stress for the beam is σ_{dov} = 157 MPa. Epoxy-fiberglass has allowable stress σ_{dov} = 98 MPa. Other material properties are shown in Table 1. Stress conditions were determined for the most unfavourable position of the blade in which gravitation and centrifugal force are of the same direction. Such case occurs when a blade tip points towards the ground.

TABLE 1
MATERIAL PROPERTIES

	steel 12 021.1	epoxy-fiberglass
modulus of elasticity E (MPa)	$2{,}6 \cdot 10^5$	$0.048 \cdot 10^5$
Poisson number μ (-)	0.28	0.28% to 0.43%
density ρ (kg/m^3)	7850	1950

Fig. 3 shows deformation of the blade along its length in steady state. Maximum yaw of the blade tip from the axis of rotation is δ = 651 mm. The blade is attached to a root attachment made of steel. Fig. 4 shows the strain in the root region of

the blade. The maximum value of reduced Von Mises strain at the end of the root section is approximately 60 MPa (yellow). Deformation of the blade increases stress within its material, which is epoxy-fiberglass.

The global assessment of a stress condition of the blade as a whole (comprising of a steel attachment and reinforcements) yields a stress state of reduced Misses strains with a value of 75.58 MPa. Such state corresponds with the solution using Poisson number with a value $\mu = 0.43$. Tab. 2 shows the values of stress on the blade under static load for four selected wind speeds and two Poisson numbers.
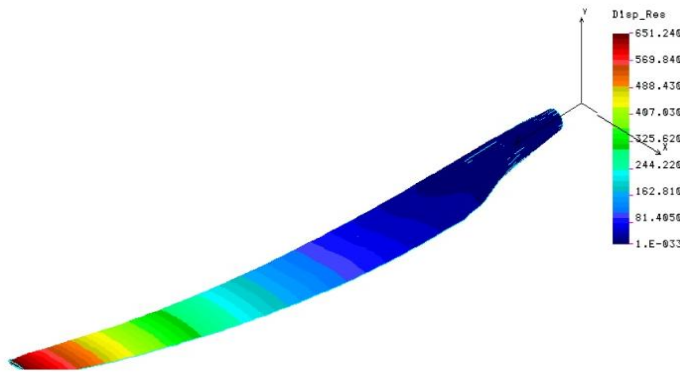
FIGURE 3: Stress state and blade deformation at wind speed $v_o = 9$ m/s
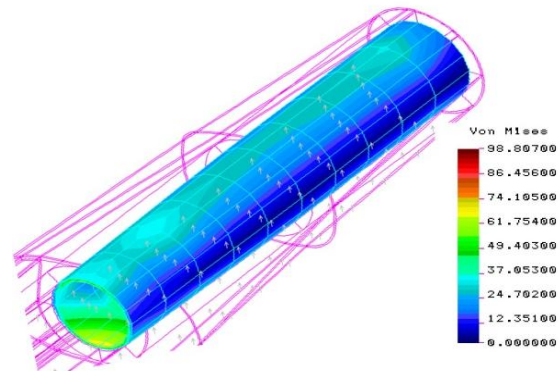
FIGURE 4: Stress in the root section

The wind turbine should work in the environment where wind speeds range between 3 and 9 m/s. Considered tip-speed ratio is $\lambda = 5.75$. Axial force coefficient c_T on the blade profile is about 0.5. If a wind speed exceeds 20m/s, the control system adjusts the pitch angle φ, so at wind speed of 12m/s revolution speed remain 2 rev/s and the power output is about 15 kW. This power output is maintained constant until wind speed exceeds 20m/s (blade pitch angle is adjusted depending on the wind speed to keep the power output constant at all times). When wind speed is over 20 m/s, the blade pitch angle at the tip φ is set to 60° and the propeller will stall. This way the energy of wind passes through the rotor without being exploited and stress in the turbine is equivalent to the stress in an operational position at wind speed of 3m/s (Tab. 2).

TABLE 2
STRESS AND DEFORMATION OF THE ROTOR BLADE WHEN CONSIDERING STATIC LOAD

v_o (m/s)	Poisson number			
	0.43		0.28	
	σ (MPa)	δ (mm)	σ (MPa)	δ (mm)
3	12.91	118.87	11.705	119.15
9	**75.578**	**651.24**	**68.77**	**653.49**
12	124.1	1070.4	112.46	1073.3
20	12.55	95.5	11.72	95.8

Airflow around the blade was modelled by software called FLUENT. The chord divides the airfoil surface into a downwind and upwind side. The downwind side has a smaller surface area ($S_n = 2.1393$ m^2) than the upwind side ($S_n = 2.1989$ m^2). Airflow around the blade causes negative pressure on the upwind side proportional to the wind speed. As the wind speed increases, air streamlines separate from the airfoil (wake occurs) and negative pressure is produced in the area of separation. There is always overpressure on the downwind side. Its amount mainly depends on the blade pitch angle relative to the plane of rotation, but also on airflow speed. It is possible to determine the amount of force exerted on the downwind (F_n) and upwind (F_z) side for a given winds speed and pitch angle. A particular value of force on a given area depends on the amount of static (p_s) and dynamic (p_d) pressure. Surface integration of the individual pressures or the total pressure ($p_{tot} = p_s + p_d$) can be used to determine the forces on both surfaces. Their difference yields resultant aerodynamic force R according to equation (8):

$$R_{tot} = \int_S dR_{tot} = \int_S p_{tot} dS = \int_S (p_s + p_d) dS \qquad (8)$$

or

$$R_{tot} = \sum_{i=1}^{n} p_{i,tot} \cdot S_i \qquad (9)$$

Based on the resultant aerodynamic force, resistance coefficient c can be determined based on formula (10).

$$c = \frac{2 \cdot R_{tot}}{\rho \cdot S_t \cdot \upsilon_o^2} \qquad (10)$$

where S_t blade surface area obtained as the product of the chord and the height of the blade.

Table 3 presents the values of the resultant forces, the static pressure R_s, dynamic pressure R_d total pressure R_{tot} acting on the downwind and upwind side of the blade.

TABLE 3
Pressures and forces on the downwind and upwind side of the blade at a wind speed υ_o = 9 m/s and blade pitch angle 12°

	R_s (N)	R_d (N)	R_{tot} (N)	p_s (Pa)	p_d (Pa)	p_{tot} (Pa)
S_z (m^2)	-606.734	121.467	-469.647	-275.929	55.241	-213.585
S_n (m^2)	397.369	250.348	641.886	185.746	117.022	300.043
ΣS (m^2)	1004.103	371.815	1111.5333	461.675	172.263	513.627

IV.   CONCLUSION

The examined stress and load conditions are on the turbine blade of a wind power plant to be located in the area with lower wind-energy potential. The maximum assumed wind speeds 30m above ground range between 5 - 9 m/s.

The airflow around the root attachment is shown in Fig. 5 and the blade tip in Fig. 6. A wake occurs on the upwind side of the root section and the flow separates from the surface of the root attachment. This is due to the fact that the root attachment has a cylindrical shape, which is, in terms of airflow, the least favourable shape. The wind speed on the upwind side reaches up to 37.6 m/s. The wake is weaker on the blade tip due to a more suitable airfoil profile. The maximum speed is about 24 m/s.
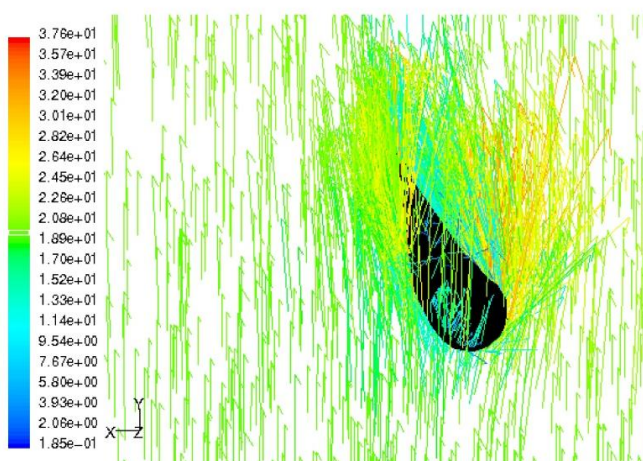
FIGURE 5 AIRFLOW AROUND THE BLADE ATTACHMENT
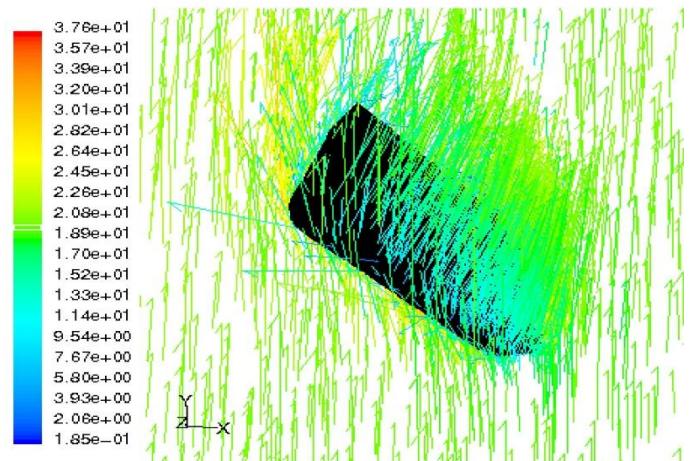
FIGURE 6 AIRFLOW AROUND THE BLADE TIP

REFERENCES

[1]   D. Rozehnal, 2000, Aerodynamic loading of wind motor with a horizontal rotation axis, Wind Power, 2 (2000) pp. 13-15.

[2]   M. Čarnogurská, D. Rozehnal , Aerodynamic characteristics of wind power plant's rotor with a blade profile of type NACA, Proc. from the 2nd conference Small water systems and alternative sources of power, DT Košice, 2003, pp. 199-204.

[3]   Le Gouriér´s, D.: Wind power plants, theory and design. Pergamon Press, Toronto-Sydney-Frankfurt. 1982.

[4]   M. Čarnogurská, M., Kozubková, M. Bojko, Flow over wind-mill rotor blade in a parking position and its stress state. ACTA MECHANICA SLOVACA, 3 (2003) pp. 323 -330.

[5]   COSMOS/M, User´s Guide, Release 2.6.

Waste Management Protocols for Iridium-192 Sources Production Laboratory Used in Cancer Treatment in Brazil

M. E. C. M. Rostelato[1], D. C. B. Souza[2], C. D. Souza[3], C. A. Zeituni[4], R. Vicente[5],
O. L. Costa[6], B. T. Rodrigues[7], J.A. Moura[8], A. Feher[9], E. S. Moura[10],
J. R. O. Marques[11], V. S. Carvalho[12], B. R. Nogueira[13]

[1-4, 6-13]Department of Radiation Technology Center, Nuclear and Energy Research Institute, Sao Paulo, Brazil
[5]Department of Waste management, Nuclear and Energy Research Institute, Sao Paulo, Brazil

Abstract—*Objective: The iridium-192 wired sources production results in radioactive waste that needs to follow the guidelines. The aim of this study is to do a radioactive waste management of wastes from iridium-192 sources production laboratory used in cancer treatment in Brazil. Methods: The wire is acquired in an alloy form with 80% platinum and 20% iridium encapsulated with 100%. Electronic microscopy, X-ray fluorescence, and posterior iridium neutron activation (to determine contaminants) are performed to ensure quality. A 50-cm twisted wire is placed in an aluminum tube. The tube is sealed and place inside the reactor irradiator system and is left for decay during 30 hours to wait for the others undesired activation products to decay. The wire is prepared for treatment with 48 cm length with 192 mCi maximum activity. All the equipment use inside the hot cell must be calibrated every four months. All the waste must be removed from the hot cell. Results: The solid waste is previously characterized in the analysis phase. The contaminants are already known and they are insignificant due to their fast half-life. The iridium-192 half-life is 74.2 days, classified as very short half-life waste. The reminiscent activity is 8mCi. Conclusion: The radioactive waste generated during the I192 wires production is solid, was a short half-life and a weakly activity of 9.7 GBq.g-1. According to the standards, this activity is too high to be discarded into the environment (limit 10 Bq.g^{-1}). The waste must be managed by the R&R (retain e retard) system.*

Keywords— ***Iridium-192, Radioactive waste, Sealed sources, Sources production, Waste management.***

I. INTRODUCTION

According to the International Agency for Research on Cancer (IARC)[1]27 million new cases of cancer are expected in the world in 2030 and around 17 million deaths. This astonishing estimate considers the increase life expectancy due to new forms of treatment. The highest incidence of cancer is observed in developing countries of South America, Africa and Asia.[1]

The "Registro de Câncer de Base Populacional e Hospitalar", People and Hospital Cancer Registry (RCBP - RHC) and the "Instituto Nacional do Câncer", National Cancer Institute in Brazil released the 2015 estimative[2]allowing the study of each cancer and for each region of the country.According with this document, 576.000 new cases occurred, and around 14 million deaths. Cancer is a major public health issue in Brazil.

Among the forms of treatment, brachytherapy is largely used due to efficient radiation dose delivery. In this form of radiotherapy, radioactive seeds, wire or pellets are placed in contact (during a period of time) or inside the region to be treated, maximizing the radiation dose inside the targeted areas.

Iridium-192 is being used in brachytherapy since 1955. It presents emission energy in the "therapy region" (370keV, 74.2 days half-life) and is easily produced in a nuclear reactor (^{191}Ir (n, γ) → ^{192}Ir).[3]Wires are an iridium-platinum alloy with 0.36 mm diameter and they can be cut in any needed length (even 3mm to be used as a radioactive seed). They can be used in severaltypes of cancer as shown in FIG. 1. The linear activity is between 1mCi/cm (37MBq/cm) and 4mCi/cm (148MBq/cm) with variations of 10%in 50 cm maximum. This activity values classified the treatment and low dose rate (0,4 à 2 Gy/h).[4]

FIGURE 1: a) Iridium-192 wire;[5]b) Example of treatment using the wire;[6]c) cartoon of a breast cancer treated with wire;[7]

1.1 Radioactive Waste management in sources production

The iridium-192 wired sources production results in radioactive waste that needs to follow the guidelines. The production facility must guarantee that radioactive exposure, for workers and public, is inside the limits presented in the guidelines. In Brazil, the "Comissão Nacional de Energia Nuclear" (CNEN), Nuclear Energy National Commission establishes the regulations for all nuclear and radioactive research and production.

Accordingto CNEN-NN 6.08 standard, radioactive concentration levels in which a waste is consider radioactive is presented for each radionuclide. To be consider common trash or chemical waste the activity value must be below the one presented. The discharge levels are calculated by the effective dose (E) received by any person, worker or public, is no greater then $10\mu Sv/year.$[8]

The solid waste management applied to the iridium-192 brachytherapy sources production is presented in FIG. 2.
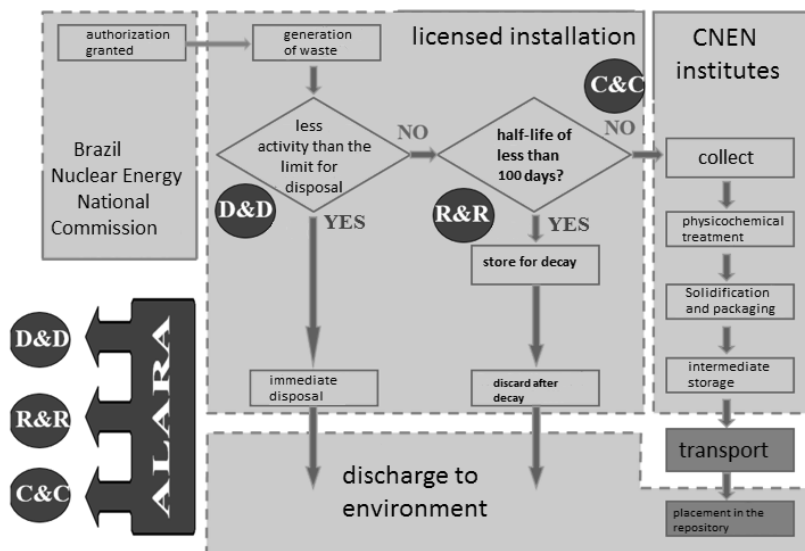
FIGURE 2: Flowchart of Brazil's radioactive waste management –D&D: Diluteand dispense; R&R: Retain and retard; C&C: Containandconfine[9].

The characterization step is where the waste is generated. This is a critical phase and requires especial attention since the results will determine the following steps. Waste can be classified by radioactive concentration (class 1, 2 or 3), physical state (solid, liquid or gaseous), and half-life (very short < 100 days, short < 30 years or long)[8].

After the characterization, the waste can be eliminated, temporarily confined for decay or permanently confined. The decision lies directly on the characteristics previously determined.

The general strategy involves minimize quantities and management cost, maintain control on every step, and understate workers and public exposure. Recommendations such asdilute and dispense (D&D), retain and retard (R&R),contain and confine (C&C) are also part of this strategy[9].

II. METHODOLOGY

The Iridium-192 wires produced in the "Instituto de PesquisasEnergéticas e Nucleares" (IPEN), Nuclear and Energy Research Institute havethe following manufacture steps:

2.1 Purchase of the iridium/platinum wire (*Goodfellow*)

The wire is acquired in an alloy form with 80% platinum and20% iridium encapsulated with 100% iridium 100%.[10]

2.2 Analysis of the material

Electronic microscopy, X-ray fluorescence, and posterior iridium neutron activation (to determine contaminants) are performed to ensure quality.

2.3   Wire activation on the IEA-R1 nuclear reactor

A 50cm twisted wire is placed in an aluminumtube (2cm diameter, 7cm length, FIG. 3.). The tube is sealed and place inside the reactor irradiator system.The irradiation parameters are: 30 hours irradiation with $5x10^{13}$ n/cm^{-2}.s^{-1}neutron flux. The tube is left for decay during 30 hours to wait for the others undesired activation productsto decay(Pt-197 e Pt-199).

(a)   **(b)**

FIGURE 3: a) Wire before irradiation; b) Twisted wire inside irradiation tube.

2.3.1   Quality control

Before its use, the wire is checked for irradiation homogeneity in its entire 50 cm length. The procedure is performed in an iridium specific hot cell. The activity is measured by an ionization chamber with lead shielding (FIG. 4). The system is attached in a *Keithley electrometer model617* charge counter. The measurement is performed at a 1cm/120s rate. The variation, in comparison with the average, must be less than 10%.[10]

2.3.2   Activity measured

The specific activity is measured by a*specific "homemade"* ionization chamber.The wire is prepared for treatment with 48 cm length (2 cm cutted) with 192mCi maximum activity (4 mCi/cm).[11]

2.3.3   Equipment maintenance

All the equipment use inside the hot cell   (FIG. 4) must be calibrated every four months. All the waste must be removed from the hot cell.
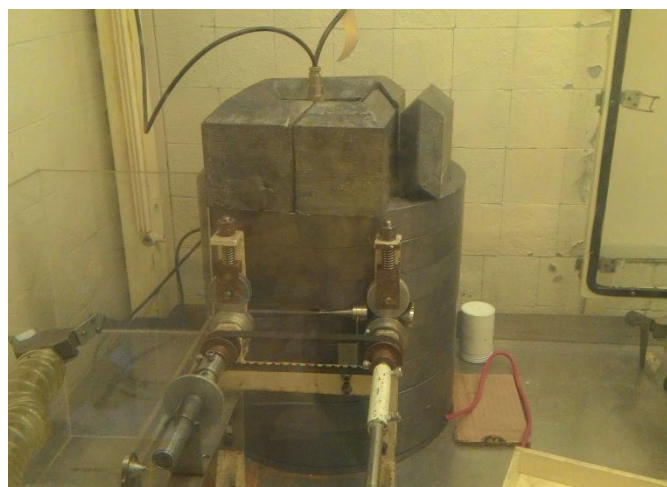
FIGURE 4: Hot cell interior: Lead shielding protecting the ionization chamber and the electrometer.

The cutting of the wire is needed due to the activation discontinuity in the extremity. This happened as a result of geometry measurements inconsistency in positioning the wire in the detection system. The cutted ends are radioactive waste.

III. RESULTS

The solid waste is previously characterized in the analysis phase. The contaminants are already known and they are insignificant due to their fast half-life. The iridium-192 half-life is74.2 days,classified as very short half-life waste. The reminiscent activity is 8mCi (2.96×10^8 Bq).According to theCNEN-NN 6.08 standard, that presents the discharge levels, the limit is 1 kBq.kg^{-1}(2.7×10^{-5} mCi.kg^{-1}).[12]

In order to estimate the total activity, the amountsare:

- Production estimate: 10 wires/week;

- Each wire (50 cm total) produces 2cm of waste;

- The discharge levels for Ir-192 waste is: 1 kBq.kg^{-1}; [12]

- The mass for the 50 cm wire is 0,73 grams;

- Waste mass and activity: 0.015 g/cm, 1-4mCi/cm, 10 wires/week, 20cm waste/week. Converting the data to mass = 0.3g/week;

- The hot cell undergo through maintenance every 4 months. The internal space needs to be clean, without any waste;

- The total waste activity per week is: 4 mCi x 20 cm waste resulting in80 mCi.week^{-1} or 2.9×10^9Bq.week^{-1}.

Weakly, 0.3 g with 2.9 GBq of Ir^{192} waste is produced. To immediate discharge, the following condition needs to occur:

$$0.3 \text{ grams of Ir192} \text{------- } 2.9 \text{ GBq}$$

$$1 \text{ gram of Ir192} \text{ -------- } 9.7 \text{ GBq (greater than 1 kBq.kg}^{-1} \text{ limit)}$$

Thus, the waste cannot be discharge. It must bemanaged through the R&R (retain e retard) system, that means, temporary storage and posterior discharge. Equation 1 is used to determine the total storage activity considering the decay (it takes into account the decay of the already stored waste for every new waste added).

$$A = \frac{f}{\lambda}\left(1 - e^{-\lambda.t}\right)$$

(1)

A: activity per time (t)

f: Entrance activity per second (Bq/s)

λ: decay constant (s^{-1})

t: time (s)

Assuming that f is obtained by the weakly waste activity generated per decay contestant (λ) and the storage time is (t: 4 months or 16 weeks):

$$f = 2.80 \; x10^9 \; {}^{Bq}/_s$$

$$\lambda = \frac{\ln 2}{T_{\frac{1}{2}}} = \frac{\ln 2}{74.2 \; x \; 24 \; x \; 60 \; x \; 60} = 1,081 \; x10^{-7} seg^{-1}$$

$$t = 4 \; months = 9.676 \; x10^6 s$$

Calculating the final activity in 4 months (scheduled maintenance):

$$A = \frac{f}{\lambda}\left(1 - e^{-\lambda t}\right) = \frac{2.8 \; x10^9}{1.081 \; x10^{-7}}\left(1 - e^{-1.081 \; x10^{-7} x \; 9.676 \; x10^6}\right) = 1.680 \; x10^{16} \; {}^{Bq}/_s \; for \; 16 \; weeks$$

$$m = \frac{0.3 \; g}{week} \; x \; 16 = 4.8 \; g in \; 16 \; weeks$$

The time that it would take to be discarded in the environment will be calculated by the decay law (Eq2):

$$A = A_0\left(e^{-\lambda.t}\right)$$

(2)

A: limit activity per time (t)

A_0: initial activity per time (t)

λ: decay constant (s^{-1})

t: time (s)

$$A = A_0\left(e^{-\lambda t}\right) \rightarrow \frac{10\, Bq}{g} = \frac{1.68\, x10^{16}Bq}{4.8\, g}\left(e^{-1.081\, x10^{-7}xt}\right) = 3.10\, x10^8 s^{-1} = 9.8\, years of storage$$

The device used for shielding and storage is presented in FIG.5:

FIGURE 5: Shielding and storage device. Dimensions: 10 cm height and 5.2 cm diameter. Volume = 212.37 cm^3.

Considering that one device used every 4 months and the waste is stored during 10 years, 30 devices are needed. Thus, all the devices will occupy:

$$V = 212.37\ cm^3 x\ 30 = 6{,}370\ cm^3$$

This volume is equivalent to a cube with ℓ=18.54 cm. The laboratory has a space (FIG. 6) delimitated by double 4.5 cm lead bricks with ℓ= 27 cm, which is enough space for store the devices for 10 years.

FIGURE 6: Waste storage area.

IV. CONCLUSIONS

The radioactive waste generated during the I^{192} wires production is solid, was a short half-life (<100 days) and a weakly activity of 9.7 GBq.g^{-1}. According to the standards, this activity is too high to be discarded into the environment (limit 10Bq.g^{-1}).The waste must bemanaged by the R&R (retain e retard) system, that means, temporary storage and posterior discharge.

Since there is maintenance every 4 months, the waste must be removed from inside the hot cell. That adds to a total activity of 1.68 x 10^{16} Bq and 4.8 g. This amount is stored inside a device made of lead that has 212.37 cm^3 volume. The waste will take 9.8 years to decay to the discharge levels.

To store 30 shielding devices during 10 years a space with 6,370 cm^{3}is necessary. The laboratory has enough space for this storage. Thus, the radioactive waste management can be performed through the R&R (retain and retard) system safely.

REFERENCES

[1]   INTERNATIONAL AGENCY FOR RESEARCH ON CANCER. IARC. World Cancer Report 2008. Available from URL: http://www.iarc.fr/en/publications/pdfs-online/wcr/2008/ [accessed 05 feb., 2014].

[2]   MINISTÉRIO DA SAÚDE. INSTITUTO NACIONAL DO CÂNCER. Estimativas 2015 Incidência de Câncer no Brasil. Available from URL: http://www.inca.gov.br/estimativa/2014/estimativa-24012014.pdf [accessed 05 feb., 2014].

[3]   ROSTELATO MECM. Estudo e desenvolvimento de uma metodologia para confecção de sementes de Iodo-125 para aplicação em braquiterapia. São Paulo: Instituto de Pesquisas Energéticas e Nucleares, 2005.

[4]   PODGORSAK EB.Radiation Oncology Physics: a Handbook for Teachers and Students. Vienna: International Atomic Energy Agency, 2005

[5]   Tabrizi SH, Aghamiri SMR, Najarian S, Jaberi R. Dosimetric evaluation of a novel high dose rate (HDR) intraluminal / interstitial brachytherapy applicator for gastrointestinal and bladder cancers. 2010. 2010;12.

[6]   Figure 1a. Available from URL:

       http://www.oncoprof.net/Generale2000/g08_Radiotherapie/Images/Levre-
       2.jpg&imgrefurl=http://www.oncoprof.net/Generale2000/g08_Radiotherapie/Photos/g08-
       gb_index24.html&h=329&w=452&tbnid=KDPfkDH_lvtRpM:&docid=KUgZwIMadd7HTM&ei=tWfEVuOsGsm9wAS45amICw&t
       bm=isch&ved=0ahUKEwij2-C75v7KAhXJHpAKHbhyCrEQMwgfKAMwAw [accessed 17 feb., 2016].

[7]   Figure 1b and c. Available from URL:

       http://www.myvmc.com/uploads/VMC/DiseaseImages/779_Brachytherapy3.jpg&imgrefurl=http://www.myvmc.com/treatments/radi
       otherapy/&h=327&w=472&tbnid=Xwk3D6Fqk8NbrM:&docid=CT2qoPwf3h2AnM&ei=tWfEVuOsGsm9wAS45amICw&tbm=isch
       &ved=0ahUKEwij2-C75v7KAhXJHpAKHbhyCrEQMwgkKAgwCA [accessed 17 feb., 2016].

[8]   COMISSÃO NACIONAL DE ENERGIA NUCLEAR. Critérios de Exclusão, Isenção e Dispensa de Requisitos de Proteção Radiológica. Posição Regulatória 3.01/001. Available from http://appasp.cnen.gov.br/seguranca/normas/pdf/pr301_01.pdf

[9]   VICENTE R. Apresentação power point: Gestão de rejeitos radioativos na indústria, medicina e pesquisa - introdução -. São Paulo: Instituto de Pesquisas Energéticas e Nucleares, 2014.

[10]   ROSTELATO MECM, RELA PR, ZEITUNI CA, et al. Development and production of radioactive sources used for cancer treatment in Brazil. Nukleonika. 2008;53: 4.

[11]   COSTA OL, ZEITUNI CA, ROSTELATO MECM, et al. Influence of the profile of iridium-192 wire in measurements of quality control for use in brachytherapy. International Nuclear Atlantic Conference. Recife, PE, Brazil. 2013.

[12]   COMISSÃO NACIONAL DE ENERGIA NUCLEAR. Gerência de Rejeitos Radioativos de Baixo e Médio Níveis de Radiação. CNEN - NN- 8.01. Available from http://appasp.cnen.gov.br/seguranca/normas/pdf/Nrm801.pdf.

Computing the weights of criteria with interval-valued fuzzy sets for MCDM problems

Chen-Tung Chen[1], Kuan-Hung Lin[2], Hui-Ling Cheng[3]

[1]Department of Information Management, National United University, Taiwan
[2]Specialist 2, Quanta Computer Inc., 211, Wen Hwa 2nd Road, Kueishan, Taoyuan, Taiwan
[3]College of General Education, Hung Kuang University, Taiwan

Abstract— *In the real world, many influenced factors or criteria should be considered in the multiple criteria decision-making (MCDM) process. Face to the uncertain environment, the decision makers or experts always cannot express their opinions exactly in the decision-making process. Under this situation, interval-valued fuzzy sets are suitable used to represent the subjective judgments of decision makers. In this paper, the fuzzy AHP method is applied to compute the fuzzy weights of each criterion based on the interval-valued fuzzy sets. The proposed method can provide a more flexible way for decision makers to express their subjective opinions. A systematic method is presented here to compute the fuzzy weights of criteria for dealing with a MCDM problem. An example is presented to illustrate the computational procedure of the proposed method. Conclusions and future research direction will be discussed at the end of this paper.*

Keywords— *MCDM, Interval-valued fuzzy set, Fuzzy AHP.*

I. INTRODUCTION

Decision making is one of the most complex administrative processes in management area (Ashtiani et al., 2009). In some situations, because of time pressure, lack of knowledge, and the decision maker's limited attention and information processing capabilities (Xu, 2006), the decision maker cannot make the optimal decision easily. In fact, both qualitative and quantitative criteria should be considered simultaneously (Erol and Ferrell Jr, 2003) in the decision making process. It calls multiple criteria decision making (MCDM) process. Saaty (1980) proposed analytic hierarchy process (AHP) method for determining the weights of criteria in a MCDM problem by a hierarchical structure and systematization. According to the pairwise comparison result, the weight of each criterion can be computed for a hierarchical problem structure.

Due to the subjective judgments of the decision makers are often uncertain in determining the pairwise comparisons, the fuzzy AHP are proposed to overcome the drawback (Buckley, 1985; Buckley et al., 2001). The fuzzy AHP allowed the experts to use fuzzy ratios in place of exact ratios to make the pairwise comparisons. Based on the concepts, there are various fuzzy AHP methods have been developed such as the geometric mean method (Buckley, 1985), the Lambda-Max method (Csutora and Buckley, 2001), fuzzy logarithmic least squares method (Wang et al., 2006), the linear goal programming method (Jung, 2011), and the logarithmic fuzzy preference programming method (Rezaei et al., 2013).

However, it is often difficult for experts to exactly quantify their opinions as a crisp number in decision making process. Therefore, the reasonable way is to represent the degree of certainty by an interval (Ashtiani et al., 2009; Vahdani et al., 2010). The membership value express as an interval value can more fit the real world situations. Interval-valued fuzzy numbers have been applied in many fields such as R&D leader selection (Ashtiani et al., 2009), risk analysis (Wei and Chen, 2009), enterprise partner selection (Ye, 2010), traditional supplier selection (Chen, 2011), bus enterprise performance evaluation (Kuo and Liang, 2012) etc. Therefore, interval-valued fuzzy sets are suitable used to represent the fuzziness of membership value of subjective opinions. In this paper, a novel method is proposed by combining interval-valued fuzzy set with fuzzy AHP to determine the fuzzy weights of each criterion.

The organization of this paper is described as follows. In section 2, we will present some notations of basic definitions and operators such as triangular fuzzy number, α-cut of fuzzy number, defuzzified method and interval valued fuzzy sets. The proposed method will be discussed at the section 3. For illustrating the proposed method clearly, an example will be implemented. Finally, the conclusion and future research are summarized at the end of this paper.

II. FUZZY NUMBERS AND LINGUISTIC VARIABLES

2.1 Triangular fuzzy number

Triangular fuzzy number (TFN) can be defined as $\widetilde{T} = (l, m, u)$, where $l < m < u$. When $l > 0$, then $\widetilde{T}$ is a positive TFN

(PTFN) (Zimmerman, 1991; Chen, 2000). The membership function of positive TFN $\tilde{T}$ can be defined as follow.

$$\mu_{\tilde{T}}(x) = \begin{cases} \dfrac{x-l}{m-l}, & l \le x \le m \\ \dfrac{u-x}{u-m}, & m \le x \le u \\ 0, & otherwis \end{cases} \tag{1}$$

The α-cut is used to transform a fuzzy set into crisp interval (Zimmerman, 1991). The α-cut can define as follow.

$$\tilde{T}^{\alpha} = [(m-l)\alpha + l, u - (u-m)\alpha],\ 0 \le \alpha \le 1 \tag{2}$$

In a short, it can be represented as $\tilde{T}^{\alpha} = [T_l^{\alpha}, T_u^{\alpha}]$. If $\tilde{T}$ is a triangular fuzzy number, the area measurement method can be defined as (Yager, 1981).

$$I(\tilde{T}) = (I_L(\tilde{T}) + I_R(\tilde{T}))/2 \tag{3}$$

where the $I_L(\tilde{T})$ represents the area bounded by the left-shape function of $\tilde{T}$, the area include the x-axis, the y-axis, the horizontal line α= 1 and the line $L_{\tilde{T}}(x)$. The $I_R(\tilde{T})$ represents the area bounded by the right-shape function, the area include the x-axis, the y-axis, the horizontal line by α= 1 and the line $R_{\tilde{T}}(x)$.

2.2 Interval-valued fuzzy set

The definition of interval-valued fuzzy set can be described as follow (Ashtiani et al., 2009; Chen, 2012).

$$\tilde{T} = \{(x, [\mu_{\tilde{T}}^L(x), \mu_{\tilde{T}}^U(x)])\}$$

$$\mu_T^L, \mu_T^U : X \rightarrow [0,1], \forall x \in X, \mu_T^L < \mu_T^U \tag{4}$$

Yao and Lin (2002) presented the interval-valued triangular fuzzy number $\tilde{T} = [\mu_{\tilde{T}}^L, \mu_{\tilde{T}}^U] = [(ll, m, u; \rho), (l, m, uu; \lambda)]$ (shown as Fig. 1), where the μ_T^L denotes the lower limit degree of membership and the μ_T^U denotes the upper limit degree of membership, and the $\mu_T^L \subset \mu_T^U$.
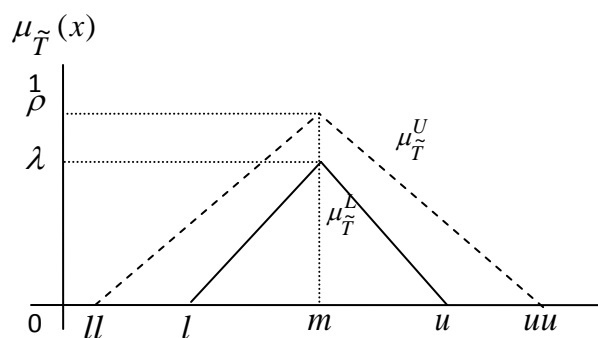
FIG. 1. INTERVAL-VALUED TRIANGULAR FUZZY NUMBER

In order to express the fuzziness more exactly, Ashtiani et. al., (2009) and Vahdani et. al (2010) used triangular interval-valued fuzzy numbers to represent the opinions of decision-makers. In many cases, an expert cannot exactly express the opinion by a crisp membership value. Under this situation, the interval-valued fuzzy number can express the uncertain opinion as an interval value. The membership value of x can be extended as $[\mu_{\tilde{T}}^L(x), \mu_{\tilde{T}}^U(x)]$. In this paper, we suppose that the lower limit degree of membership and upper limit degree of membership at m are equal to 1. It represents a normal interval-valued triangular fuzzy number (IFVNs).

Assume that there are two interval-valued triangular fuzzy numbers $\tilde{T}_1$ and $\tilde{T}_2$, where $\tilde{T}_1 = ([ll_1, l_1], m_1, [u_1, uu_1]$ and $\tilde{T}_2 = ([ll_2, l_2], m_2, [u_2, uu_2]$, the arithmetic operations can be calculated as follows (Kuo and Liang, 2012).

$$\tilde{T}_1 + \tilde{T}_2 = ([ll_1 + ll_2, l_1 + l_2], m_1 + m_2, [u_1 + u_2, uu_1 + uu_2]) \tag{5}$$

$$\tilde{T}_1 - \tilde{T}_2 = ([ll_1 - uu_2, l_1 - u_2], m_1 - m_2, [u_1 - l_2, uu_1 + ll_2]) \tag{6}$$

$$\tilde{T}_1 \otimes \tilde{T}_2 \approx ([ll_1 \otimes ll_2, l_1 \otimes l_2], m_1 \otimes m_2, [u_1 \otimes u_2, uu_1 \otimes uu_2]) \tag{7}$$

$$\tilde{T}_1 \div \tilde{T}_2 \approx ([ll_1 \div uu_2, l_1 \div u_2], m_1 \div m_2, [u_1 \div l_2, uu_1 \div ll_2]) \tag{8}$$

III. PROPOSED METHOD

Based on interval-valued fuzzy sets, the Lambda-Max method (Csutora and Buckley, 2001) is applied to compute the fuzzy weight of each criterion. The computational procedure is shown as follows.

Step 1. Establish hierarchical structure.

Establish a hierarchical framework of decision-making problem. Within the hierarchical framework, there may contain several criterion and sub-criterion.

Step 2. The expert uses the interval-valued linguistic variable to make the pairwise comparison in the criteria and sub-criteria levels.

Step 3. Using interval-valued fuzzy AHP, the weights of criteria and sub-criteria can be computed and expressed as interval-valued fuzzy numbers. The computational procedure of calculation steps as follow.

1) Construct the fuzzy positive reciprocal matrix.

The experts are allowed to use interval-valued fuzzy ratios (see Table 1) in place of exact ratios. The $\tilde{T}_{ij}$, $i \neq j$, can now be interval-valued fuzzy numbers in any positive reciprocal matrix. The fuzzy positive reciprocal matrix is defined as $\tilde{T} = [\tilde{T}_{ij}]_{n \times n}$, where $\tilde{T}_{ij} = 1, \ \forall i = j$, $\tilde{T}_{ji} = \dfrac{1}{\tilde{T}_{ij}}, \ \forall i, j = 1, 2, \dots, n$. If $\tilde{T}_{ij} = ([ll, l]m, [u, uu])$, then $\tilde{T}_{ij}^{-1} = ([uu^{-1}, u^{-1}], m^{-1}, [l^{-1}, ll^{-1}])$.

TABLE 1
LINGUISTIC VARIABLE FOR IMPORTANCE

Symbol	Linguistic variables	Interval-value fuzzy number
①	Extremely Equal Importance	([1,1] ,1, [1,1])
②	Equal Importance	([1,1] ,1, [2,3])
③	Intermediate values	([1,1] ,2, [3,4])
④	Weak Importance	([1,2] ,3, [4,5])
⑤	Intermediate values	([2,3] ,4, [5,6])
⑥	Essential Importance	([3,4] ,5, [6,7])
⑦	Intermediate values	([4,5] ,6, [7,8])
⑧	Very Strong Importance	([5,6] ,7, [8,9])
⑨	Intermediate values	([6,7] ,8, [9,9])
⑩	Absolute Importance	([7,8] ,9, [9,9])

2)   Compute the interval-valued fuzzy weights of criteria.

According to the Lambda-Max method (Csutora and Buckley, 2001), a sequence of fuzzy positive reciprocal matrix is applied to determine the relative weights of each criterion. The procedure of all calculation steps as follow.

   a.   Let α = 1, using α-cut to obtain $\tilde{T}_m^1 = [t_{ijm}]_{n \times n}$, it represent the decision-makers give the crisp positive reciprocal matrix $\tilde{T}$, and determine the fuzzy weight $\tilde{W}_m$, for $\tilde{W}_m = [W_{im}]$, $i = 1,2,...,n$.

   b.   Let α = 0, using α-cut to obtain the $\tilde{T}_u^0 = [t_{iju}]_{n \times n}$, $\tilde{T}_{uu}^0 = [t_{ijuu}]_{n \times n}$, $\tilde{T}_{ll}^0 = [t_{ijll}]_{n \times n}$, and $T_l^0 = [t_{ijl}]_{n \times n}$ in accordance with the fuzzy positive reciprocal matrix. Next, computing the fuzzy weights $\tilde{W}_{ll}, \tilde{W}_l$, $\tilde{W}_u$ and $\tilde{W}_{uu}$, where $\tilde{W}_{ll} = [W_{ill}]$, $\tilde{W}_l = [W_{il}]$, $\tilde{W}_u = [W_{iu}]$, and $\tilde{W}_{uu} = [W_{iuu}]$, $i = 1,2,...,n$.

   c.   In order to make sure the fuzzy weights are still normal fuzzy sets, the following formula is used to adjust these weights. First, we can determine lower bounds triangular fuzzy weights as $Q_l = \min\{\frac{W_{im}}{W_{il}} | 1 \le i \le n\}$ and

$$Q_u = \max\{\frac{W_{im}}{W_{iu}} | 1 \le i \le n\}.$$

The constants Q_l and Q_u are used to calculate the new weight as $W_{il}^* = Q_l \times W_{il}$ and $W_{iu}^* = Q_u \times W_{iu}$.

Second, we use the new fuzzy weight of lower limit and upper limit to determine the upper bounds triangular fuzzy weights as $Q_{ll} = \min\{\frac{W_{il}^*}{W_{ill}} | 1 \le i \le n\}$ and $Q_{uu} = \max\{\frac{W_{iu}^*}{W_{iuu}} | 1 \le i \le n\}$.

Then, the constants Q_{ll} and Q_{uu} are used to determine the new upper bounds triangular fuzzy weights as $W_{ill}^* = Q_{ll} \times W_{ill}$ and $W_{iuu}^* = Q_{uu} \times W_{iuu}$.

Finally, we can get the new fuzzy weights $W_{ll}^* = [W_{ill}^*]$, $W_l^* = [W_{il}^*]$, $W_u^* = [W_{iu}^*]$, and $W_{uu}^* = [W_{iuu}^*]$, for i=1,2,…n.

   d.   To integrate W_{ll}^*, W_l^*, W_m, W_u^* and W_{uu}^*, we can obtain the positive triangular fuzzy weight matrix for decision-makers. The fuzzy weights of i-th criterion can be represented as $\tilde{W}_i = ([W_{ill}^*, W_{il}^*], W_{im}, [W_{iu}^*, W_{iuu}^*])$.

   e.   Defuzzy the interval-valued fuzzy weights.

Applying the area measurement method (Yager, 1981) to transfer the interval-valued fuzzy number into interval value as $W_j = [W_j^{\min}, W_j^{\max}]$, where W_j represents the interval weight of criterion j, the $W_j^{\min} = \frac{W_{jll} + 2W_{jm} + W_{jl}}{4}$ represents the lower limit of the interval and $W_j^{\max} = \frac{W_{ju} + 2W_{jm} + W_{juu}}{4}$ represents the upper limit of the interval.

3)   Repeating the process of step (B), the weights of sub-criteria can be computed with respect to each criterion.

<div align="center">

IV.   NUMERICAL EXAMPLE

</div>

Suppose that a company desires to select an information system to serve their customer. A committee of three decision-makers (or experts) (p_1, p_2, p_3) has been formed to evaluate the importance of each criterion. After the reviewing by the committee, three criteria and nine sub-criteria (C_{11}, C_{12}, …, C_{33}) are considered to select the suitable vendor. The computation process of proposed method is shown as follows.

Step 1. According to the description, the hierarchical structure of problem is shown as Fig.2.

Step 2. Each expert uses the interval-value linguistic variables to make the pairwise comparisons among criteria as Table 2.
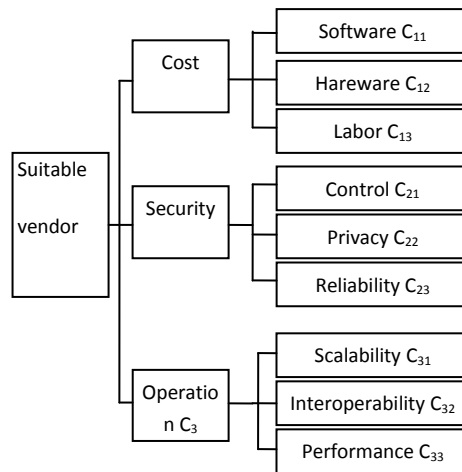
FIG. 2. THE EVALUATION STRUCTURE

TABLE 2
PAIRWISE COMPARISONS OF THREE EXPERTS

		C_1	C_2	C_3		C_{11}	C_{12}	C_{13}		C_{21}	C_{22}	C_{23}		C_{31}	C_{32}	C_{33}
P_1	C_1	①	③	⑤	C_{11}	①	⑥$^{-1}$	⑧$^{-1}$	C_{21}	①	④	⑥$^{-1}$	C_{31}	①	⑤$^{-1}$	③
	C_2	③$^{-1}$	①	②$^{-1}$	C_{12}	⑥	①	③$^{-1}$	C_{22}	④$^{-1}$	①	⑩$^{-1}$	C_{32}	⑤	①	⑨
	C_3	⑤$^{-1}$	②	①	C_{13}	⑧	③	①	C_{23}	⑥	⑩	①	C_{33}	③$^{-1}$	⑨$^{-1}$	①
		C_1	C_2	C_3		C_{11}	C_{12}	C_{13}		C_{21}	C_{22}	C_{23}		C_{31}	C_{32}	C_{33}
P_2	C_1	①	⑥	⑤	C_{11}	①	③$^{-1}$	②$^{-1}$	C_{21}	①	⑦$^{-1}$	④	C_{31}	①	⑤	③
	C_2	⑥$^{-1}$	①	③	C_{12}	③	①	⑤$^{-1}$	C_{22}	⑦	①	⑧	C_{32}	⑤$^{-1}$	①	⑧
	C_3	⑤$^{-1}$	③$^{-1}$	①	C_{13}	②	⑤	①	C_{23}	④$^{-1}$	⑧$^{-1}$	①	C_{33}	③$^{-1}$	⑧$^{-1}$	①
		C_1	C_2	C_3		C_{11}	C_{12}	C_{13}		C_{21}	C_{22}	C_{23}		C_{31}	C_{32}	C_{33}
P_3	C_1	①	⑦$^{-1}$	⑥$^{-1}$	C_{11}	①	④	③	C_{21}	①	⑤	⑨	C_{31}	①	③$^{-1}$	⑨$^{-1}$
	C_2	⑦	①	③$^{-1}$	C_{12}	④$^{-1}$	①	⑤	C_{22}	⑤$^{-1}$	①	③	C_{32}	③	①	⑤$^{-1}$
	C_3	⑥	③	①	C_{13}	③$^{-1}$	⑤$^{-1}$	①	C_{23}	⑨$^{-1}$	③$^{-1}$	①	C_{33}	⑨	⑤	①

Step 3. Compute the interval-valued fuzzy weights of criteria.

i.   The fuzzy positive reciprocal matrix is shown as Table 2.

ii.   According to the fuzzy reciprocal matrix for three criteria, the criteria weights of the expert P_1 can be computed as follows

(1)   Let α = 1, using α-cut to obtain $\tilde{T}_m^1 = \begin{bmatrix} 1 & 2 & 4 \\ 1/2 & 1 & 1 \\ 1/4 & 1 & 1 \end{bmatrix}$, and determine the fuzzy weight as $W_m = [0.584, 0.232, 0.184]$.

(2)   Let α = 0, using α-cut to obtain the positive reciprocal matrix as $\tilde{T}_{ll}^0 = \begin{bmatrix} 1 & 1 & 2 \\ 1/4 & 1 & 1/3 \\ 1/6 & 1 & 1 \end{bmatrix}$, $\tilde{T}_l^0 = \begin{bmatrix} 1 & 1 & 3 \\ 1/3 & 1 & 1/2 \\ 1/5 & 1 & 1 \end{bmatrix}$,

$\tilde{T}_u^0 = \begin{bmatrix} 1 & 3 & 5 \\ 1 & 1 & 1 \\ 1/3 & 2 & 1 \end{bmatrix}$, $\tilde{T}_{uu}^0 = \begin{bmatrix} 1 & 4 & 6 \\ 1 & 1 & 1 \\ 1/2 & 3 & 1 \end{bmatrix}$. Next, we can compute the fuzzy weights of each matrix as

$W_{ll}^0 = [0.570, 0.189, 0.241]$, $W_l^0 = [0.579, 0.204, 0.217]$, $W_u^0 = [0.553, 0.239, 0.208]$,

$W_{uu}^0 = [0.565, 0.205, 0.230]$.

(3)   In order to make sure the weights are still normal fuzzy sets, first we adjust lower bounds triangular fuzzy weights and find the constants $Q_l = 0.849$ and $Q_u = 1.056$. And then, obtain the new weights $W_l^* = [0.491, 0.173, 0.184]$ and

$W_u^* = [0.584, 0.253, 0.220]$. Next we adjust upper bounds triangular fuzzy weights, and find the constants $Q_{ll} = 0.763$ and $Q_{uu} = 1.236$. Then, obtain the new weights $W_{ll}^* = [0.435, 0.144, 0.184]$ and $W_{uu}^* = [0.699, 0.253, 0.285]$.

(4)   To combine the weight matrix $[W_{ll}^*, W_l^*], W_m, [W_u^*, W_{uu}^*]$, we can obtain the interval-valued fuzzy weight of expert P_1 for three criteria as

$$\widetilde{W}_1 = ([0.435, 0.491], 0.584, [0.584, 0.699]) \quad \widetilde{W}_2 = ([0.144, 0.173], 0.232, [0.253, 0.253])$$

$$\widetilde{W}_3 = ([0.184, 0.184], 0.184, [0.220, 0.285]).$$

(5)   Integrate the interval-valued fuzzy weights of three experts; the area measurement method is applied to transform the interval-valued fuzzy set into interval value. The weights of criteria can be computed as $W_1 = [0.422, 0.454]$, $W_2 = [0.256, 0.264]$ and $W_3 = [0.287, 0.303]$.

iii.   The computational procedures of sub-criteria weights are illustrated as step B and the result can be shown as Table 3.

TABLE 3
THE WEIGHTS OF SUB-CRITERIA

Sub-criteria	Weights	Sub-criteria	Weights	Sub-criteria	Weights
C_{11}	[0.261,0.283]	C_{21}	[0.347,0.366]	C_{31}	[0.267,0.285]
C_{12}	[0.299,0.316]	C_{22}	[0.259,0.341]	C_{32}	[0.409,0.424]
C_{13}	[0.416,0.439]	C_{23}	[0.289,0.307]	C_{33}	[0.308,0.317]

V.   CONCLUSIONS AND FUTURE RESEARCH

In general, many quantitative and qualitative factors will influence the expert to make a decision in the decision-making process. Under this situation, decision makers always difficult to express their opinions by the membership value exactly. Therefore, the interval-valued fuzzy sets are suitable to express the subjective opinion of each decision maker in a decision environment. In this paper, the fuzzy AHP method is extended to compute the fuzzy weights of all criteria based on the interval-value fuzzy sets. Applying the proposed method, a systematic way is presented here to compute the fuzzy weights of criteria. In the future, a decision analysis system will be designed and developed based on this proposed method to reduce the computational time and improve the decision-making quality.

ACKNOWLEDGEMENT

REFERENCES

[1]   B. Ashtiani, F. Haghighirad, A. Makui and G. A. Montazer, "Extension of fuzzy TOPSIS method based on interval-valued fuzzy sets," Applied Soft Computing, Vol.9, 2009, pp.457–461.

[2]   J. J. Buckley, "Fuzzy hierarchical analysis," Fuzzy Sets and Systems, Vol.17, 1985, pp.233–247.

[3]   J. J.Buckley, T. Feuring, and Y. Hayashi, "Fuzzy hierarchical analysis revisited," Fuzzy Sets and Systems, Vol.129, 2001, pp. 48-64.

[4]   C. T. Chen, "Extensions of the TOPSIS for group decision-making under fuzzy environment," Fuzzy sets and systems, Vol.114, No. 1, 2000, pp.1-9.

[5]   T. Y. Chen, "Optimistic and pessimistic decision making with dissonance reduction using interval-valued fuzzy sets," Information Sciences, Vol.181, No.3, 2011, pp.479-502.

[6]   T. Y. Chen, "Comparative analysis of SAW and TOPSIS based on interval-valued fuzzy sets: Discussions on score functions and weight constraints," Expert Systems with Applications, Vol.39, No.2, 2012, pp.1848-1861.

[7]   R. Csutora and J. J. Buckley, "Fuzzy hierarchical analysis: the Lambda-Max method," Fuzzy Sets and Systems, Vol.120, 2001, pp.181-195.

[8]   I. Erol and Jr, W. G. Ferrell, "A methodology for selection problems with multiple, conflicting objectives and both qualitative and quantitative criteria," International Journal of Production Economics, Vol.86, No.3, 2003, pp.187-199.

[9]   H. Jung, "A fuzzy AHP–GP approach for integrated production-planning considering manufacturing partners," Expert systems with Applications, Vol.38, No.5, 2011, pp.5833-5840.

[10] M. S. Kuo and G. S. Liang, "A soft computing method of performance evaluation with MCDM based on interval-valued fuzzy numbers," Applied Soft Computing, Vol.12, No.1, 2012, pp.476-485.

[11] J. Rezaei, R. Ortt and V. Scholten, "An improved fuzzy preference programming to evaluate entrepreneurship orientation," Applied Soft Computing, Vol.13, No.5, 2013, pp.2749-2758.

[12] T. L. Saaty, "The Analytic Hierarchy Process," New York: McGraw-Hill, 1980.

[13] B. Vahdani,H. Hadipour, J. S. Sadaghiani and M. Amiri,"Extension of VIKOR method based on interval-valued fuzzy sets," The International Journal of Advanced Manufacturing Technology, Vol.47, No.9-12, 2010, pp. 1231-1239.

[14] Y. M. Wang, T. Elhag and Z. Hua, "A modified fuzzy logarithmic least squares method for fuzzy analytic hierarchy process," Fuzzy Sets and Systems, Vol.157, No.23, 2006, pp.3055-3071.

[15] Z. S. Xu, " Induced uncertain linguistic OWA operators applied to group decision making," Information Fusion, Vol.7, 2006, pp.231-238.

[16] R. R. Yager, "A procedure for ordering fuzzy subsets of the unit interval," Information Sciences, Vol.24, 1981, pp.143-161.

[17] J. S. Yao and F. T. Lin, "Constructing a fuzzy flow-shop sequencing model based on statistical data," International Journal of Approximate Reasoning, Vol.29, 2002, pp.215-234.

[18] F. Ye, "An extended TOPSIS method with interval-valued intuitionistic fuzzy numbers for virtual enterprise partner selection," Expert Systems with Applications, Vol.37, No.10, 2010, pp.7050-7055.

[19] H. J. Zimmerman, "Fuzzy Set Theory and its Applications," Boston: Kluwer Academic Publishers, 1991.

Examination of essential oils used in PLA with GC-MS method

Kinga Tamasi[1], Gabriella Zsoldos[2]

Institute of Ceramics and Polymer Engineering, University of Miskolc, Hungary

Abstract— *Upto date, many experiments have been carried out successfully in producing and using essential oil-treated biodegradable polylactid acid (PLA), but the examinations revealed. That essential oils, theoretically consisting the same composition, (like cinnamonoil, majoram oil, orclaryoil) crystallize differently in the PLA base, weakening its mechanical, optical, and thermal properties. The aim of the experiment is to define the exact components with a Gas-Chromatography instrument with MS-detector. It has been found that among the compounds detected in different cinnamon oil samples, there are indeed other potentially harmful components, such as serpentines, alcoholic derivatives, mineral oils and phthalic acid esters, which have caused the condition to deteriorate.*

Keywords— *biopolymer, essential oils, GC-MS, phtalic acid esters, PLA.*

I.   INTRODUCTION

One of the major environmental problems of the 21st century is non-degradable polymers, which are manufactured in huge amounts all over the world because their cheap prices and their easy use make our lives easier. In Hungary, the amount of usable plastic waste is increasing every year. Nowadays, the primary aim of our polymer research is to produce polymers that meet the requirements of this age, that are biodegradable, and compatible with the tissues of the human body.

In one of our former research we compared the mechanical, optical, and thermical properties of samples containing different antimicrobial additives, a base material, and a polyoleicacid type suitable for foil making. It was necessary for the additives to not weaken the material's above-mentioned properties. The research revealed that essential oils, theoretically consisting of the same composition (like cinnamon-oil, majoram-oil, orclary-oil) crystallize differently in the PLA base, making differences in its mechanical, optical, and thermal properties.

II.   MATERIALS

2.1   Polylacticacid (PLA)

Biopolymers can be sorted based on their raw materials and the method of production. There are three different types of biopolymers: polysaccharide- based (starch, cellulose), protein-based (collagen, gelatin, casein, keratin), and polymers with vegetal origin (wheat gluten, maize casein, soy protein). These function as raw materials for long-used natural based plastics.

An important group of biopolymers are the polymers made by monomers produced by fermentation. These include polylactides such as polylactic acid and poly-hydroxy-alcanoates. Polyester amide, polyester urethane, polyglycolic acid and polylactides are biodegradable synthetic polymers, but we can also find degradable polymers consisting of organic or synthetic components such as the starch/PVAL, or starch/PLA coupling. The polylactic acid, as the material that meets the above-mentioned requirements has been at the center of researches for decades, and the analysis of its reactions in the literature is really important. PLA is a biodegradable, thermoplastic polymer, which can be produced from renewable raw materials. Due to its properties, it has proven to be suitable to make deep-drawing products (for example glasses, or fruit boxes) and can also be used in packaging technologies. The production of lactic acid (LA) based on crops has revolutionized the production of PLA, thus opening the way for the production of custom plastics and packaging materials. Nowadays, this technology represents 80% of the used methods. The quantitative distribution of PLA produced in the world is shown in Figure 1:
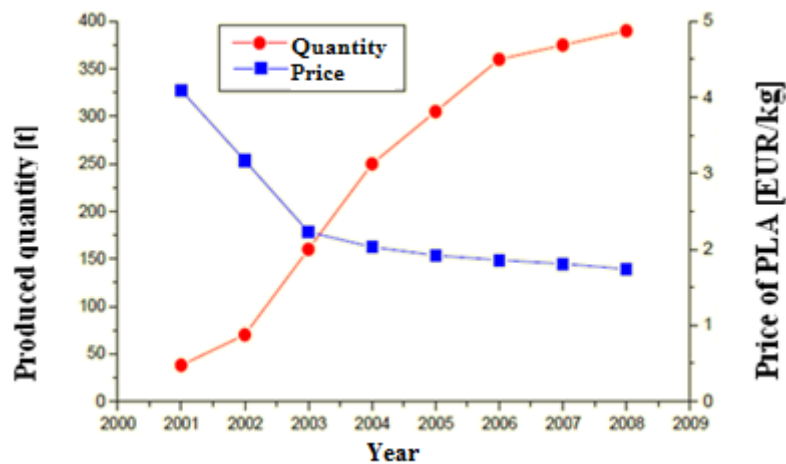
FIGURE 1. The relationship between the quantity (EUR / kg) of PLA produced from 2000 up to 2009. [1]

Lactic acid (also known as 2-hydroxypropanoic acid, C3H6O3) is an organic acid that play a role in many biochemical processes (Scheele, 1780.) The molecule consists of a carboxyl group and a hydroxyl group, this way creating an alpha hydroxy-acid (AHA). A proton from a carboxyl group leads to solution, and the resulting ion is called lactate. It is hygroscopic, and highly miscible with water or ethanol. A chiral molecule having an asymmetric carbon atom has two distinct spatial isomers (Figure 2). One of them is L - (+) - lactic acid, while its mirror image is called D (-) - lactic acid. Only the L – (+) – lactic acid is significant biologically, typically a product of anaerobic metabolisms. By hydrogenating the pyruvic acid, the following isomers may be formed:
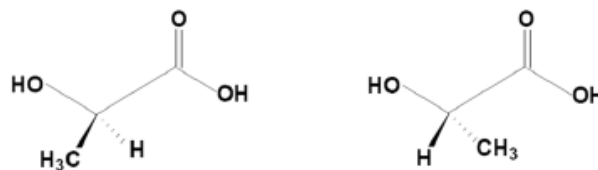
FIGURE 2. Two isomers of lactic acid: D - (-) lactic acid and L - (+) lactic acid [2]

D-lactic acid occurs in natural yeast and sour cabbage, while L-lactic acid can be found in beef and lump milk. Two lactic acid molecules form a cyclic compound in water, which is the dimer of lactic acid: lactide, which exists in three spatial forms due to an asymmetric carbon atom in lactic acid [3]:
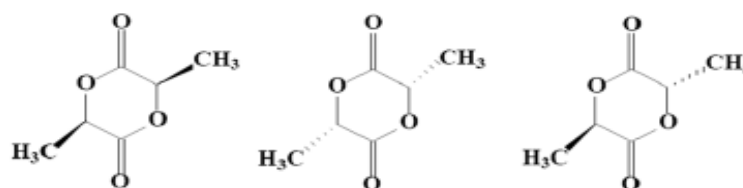
FIGURE 2. Dimers of lactic acid [3]:
A. L-lactide **B.** D-lactide and **C.** Meso-lactide

The structure and properties of PLA. PLA belongs to the group of polylactides which is a linear aliphatic polyester.The repeating unit is lactic acid (Figure 3.), its physical properties are influenced by many factors: structure, molecular characteristics, crystallinity, morphology and chain orientation. Physical, chemical and biological properties determine its usability.
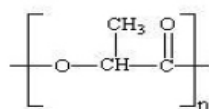
FIGURE 3. Lactic acid, the monomer of PLA [3]

The physical properties of PLA are improving if the material is orientated, in case of making a fiber, a two-way film or a deep drawn product. Today, a monomer mixture is used, which consists mostly of a mixture of L, and D-lactic acid in ~ 0.1 to 10 % content. The mechanical properties, the crystallinity, the degradability of the PLA can be adjusted within the ratio of L- and D-lactic acid (higher crystallinity PLA decreases slower). If PLA contains less than 8 % D-lactic acid, it partially crystallizes by frothing, tempering or stretching. Strength and heat resistance increase with crystallinity. When the D-isomer ratio decreases in the chain, the melting point of the PLA increases and could reach 170-190 ° C. PLA's surface tension is 38 N/m, therefore the printing or metal coating of the material is relatively simple. Of course, in the case of a particular structure, the conditions of manufacturing also significantly influence the properties of the polymers.

2.2   Essential oils

Essential oils extracted from plants, there have antibacterial effects and each other has other beneficial (medicinal) effects depending on their composition. There is also a difference between the microbial effect of essential oils, many examples of which are found in the literature [4, 5, 6, 7, 8]. Essential oils can consist of more than 50 ingredients, including up to 85 % of the main components, while some minor components can only be traced. Essential oils are mainly composed of terpenes and terpenoids (oxygen-containing terpenes): monoterpenes (C10) or sesquiterpenes (C15) but in smaller amounts diterpenes (C20) and triterpenes can also be found (Figure 4.). In addition to the terpenes, other major constituents may be the various low molecular weight aliphatic and aromatic compounds, e.g. hydrocarbons, acids, alcohols, aldehydes, lactones and sulfur-containing volatile compounds. The amount and proportion of components may vary depending on weather, geographical distribution, and individual variation within plants (Burt, 2004) [6, 7, 8].
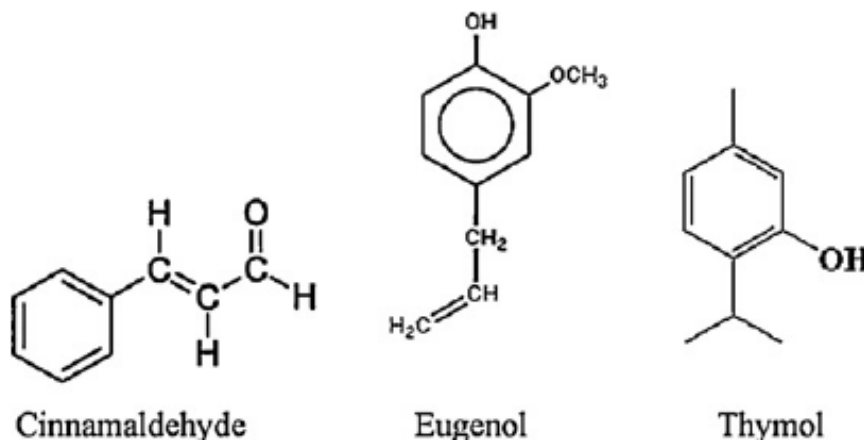
FIGURE 4. The structure of some essential oil components [9]

In the essential oils approx. 90% monoterpenes are found as the main ingredient. Monoterpenes are formed by the condensation of two isoprene molecules and can be classified into several groups based on their diverse functional groups: hydrocarbons, which may also be cyclically structured (terpines, pinenes, sabin); alcohols (linalool, geraniol); aldehydes (geranium, neral); ketones (carved, camphor); esters (linalyl acetate), phenols (thymol, carvacrol). Components containing aromatic rings, such as cinnamaldehyde, cinnamon alcohol, eugenol, estragol, etc., are less common (Bakkali et al., 2008).

2.3   Chemical composition of controlled oil samples

A.   Cinnamon oil (Aetheroleum cinnamomi)

Obtained by distillation of water or steam through Ceylon cinnamon tree belonging to the Lauraceae family (Lauraceae) (Cinnamomumverum, syn.: C. ceylanicum) inner bark and Chinese cassia cinnamon (C. aromaticum, syn .: C. cassia) Unpurified bark where the yield of the oil is around 0.5 to 4.0%. In addition to the bark, the cinnamon leaf leaves and leafy shoots also produce essential oils, the main components of cinnamon aldehyde and eugenol, the total amount of compounds for bark oils: 65-75% or 5-18%, and 3-5% in leaf (cinnamon aldehyde) or 70-90% (eugenol).

B.   Majoram oil (Aetheroleum majoranae)

Majoranna oil is extracted from the dry shoots of majoranna (Origanummajorana) by steam distillation. Pale yellow, yellowish or amber, strongly spicy and penetrating. Component: terpinen-4-ol (38.4%), cis-szabinene hydrate (15.0%), p-cymol (7.0%) and γ-terpinene (6.9%) [10].

C.   Musk oil (Salvia sclarea)

It is obtained from the musk oxide by steam distillation. In addition to the cosmetics industry, it is also used in the food industry and in medicine because it has an antiseptic effect. Component: Linalil-acetate and linalool make up nearly 80%, approx. 10% sclararene and a much smaller amount of camphor, mircene, geraniol, caryophylline, germacle, terpinol, peacock, pineapple and borneol. [11]

D.   Ginger oil (Aetheroleumzingiberis)

Obtained from the root gum by steam distillation. It is a spicy, sweet, slightly lemon, with a spicy aroma. Its color is yellow, pale. Component: Sesquiterpenes: α- and β-zingiberen (30-40%), turmeric (18%), bizabenol (10-15%) [11].

III.   GC-MS ANALYSIS METHOD

The purpose of the chromatographic procedures is to ensure the qualitative and quantitative determination of the volatile organic matter content of the samples. Separation is based on the re-distribution of components between two phases, and chromatographic procedures differ from other distribution-based separation methods (eg liquid-liquid extraction, distillation) so that one of the phases involved in separation is in motion (mobile phase), the other phase is stationary (stationary phase). The chromatogram is generated by the eluting components of the column to represent the intensity of the signal induced in the detector by the time.
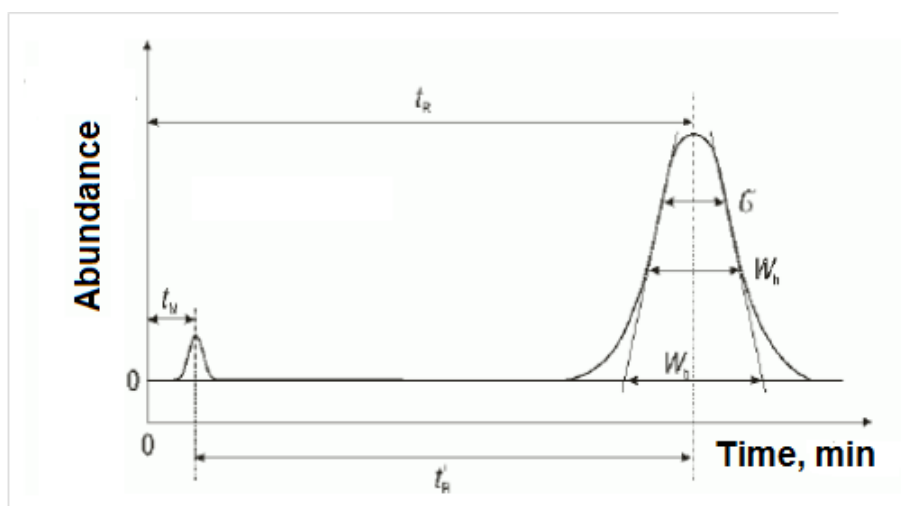
FIGURE 5. An ideal chromatogram

3.1   Description of gas chromatography processes

Retention time (Rt) of a given component is the time from injection to detection (peak maximum). All components spend the same time in the carrier gas. Components that do not interact with the stationary phase simply pass through the carrier gas on the column, their passage time is the dead time (tm) determined by the column length and the flow rate of the carrier gas which is dependent on the temperature of the column. The partition coefficient (K):

$$K = \frac{C\ (stationary\ )}{C\ (carrier\ )} \qquad\qquad (1)$$

Where:

- K: the partition ratio of a given component,
- $C_{stationary\ phase}$: equilibrium concentration of a given component in the stationary phase,
- $C_{carrier}$: equilibrium concentration of a given component in the carrier gas.

The partition coefficient characterizes the affinity of each component to the stationary phase at a given temperature. The higher the K value for a given component the longer the time is spent in the stationary phase, the greater its retention time. So, injected at once 59 components reach the end of the column in different times, so separation can occur. While the time

spent in the carrier gas can be characterized by dead time, the time spent in the stationary phase is given by the corrected retention time (tR '):

$$tR^{'} = tR - Tm \tag{2}$$

In the chromatogram the quality information provided by retention times and the volume is carried by the areas under the peaks. To determine the quality of each component, the retention data is sufficient only if the sample profile of the sample is known (in our case it contains explosive substances but no interfering components). If we do not have such information, the identification of the components can be done only by using suitable detectors (eg MS) [12].

IV.   RESULTS

The relationship between the concentration of the samples and the analytical signal (peak area) is determined by calibration. The area of the peaks of the chromatogram shows a linear relationship with the amount of material in the detector generally, increasing the amount of material to saturation. For quantitative analysis, usually the straight section of the curve (dynamic range of the detector) can be applied. Since the sensitivity of the detectors (the slope of the calibration line) is different for each material, the calibration should be performed for each component to be determined. As expected, there were significant differences in the composition of cinnamon oil samples, which can be seen in Figures 6 and 7:
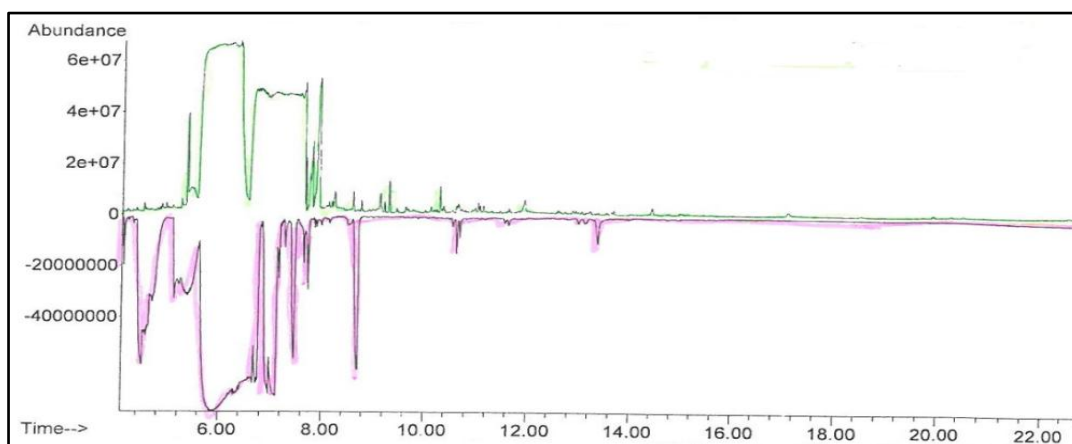
FIGURE 6. Comparative chromatogram of cinnamon oil samples

It can be stated that the chromatograms differ significantly of sample 1 of cinnamon oil (green line) and cinnamon oil sample 2 from the 7th minute, which means that their chemical composition is different. After the qualitative determination, the components detected in the samples were compared for given retention times. Alignment until t = 5.81 min retention time was observed, indicating the presence of cinnamaldehyde in all four samples. It can be said that the main component is present in the system. There are now significant differences in the chromatogram, for example at t = 6.94 minutes in the cinnamon oil sample 2, 2-propen-1-ol and at t = 8.50 min. benzyl benzoate was detected, while in cinnamon oil sample 1 none of them was detected at all. It can be assumed that they are components that can cause the crystallization difference.
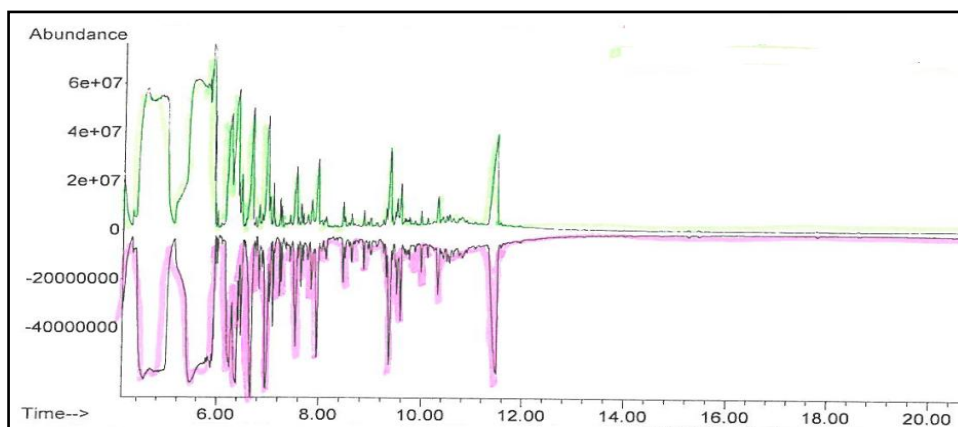
FIGURE 7. Additional chromatograms of cinnamon oil samples

V.   SUMMARY

The GC-MS chromatographic analysis of the PLA biopolymer containing different essential oils showed that there was a significant difference between the composition of the cinnamon oil samples and not between the muscatel sage and the ginger oil samples. The measurement results were not influenced by the sample preparation method, since the essential oils were naturally solved so that the decomposition could be more easily made in the system and it was easier to detect the components that formed the oils. In addition to the components already disclosed, the following compound, such as benzyl benzoate *(Figure 8),* which is used as a solvent for perfume for tobacco, as well as for improving the plasticity of polymers and cellulose, has been detected.
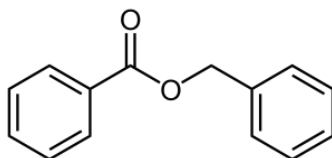
FIGURE 8. Structural Formula for Benzylbenzoate [13]

ACKNOWLEDGEMENTS

REFERENCES

[1] Tamási K.: Antibakteriális adalékanyagok (illóolajak, nizin és PHMB) hatása a politejsav mechanikai és optikai tulajdonságaira. Szakdolgozat, Miskolci Egyetem, 2011.

[2] Furka Á.: Szerves kémia. Nemzeti Tankönyvkiadó, Budapest 1998.

[3] Guba F. : Orvosi biokémia. Medicina, Budapest 1988.

[4] S.Inouyea, T. Takizawa, H. Yamaguchi: Antibacterialactivity of essentialoils and their major constituents again strespiratory tract pathogens by ganeous contact. Journal of Antimicrobial Chemotherapy, Vol. 47, Issue 5, Pg. 565-573. 2001.

[5] C. F. Carson, T. V. Riley: Antimicrobialactivity of the major components

[6] S.Prabuseenivasan, M. Jayakumar, S. Ignacimuthu: In vitro antibacterialactivity of someplantessential oils. BMC Complementary and AlternativeMedicine,Issue 6, Pg. 392006.

[7] O.Mejlholm, P. Dalgaard: Antimicrobialeffect of essentialoilstheseafoodspoilagemicro-organism Photobacterium phosphoreum in liquidmedia and fishproducts. Journal of AppliedMicrobiology, Vol.34, Issue 1, Pg. 27-31, 2002.

[8] Tserennadmid R, Takó M, Galgóczy L, Papp T, Vágvölgyi Cs, Gerő L, Krisch J: Antibacterialeffect of essentialoils and interactionwithfoodcomponents.Central European Journal of Biology,Issue5, Pg. 641-648. 2010.

[9] Rentsenkhand T.: Illóolajok és kombinációk hatása élelmiszerromlást okozó mikroorganizmusokra, PhD. értekezés, Szegedi Tudományegyetem, Pg. 8. 2010.

[10] **R. R. Vera*** **and J. Chane-Ming.:** Composition of theessentialoil of marjoram (Origanummajorana L.) from Reunion Island. References and further reading may be available for this article. To view references and further reading you must purchase this article.FoodChemistry, Vol. 66, Issue 2, Pg.143-145, 1999.

[11] www. wikipedia.hu, 2011.04.02.

[12] Tamási K.: Sporteszközök vizsgálata ED-XRF spektrométerrel és GC-MS kromatográffal. Diplomamunka, Miskolci Egyetem, 2014.

[13] https://hu.wikipedia.org/wiki/Benzil-benzo%C3%A1tv (2014.05.29).

Theory of Dipole-Exchange Spin Excitations in a Spherical Ferromagnetic Nanoshell, consideration of the Boundary Conditions

V.V. Kulish

Department of general and experimental physics, National Technical University of Ukraine "Igor Sikorsky Kyiv Polytechnic Institute", 37 Peremogy prosp., 03056, Kyiv, Ukraine

Abstract— The paper continues study of dipole-exchange spin excitations in a spherical ferromagnetic nanoshell started by the author in the previous paper. The proposed model considers the magnetic dipole-dipole interaction, the exchange interaction, the anisotropy effects and the damping effects. A new method of obtaining the values' spectrum of the wavenumbers for the investigated excitations – the method based on the application of general boundary conditions – is proposed. Consequently, the values' spectra of the wavenumbers and the frequencies of the investigated excitations are obtained in addition to the previously obtained dispersion law. Exploitation of the above-mentioned method essentially extends the area of application of the obtained results compared to the previous paper. The obtained dependence of the wavenumber on the angular mode number is shown to be weak and close to linear. On the other hand, the obtained dependence of the wavenumber on the radial mode number is shown to be essential. The obtained spectrum of wavenumbers' values is shown to transform to a quasi-one-dimensional form once specific conditions are satisfied; these conditions are found.

Keywords— Magnetic dynamics, Spin excitation, Dipole-exchange theory, Ferromagnetic nanosystem, Spherical nanoshell.

I. INTRODUCTION

Nowadays, a rapidly developing sub-field of information technologies is dedicated to creating data storage, transfer and processing devices based on the applications of spin waves in nanosystems [1-3]. One of the key problems for developing such technologies is theoretical modeling of spin-wave processes in these nanosystems. Such modeling is required not only for direct applications of spin waves, but also for synthesizing materials with preset magnetic properties as these properties are often influenced by spin-wave processes. This modeling, in turn, requires deeper understanding of the corresponding processes in magnetic nanosystems. In the proposed paper, one of the problems of the above-described type is solved.

As it has been shown by numerous studies (see, e.g., the review [4]), properties of nanosystems – in particular, spin-wave properties – depend essentially on their size and shape. Unfortunately, a general theory of spin waves in magnetic nanosystems has not been created at the moment. Therefore, spin waves in nanosystems of different geometries are studied separately. Among the variety of magnetic nanosystems of different configurations, a special class is represented by shell-type ferromagnetic nanosystems (nanoshells, nanotubes and others). These nanosystems exhibit unique – not inherent to traditional continuous nanosystems – properties that are prospective for numerous technical applications. In particular, magnetic properties of such nanosystems can be regulated more flexibly than properties of corresponding continuous nanosystems [5]. However, such nanosystems remain poorly researched at the moment. In particular, study of spin-wave processes in synthesized recently ferromagnetic nanoshells [5-7] represent and actual topic of research.

The paper continues the study of dipole-exchange spin excitations in a spherical ferromagnetic nanoshell started by the author in the paper [8]. The magnetic dipole-dipole interaction, the exchange interaction, the anisotropy effects and the damping effects are considered. In the previous paper of the author [8], a dispersion relation for the above-described spin excitations has been obtained. However, for complete description of such excitations, this relation should be complemented by a values' spectrum of the wavenumber (in particular, this allows to obtain the spectrum of values of the spin excitations' frequencies). For the most nanosystems, that represents more challenging task than just finding the dispersion relation. In the paper [8], the above-mentioned spectrum has been obtained only for a very specific particular case (the material outside the nanoshell has been assumed to be a high-conductivity metal) thus essentially limiting the area of application of the entire obtained result. The proposed paper overcomes this limitation by applying a different – essentially more general – method of obtaining the above-mentioned spectrum. As a result, the values' spectrum of the spin excitation wavenumbers and

frequencies – that can be applied for much wider range of nanoshell configurations – are obtained for an essentially more general case of the nanoshell configuration. The obtained spectrum of wavenumbers is shown to transform to a quasi-one-dimensional form once specific conditions are satisfied; these conditions are found.

II.   PROBLEM STATEMENT: MODEL DESCRIPTION

Let us consider a spherical ferromagnetic nanoshell composed of a uniaxial ferromagnet of the "easy axis" type. Let us denote the ferromagnet parameters as follows: the exchange constant α, the uniaxial anisotropy parameter β, the gyromagnetic ratio γ, the ground state magnetization $\vec{M}_0$ (is considered constant in absolute value inside the shell), the dissipation parameter α_G (the Hilbert term is used for consideration of the dissipation). We assume that the external magnetic field is absent, and the easy magnetization axis – and, therefore, the ground state magnetization – is directed radially inside the nanoshell. Let us denote the internal shell radius a and the external radius b (see Fig.1.).
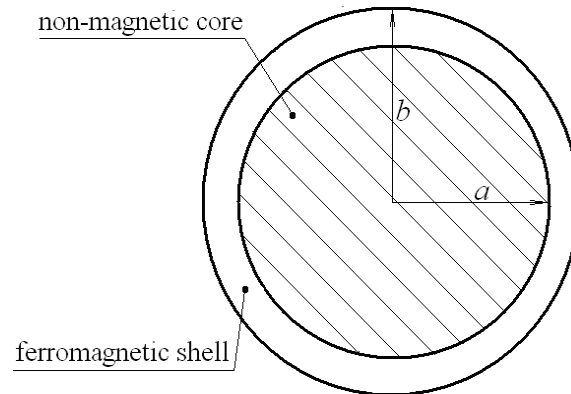

FIGURE 1. The spherical nanoshell that is studied in the paper.

Let us consider a spin wave (spin excitation in a form of standing wave, to be exact) propagating in the nanoshell so that the magnetization $\vec{m}$ and the magnetic field $\vec{h}$ of the wave are small perturbations of the overall magnetization $\vec{M}$ and the magnetic field inside the ferromagnet $\vec{H}^{(i)}$, correspondingly (linear wave). Thus, the relations $|\vec{m}| << |\vec{M}_0|$, $|\vec{h}| << |\vec{H}_0^{(i)}|$ fulfill, where $\vec{H}_0^{(i)}$ is the ground state internal magnetic field (so that $\vec{M} = \vec{M}_0 + \vec{m}$, $\vec{H}^{(i)} = \vec{H}_0^{(i)} + \vec{h}$). Let us find the dispersion relation and the wavenumber values' spectrum for such linear spin excitations.

For the investigated spin excitation, let us use the magnetostatic approximation, assuming that the magnetic potential Φ exists and, therefore, $\vec{h} = -\nabla\Phi$. After introducing amplitudes $\vec{m}_0$, $\vec{h}_0$ for the magnetization and the magnetic field perturbations, correspondingly (so that $\vec{m}(\vec{r},t) = \vec{m}_0(\vec{r})\exp(i\omega t)$, $\vec{h}(\vec{r},t) = \vec{h}_0(\vec{r})\exp(i\omega t)$, where ω is the wave frequency), we can write down the following relations for the magnetic potential: $\vec{h}_0 = -\nabla\Phi_0$, $\Phi = \Phi_0 \exp(i\omega t)$. The outside material is considered non-magnetic so the relations $\vec{m}_0 = 0$, $\Delta\Phi_0 = 0$ fulfill outside the investigated ferromagnet. After combining the linearized Landau-Lishitz equation with the Maxwell equation $div\vec{H}^{(i)} = -4\pi div\vec{M}$ and eliminating the magnetization amplitude in the resulting system of equations, the following equation for the magnetic potential of the investigated waves can be obtained:

$$\left(\frac{\omega^2}{\gamma^2 M_0^2} - \left(\tilde{\beta} - i\frac{\alpha_G \omega}{\gamma M_0} - \alpha\Delta \right)\left(\tilde{\beta} - i\frac{\alpha_G \omega}{\gamma M_0} + 4\pi - \alpha\Delta \right) \right)\Delta\Phi_0 + 4\pi\left(\tilde{\beta} - i\frac{\alpha_G \omega}{\gamma M_0} - \alpha\Delta \right)\frac{1}{r^2}\frac{\partial}{\partial r}\left(r^2 \frac{\partial\Phi_0}{\partial r} \right) = 0 \quad (1)$$

(see [8]), here the spherical coordinates (r,θ,φ) are used and the value $\tilde{\beta} = \beta + H_0^{(i)}/M_0$.

In order to obtain the values' spectrum of wavenumbers of the investigated spin excitation, let us use the boundary conditions for the magnetic field. Assuming that standard boundary conditions fulfill for the ground state magnetization and the magnetic field, we can write down $b_{1n}=b_{2n}$, $h_{1\tau}=h_{2\tau}$ on the boundary of the considered ferromagnet (here medium 1 is the ferromagnet, medium 2 is the external medium, n means normal and τ – tangential to the boundary vector component, $\vec{b}$ is the magnetic induction vector of the wave). For the vectors $\vec{h}$, $\vec{m}$ we obtain $h_{1n}-h_{2n}=4\pi m_n$, $h_{1\tau}=h_{2\tau}$ (as the outside

environment is non-magnetic). For the magnetic potential, these conditions together with the condition of the potential continuity on the ferromagnet boundary can be written in the following form:

$$
\begin{cases}
\Phi_0\big|_1 = \Phi_0\big|_2 \\
\left(\nabla\Phi_0\right)_{1\tau} = \left(\nabla\Phi_0\right)_{2\tau} \\
\dfrac{\partial\Phi_0}{\partial n}\bigg|_1 - \dfrac{\partial\Phi_0}{\partial n}\bigg|_2 = 4\pi m_{0n}
\end{cases}
\tag{2}
$$

Note that the conditions (2) contains not only the magnetic potential, but also a normal component of the magnetization of the wave, so for the complete solution of the problem, generally speaking, the above-mentioned magnetization should be found. For the investigated nanosystem, however, the ground state magnetization is directed radially. As the spin wave magnetization $\vec{m}_0$ is normal to this direction, the component m_{0n} on the nanoshell boundary vanishes: $m_{0n}=0$. Therefore, the last condition in (2) can be rewritten as follows:

$$
\frac{\partial\Phi_0}{\partial n}\bigg|_1 - \frac{\partial\Phi_0}{\partial n}\bigg|_2 = 0
\tag{3}
$$

In other nanosystem configuratons such simplification can be made, for instance, by the means of imposing fixed boundary conditions for the magnetization.

The system (2) together with the boundary conditions (2), (3) will be used as starting relations during the investigation of the above-described spin excitations.

III.   SPECTRAL CHARACTERISTICS OF THE SPIN ESCITATIONS

An approximate solution of the equation for the magnetic potential (1) can be written in the form $\Phi_0\left(r,\theta,\varphi\right) = \left(A_1 j_l\left(kr\right) + A_2 n_l\left(kr\right)\right)Y_{lm}\left(\theta,\varphi\right)$, here l and m are integers ($-l \le m \le l$), numbers of the angular excitation mode, j_l and n_l are the spherical Bessel and Neumann functions of the order l, correspondingly, Y_{lm} are the spherical polynomials, k is the radial wavenumber and A_1, A_2 are constants. This form of solution can be used when the expression $l(l+1)/r^2$ can be considered approximately constant inside the shell or small compared to k^2. The first condition is satisfied, in particular, when the shell is thin, so the relation $(b^2-a^2)/a^2 \ll 1$ fulfills. The second condition is satisfied, in particular, in the case of short waves ($ka \gg l$) and in the case of purely radial spin excitations ($l=0$), see [8]. In the case of thin nanoshell ($b^2-a^2)/a^2 \ll 1$ after substituting the given above solution into the equation (4) the following approximate dispersion relation can be obtained:

$$
\omega = \frac{|\gamma|M_0}{1+\alpha_G^2}\left(\sqrt{\left(1+\alpha_G^2\right)\left(\alpha^2 k^4 + 2\alpha\tilde{\beta}k^2 + \tilde{\beta}^2 + 4\pi\alpha\left(1+\frac{\tilde{\beta}}{\alpha k^2}\right)\frac{l(l+1)}{r_0^2}\right) - \alpha_G^2\left(\frac{K}{k}\right)^4} - i\alpha_G\left(\frac{K}{k}\right)^2\right)
\tag{4}
$$

here $K^2(k) = \alpha k^4 + \tilde{\beta}k^2 + 2\pi l(l+1)/r_0^2$, $r_0 = \sqrt{\left(b^2 + a^2\right)/2}$ (see [8]). For a spin wave that can practically be excited, the dissipation parameter α_G should be less or of an order of 0.1 so that $\alpha_G^2 \ll 1$ and, therefore, everywhere in (4) the replacement $1 + \alpha_G^2 \to 1$ can be made. After that, the dispersion relation (4) can be rewritten as follows:

$$
\omega = |\gamma|M_0\left(\sqrt{\alpha^2 k^4 + 2\alpha\tilde{\beta}k^2 + \tilde{\beta}^2 + 8\pi\alpha\left(1+\frac{\tilde{\beta}}{\alpha k^2}\right)\frac{l(l+1)}{b^2+a^2}} - i\alpha_G\left(\alpha k^2 + \tilde{\beta} + \frac{4\pi l(l+1)}{k^2\left(b^2+a^2\right)}\right)\right)
\tag{5}
$$

It was mentioned in the Introduction that in order to complete the presented theoretical analysis, the spectrum of values of the radial wavenumber also needs to be found. In the previous paper of the author [8], the above-mentioned spectrum has been obtained only for a very specific particular case (the material outside the nanoshell has been assumed to be a high-conductivity metal) thus essentially limiting the area of application of the entire obtained result. On the other hand, using

consideration described in the Section 2 of the current paper allows obtaining the specified spectrum in a very general case. The area of application of the result will be limited only by the nanoshell model described in the Section 2.

The absence of the radial excitations ($k=0$) for the investigated nanoshell corresponds to the spatially uniform spin oscillations (ferromagnetic resonance). In particular, this takes place when the shell thickness is less than the exchange length so radial modes of excitations are not possible. When the radial excitations are present ($k\neq 0$), the magnetic potential outside the nanoshell can be sought in the form $\Phi_0^e(r,\theta,\varphi)=F^e(r)Y_{lm}(\theta,\varphi)$, where the function F^e satisfies the following equation:

$$F^{e\,\prime\prime}+\frac{2}{r}F^{e\,\prime}-\frac{l(l+1)}{r^2}F^e=0 \tag{6}$$

Solution of this equation that satisfies the continuity condition on the nanoshell boundary and is limited when $r\to\infty$ as well as in the point $r=0$ can be written in the following form:

$$F^e=\begin{bmatrix}\big(B_1 j_l(ka)+B_2 n_l(ka)\big)(r/a)^l,\quad r\le a\\ \big(C_1 j_l(kb)+C_2 n_l(kb)\big)(r/b)^{-(l+1)},\quad r>b\end{bmatrix} \tag{7}$$

here B_1, B_2, C_1, C_2, are constants. The corresponding magnetic potential satisfies the Laplace equation and both the first and the second conditions in (2). Finaly, from the condition (3) the sought expression for the wavenumber can be found. This expression is implicit and can be written as follows:

$$\frac{k j_l{}'(kb)+\big((l+1)/b\big)j_l(kb)}{-k n_l{}'(kb)-\big((l+1)/b\big)n_l(kb)}=\frac{k j_l{}'(ka)-(l/a)j_l(ka)}{-k n_l{}'(ka)+(l/a)n_l(ka)} \tag{8}$$

Let us take advantage of the fact that the investigated nanoshell is thin: $(b-a)/a<<1$ and, therefore, $ka>>1$, $kb>>1$ for typical nanoshells. This allows simplifying the obtained spectrum by means of applying the asymptotics of the spherical Bessel and Neumann functions. For $\cos(ka)\neq 0$, $\cos(kb)\neq 0$ (8) can be rewritten as follows:

$$\mathrm{tg}\big(k(b-a)\big)=\frac{k\big((l+1)b+la\big)}{k^2 ab-l(l+1)} \tag{9}$$

If the additional condition $k^2 ab>>l(l+1)$ fulfills, the right hand side in the last relation can be neglected ($\mathrm{tg}\big(k(b-a)\big)=0$) and, therefore, the spectrum for the radial wavenumber has an explicit – quasi-one-dimensional – form:

$$k=\frac{\pi n}{b-a} \tag{10}$$

where n is an integer, the number of the radial excitations mode. A spectrum of such form can be expected for effectively one-dimensional nanosystem, e.g., a flat ferromagnetic film. Therefore, in the particular case when $k^2 ab>>l(l+1)$ (so the angular excitations are neglected), the frequencies' spectrum of the considered spin excitations can be written as follows:

$$\omega=|\gamma|M_0\left(\sqrt{\alpha^2\left(\frac{\pi n}{b-a}\right)^4+2\alpha\tilde{\beta}\left(\frac{\pi n}{b-a}\right)^2+\tilde{\beta}^2+8\pi\alpha\left(1+\frac{\tilde{\beta}}{\alpha}\left(\frac{\pi n}{b-a}\right)^{-2}\right)\frac{l(l+1)}{b^2+a^2}}-i\alpha_G\left(\alpha\left(\frac{\pi n}{b-a}\right)^2+\tilde{\beta}+\frac{4l(l+1)(b-a)^2}{\pi n^2\big(b^2+a^2\big)}\right)\right) \tag{11}$$

In a general case – when the condition $k^2 ab>>l(l+1)$ is not satisfied – this spectrum is defined by the equation (5) with the values of k that satisfy the relation (9). Note that the condition $k^2 ab>>l(l+1)$ for a set values of a, b corresponds to either large value of k or small value of l, depending on which of these values is set.

Analogous considerations can be used for the case of short waves ($ka>>l$) and in the case of purely radial spin excitations ($l=0$). Dispersion relation for such cases can be written in the following form:

$$\omega = \frac{|\gamma| M_0}{1+\alpha_G^2}\left(\tilde{\beta}+\alpha k^2\right)\left(1-i\alpha_G\right) \tag{12}$$

For such cases, the relation $k^2 ab \gg l(l+1)$ always fulfill and, therefore, a quasi-one-dimensional spectrum (10) for the radial wavenumber can be used. After replacing $1+\alpha_G^2 \rightarrow 1$ we obtain the values' spectrum of the frequencies as follows:

$$\omega = |\gamma| M_0\left(\tilde{\beta}+\alpha\left(\frac{\pi n}{b-a}\right)^2\right)\left(1-i\alpha_G\right) \tag{13}$$

Let us analyze the obtained relations.

IV.   DISCUSSION

First, let us point out that for the investigated nanoshell the spin excitations' frequencies spectrum becomes essentially discrete (unlike the nanosystems that are nanosized only in two dimensions – nanotubes, nanowires and so on). This fact implies from the obtained relations (5), (9), (10).

Then, let us make numerical estimations of the spin excitations' frequency in the considered nanoshell. Note that the wavenumber k is restricted, on the one hand, by the nanoshell thickness $b-a$ (unities to tens of nanometers for typical nanoshells), and, on the other hand, by the interatomic distance d_0 (several angstroms for typical materials). Therefore, the wavenumber lies in the interval 10^3-10^5 m^{-1} and the sought frequency for typical ferromagnet parameters ($\beta \sim 1$, $\alpha \sim 10^{-12}$ cm^{-2}, $\gamma = 10^7$ Hz/Gs, $M_0 = 10^3$ Gs) lies in the interval 10^{10}-10^{12} Hz. That, really, corresponds to the typical spin waves' frequencies. The above-mentioned considerations also limit the numbers of angular and radial modes: the number of possible radial modes for typical nanoshells is $n_{max} \sim (b-a)/d_0 \sim 10 \div 100$, and the number of possible angular modes is $l_{max} \sim 2\pi r_0/d_0 \sim 50 \div 500$.
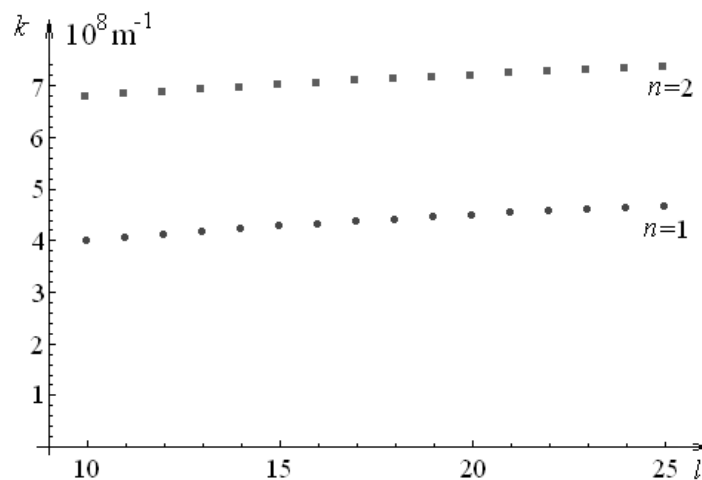
FIGURE 2. The dependence of the radial wavenumber on the angular mode number l for the first two radial modes ($n=1$, $n=2$). Round dots (lower set) represents the dependence for $n=1$, square (upper set) – for $n=2$.

Finally, let us analyze the obtained expression for the wavenumbers' spectrum in the case when it is not quasi-one-dimensional – the condition $k^2 ab \gg l(l+1)$ does not fulfill, so the relation (9) must be used. Numerical analysis shows that for a given l, there exists a number of solutions of (9) that correspond to different radial modes. Let us choose typical values $a=50$ nm, $b=60$ nm. Then, the condition $k^2 ab \gg l(l+1)$ does not fulfill starting from $l \sim 10$ and possible values of k start from $k_{min} \sim \pi/(b-a) \sim 3 \cdot 10^8$ m^{-1}. Numerical analysis shows that for a given n, the wavenumber dependence on l is weak, increasing and close to linear (see Fig. 2) until the next branch of k values becomes possible for the given a, b. (The last mentioned effect in most cases can be practically neglected – for instance, for the above-mentioned nanoshell sizes such passage takes place when $l \sim 300$). On the other hand, the dependence of the wavenumber on the radial mode number is essential. It can be seen from the graph for $n=1$ and $n=2$, and from numerical analysts for higher values of n. For instance, for $n=3$ in the same range of l the wavenumber ranges from approximately $9.8 \cdot 10^8$ m^{-1} to approximately $10.2 \cdot 10^8$ m^{-1}.

V.   CONCLUSION

Thus, dipole-exchange spin excitations in a spherical ferromagnetic nanoshell have been investigated in the paper. The magnetic dipole-dipole interaction, the exchange interaction, the anisotropy effects and the damping effects have been considered. The dispersion law for the above-mentioned excitations – obtained in the previous paper of the author – has been complemented with the spectra of wavenumber values and the frequencies' values. The above-mentioned spectra have been obtained using general boundary conditions for the magnetic field. In the previous paper of the author [8], the above-mentioned spectra have been obtained only for a very specific particular case (the material outside the nanoshell has been assumed to be a high-conductivity metal) thus essentially limiting the area of application of the entire obtained result. On the other hand, the method proposed in the current paper does not require any additional assumptions. Therefore, the obtained results can be used for any spherical ferromagnetic nanoshell of the studied configuration as long as the general nanoshell model used in the paper (thin nanoshell, linear excitations, constant absolute value of the magnetization vector etc.) can be applied – and the mentioned model is applicable for typical spherical ferromagnetic nanoshells synthesized nowadays.

A graphical representation of the obtained spectrum has been given and the numerical analysis of the obtained results has been performed. The analysis has shown that the dependence of the wavenumber on the angular mode number is weak and close to linear, while the dependence of the wavenumber on the radial mode number is essential. It has also been shown that if the condition of large wavenumber or the condition of small number of an angular mode is satisfied, the obtained spectrum transforms to a quasi-one-dimensional form (analogous to one observed in a flat film).

The method proposed in the paper can be applied to nanoshells of more complex configurations – for instance, a nanorice nanoshell – as well as for more complex configurations of shell-type nanosystems in general. However, one have to bear in mind that for configurations of ground state magnetization different from the one used in the paper, additional conditions (for instance, fixed boundary conditions for the magnetization) should be applied.

ACKNOWLEDGEMENTS

REFERENCES

[1]   C. Chappert, A. Fert, and F.N. Van Dau, "The emergence of spin electronics in data storage", Nat. Mater., vol.6, No.11, pp. 813–823, November 2007.

[2]   S. Neusser and D. Grundler, "Magnonics: spin waves on the nanoscale", Adv. Mater., vol.21, pp. 2927–2932, June 2009.

[3]   T. Schneider, A.A. Serga, B. Leven, B. Hillebrands, R.L. Stamps, and M.P. Kostylev, "Realization of spin-wave logic gates", Appl. Phys. Lett., vol.92, 022505, January 2008.

[4]   A.H. Lu, E.E. Salabas, and F. Schüth, "Magnetic nanoparticles: synthesis, protection, functionalization, and application", Angewandte Chemie International Edition, vol.46, pp. 1222-1244, February 2007.

[5]   M. Sanles-Sobrido, M. Bañobre-López, V. Salgueiriño, M.A. Correa-Duarte, B. Rodríguez-González, J. Rivas, and L.M. Liz-Marzán, "Tailoring the magnetic properties of nickel nanoshells through controlled chemical growth", Journ. Mat. Chem., vol.20, pp. 7360-7365, July 2010.

[6]   C.G. Hu, Y. Li, J.P. Liu, Y.Y. Zhang, G. Bao, B. Buchine, and Z.L. Wang, "Sonochemical synthesis of ferromagnetic core–shell Fe_3O_4–FeP nanoparticles and FeP nanoshells", Chem. Phys. Lett., vol.428, pp. 343-347, September 2006.

[7]   M.N. Hansen, L.S. Chang, and A. Wei, "Resorcinarene-encapsulated gold nanorods: solvatochromatism and magnetic nanoshell formation", Supramolecular chemistry, vol.20, pp. 35-40, April 2008.

[8]   Yu.I. Gorobets and V.V. Kulish, "Dipole-exchange spin excitations in a thin ferromagnetic nanoshell", Central European Journal of Physics, No.11(3), pp. 375-379, March 2013.

Secure Outsourced Association Rule Mining using Homomorphic Encryption

Sandeep Varma[1], LijiP I[2]

Department of CSE, College of Engineering, Trivandrum

Abstract—Several techniques are used in data analysis, where frequent itemset mining and association rule mining are very popular among them. The motivation for 'Data Mining as a Service' (DMaaS) paradigm is that when the data owners are not capable of doing mining tasks internally they have to outsource the mining work to a trusted third party. Multiple data owners can also collaboratively mine by combining their databases. In such cases the privacy of outsourced data is a major issue. Here the context includes necessity of 'corporate privacy' which means other than the data, the result of mining should also preserve privacy requirements. The system proposed uses Advanced Encryption Standard (AES) to encrypt the data items before outsourcing in order to prevent the vulnerability of 'Known Plaintext' attack in the existing system. Fictitious transactions are inserted to the databases using k-anonymity method to counter the frequency analysis attack. A symmetric homomorphic encryption scheme is applied in the databases for performing the mining securely. Based on the experiments and findings, though the running time of proposed solution is slightly greater than the existing system, it provides better security to the data items. Since the computations tasks are performed by the third party server, consumption of resources at the data owners' side is very less.

Keywords—privacy preserving, association rule mining, data mining, vertically partitioned databases, homomorphic encryption.

I. INTRODUCTION

The method of evaluating data from different angles and summarizing it into favorable information is the essence of data mining [14]. Reviewing the data or mining information can be very useful to a business. The extracted information can be used to raise revenue, reduce costs, or both. The method is also called data or knowledge discovery. The term data mining refers to extracting or mining information from massive quantity of data. There are several analytical tools for analyzing data. Data mining software is one among them. The data analyzed from different angles or dimensions are categorized and the identified relationships are summarized. Identifying the inter relations or patterns from large relational databases is carried out in data mining. Data mining is particularly vulnerable to misuse. So, the requirement of protecting privacy is a major concern in data mining.

In data mining the term privacy [6] is referred for finding valuable information. There is an enormous collection of large amounts of personal data such as criminal records, purchase details, health records etc. Each individual has the right to control their personal information. When the control in privacy is lost, the major issues which can be occurred are misuse of private information, handling misinformation and granulated access to personal information.

The datasets can be analyzed by techniques called frequent itemsets mining and association rule mining [3]. The former method is used to find data items or itemsets that co-occur frequently and the latter method is used for identifying exciting association coherence between data items in heavy transaction databases. The consistency between the products in large transaction databases are found out using association rules and an event which involves one or more products (items) in the trade or domain is referred as a transaction. For example, purchasing of items by a customer in a supermarket is a transaction. A set of items is called an "itemset" and an itemset with "k" number of items is called "k-itemset".

The context dealt here includes multiple data owners collaboratively mining from their joint data to learn frequent itemsets and association rules. The major issue of privacy pull back the data owners from sending their unprocessed data to a central station. In a horizontally partitioned database, one or more tuples (i.e., transactions) in the combined database are possessed by every data owner while in a vertically partitioned database the data owners possess one or more attributes in the joint database. This work focus on vertically partitioned databases which are beneficial in market basket analysis [3].

II.   BACKGROUND

2.1   Pattern Mining Task

The formal definition of problem of mining association rules can be stated as follows [1]: Let $L = \{l_1, l_2, \dots, l_n\}$ be a set of literals called items. Suppose a set of transactions is represented by T, where each transaction t is a set of items such that $t \subseteq L$. A unique identifier called Transaction ID (TID) is integrated with each transaction. It is said that transaction t contains P, a set of some items in L, if $P \subseteq t$. An association rule is an implication like $P \implies Q$, where $P \subseteq L, Q \subseteq L$, and $P \cap Q = \phi$. The rule $P \implies Q$ exists in the transaction set T with confidence value c, if c% of the transactions in T that contain P also contain Q. The rule $P \implies Q$ has support value s in the transaction set T, if s% of the transactions in T contains $P \cup Q$. If the support value of an itemset P is greater than or equal to the *minimum support* threshold, then it is called *large* or *frequent* itemset. Our aim is to discover all frequent itemsets and generate association rules from them.

2.2   Cryptographic Hash Function

A cryptographic hash function $H()$ is a one-way function. If we have a hash value $\hat{h}$, it is arithmetically not feasible to discover another plaintext m such that $H(m) = \hat{h}$. The hash function has two properties called weak and strong collision resistance. Collision resistance is the property in which the collision of two hash values doesn't occur i.e., it is arithmetically not feasible to discover two different plaintexts m1 and m2 such that $H(m_1) = H(m_2)$. SHA-1 and SHA-2 are two widely used cryptographic hash functions.

2.3   Homomorphic Encryption

In homomorphic encryption schemes, the operations we perform on plaintexts can be done on ciphertexts without any error. The main operations used are addition and multiplications. In additive homomorphic encryption schemes, only addition operation is allowed. Similarly, multiplicative homomorphic encryption only allows multiplication operation. When only one of the operation is allowed it is partially homomorphic and if both operations are allowed it is fully homomorphic encryption scheme.

In an homomorphic encryption which is additive, the ciphertext of the total of two messages, $m_1 + m_2$, can be calculated using some operation "•" on the encrypted version of m_1 and m_2, without initially deciphering m_1 and m_2 or carrying the key for decryption.

In a multiplicative homomorphic encryption, the ciphertext of the product of two messages, $m_1 \times m_2$, can be calculated with an operation "⊗" on the encrypted version of m_1 and m_2, without initially deciphering m_1 and m_2 or carrying the key for decryption.

III.   RELATED WORKS

Association rules are statements of the form 'if … then'[14]. They are used to find relationships among large data in a relational database or some other data depository even though the data may seem unrelated. "If a customer buys shoes, he is 70% likely to purchase socks also" is an example for an association rule as statement. An antecedent (if) and a consequent (then) are two parts of an association rule. An antecedent is an element encountered in the data. A consequent is an element that happens in association with the antecedent. Association rules are generated on the basis of support and confidence by evaluating data for frequent if/then patterns to determine the utmost relevant relationships. Support value shows how frequently the data items appear in the database. Confidence value point out how many times the if/then statements become true. In data mining techniques, association rules are widely used for analyzing and anticipating customer behavior. They have an important role in shopping basket data analysis, product clustering, catalog design and store layout.

3.1   Vaidya and Clifton Algorithm (VDC)

The first work which recognized and addressed the privacy concerns in vertically partitioned databases is done by Vaidya and Clifton [8]. They proposed a protocol for finding scalar product securely and a solution for mining frequent itemsets preserving owner's privacy which is built based on that protocol. Association rules can be generated from the result of frequent itemset mining and their support values.

The VDC algorithm is designed for only two parties to find out the frequent itemsets having minimum support values. The individual transaction values are not revealed by both the parties. The algorithm is based on the classic data mining algorithm

called Apriori [2]. The function apriori-gen is used to generate all candidate itemsets. For each candidate itemset, the algorithm counts the support value by secure computation of the scalar product.

Secure computation of scalar product is the crucial part of the protocol. They proposed an algebraic solution that hides genuine values by putting them in equations masked with arbitrary values.

Drawbacks: First, to find the support of each itemset the parties has to communicate every time. Both parties get the true support of each itemset. This may lead to exposure of information in some cases. The method can only be used to mine boolean association rules. Since the input values are restrained to 0 or 1, it also creates exposure risk.

3.2   Vaidya and Clifton N-Party Protocols (VDCN)

There are two protocols defined in [9]. The first one addresses the scenario where several parties are involved. It refers to the problem of secure computation of the size of intersection. The parties in the protocol have sets of items from a common domain. The target is to compute the cardinality of the intersection of those sets securely. In formal, k parties $P_1, ..., P_k$ having local sets $S_1, ..., S_k$ are given. The aim is to compute $|S_1 \cap ... \cap S_k|$ securely.

The basic idea is to encrypt all items using a parametric commutative encryption function. RSA public key encryption is used for that. Each party encrypts their items with their own key and the sets are passed on to another party. The received parties also encrypt the items and pass them to next party. This continues until all parties have encrypted all items. If the values are same the ciphertext generated by different sets will be equal because the commutative property of encryption. Finally any party can calculate the total number of values present in all of the encrypted itemsets. The parties would not know which of the items are present in a particular site.

The other protocol in [9] is called VDCN protocol. It is an extension of the VDC algorithm. VDCN is for N-parties whereas VDC is for two parties. This algorithm uses the first protocol to find the frequent itemsets having minimum support values. The apriori-gen function is used in the algorithm for generating candidate itemsets. For each candidate itemset, the parties run the protocol to compute support value. These support values are shared among all the parties.

Drawbacks: The drawbacks of the two-party algorithm are present here also because the support values and frequent itemsets are known by everyone. A site can learn the exact support of an itemset from the result of secure computation. With that knowledge, the site sayA can find the probability that an item in the set supported by A has a property in another site say B. It can be calculated as the ratio of the actual support to A's support.

3.3   Association rules mining in vertically partitioned databases

The work done by B. Rozenberg and E. Gudes [7] is the most relevant one among different privacy-preserving mining solutions. Two algorithms are proposed by them. The first algorithm is for two parties and the parties are symmetric. One party is named Master and the other party is named Slave. The protocol initiation is done my master. Slave only contributes its information. Only master do global computations. The master finds all frequent itemsets from its own real transactions. Then master check whether those itemsets are present in the slave's real transactions or not. This process is done either by a trusted third party or using secure computation. Then the two parties swap their roles and repeat the method. Second algorithm is for N parties. It is an extension to the first algorithm. It contains N-1 slaves and one master. Master do the global computations and inform the result to slaves.

The mining process is done by master. The fictitious transactions are injected by slaves to their individual database and transmit them to the master. A group of IDs of legitimate transactions are sent to a semi-trusted third party by all slaves. Master discovers association rules from the joined database. Since that database contains fictitious data, master transmits the ID lists of the transactions containing $P \cap Q$ for all association rules $P \implies Q$ to the third party for verification.

Drawbacks: This method cannot be called as an outsourced mining solution since a data owner (named master) performs the computations. The information about the raw data of data owners is available to the master even if it contains fictitious transactions.

3.4   Privacy Preserving Algorithms for Distributed Mining of Frequent Itemsets

In [11], there are two algorithms proposed for vertically partitioned databases and they have two levels of privacy. Both the algorithms are two party algorithms. One is weakly privacy-preserving and the other is strongly privacy-preserving. The

transaction database is represented as a boolean matrix. The overview of the context considered is: The private inputs of A and B are $(p_1, \ldots, p_n)$ and $(q_1, \ldots, q_n)$. The goal is to decide whether $\sum_{i=1}^{n} p_i q_i > s$, where s is a public input.

Probabilistic public-key encryption is the basis of algorithm having weak privacy-level. The algorithm has 3 steps. In Step 1, A encrypts $(p_1, \ldots, p_n)$ using her *own* public key (so that B cannot decrypt them) and sends the ciphers to B. In Step 2, the encryption of $(p_1 q_1, \ldots, p_n q_n)$ is calculated by B from the received ciphertexts. Then the newly generated ciphertexts are re-randomized and re-permuted by B and sent to A. In the last step, the cipher obtained from B is decrypted by A and the numbers of 1s are counted to compare with the threshold.

Anhomomorphic encryption scheme is the basis of the second algorithm having strong privacy level. This algorithm also has 3 steps. In Step 1, A encrypts $(p_1, \ldots, q_n)$ using her *own* public key (so that B cannot decrypt them) and sends the ciphers to B. In Step 2, the encryption of $(k_1(T-s-1), \ldots, k_n(T-s-n))$ is calculated by B where T is the support count of candidate itemset and k_i is random string. Then the newly generated ciphertexts are re-randomized and re-permuted by B and sent to A. In the final step, Achecks whether there is a ciphertext available which can be decrypted to 0.

Drawbacks: The first solution unravels the true supports, which is not acceptable. The next solution does not reveal the true supports but association rules cannot be discovered based on the result of this method since confidence values cannot be calculated without the true supports. Since computing confidence value securely is very complicated than computing support, this method cannot be used to generate association rules.

3.5   Privacy-preserving mining of association rules from outsourced transaction databases

The work done in [4] deals with mining of frequent itemsets and generation of association rules in privacy-preserving manner when the data is outsourced in the scenario of only one data owner. The data owner encrypts the data items using a substitution cipher in order to maintain the unprocessed data confidential. Since the substitution cipher is vulnerable to frequency analysis attack, a solution made from the concept called 'k-anonymity' is used for hiding the true frequencies. K-anonymity is a method used in data anonymization.

Fictitious transactions are added to the database before encryption to resist the attack by frequency analysis. The frequency of each data item will be same as at least k-1 other data items. After the encryption, the data owner exports the encrypted data to the server for performing mining process. The server is supposed to do the mining task using a standard algorithm for frequent itemset mining. Then the results are send to data owner. Since the outsourced database contains fictitious transactions, data owner has to subtract the support of fictitious transactions from the mining results to get the real support values of itemsets. At last, the itemsets which has support higher than a threshold are decrypted.

Drawbacks: To conserve privacy of data in the vertically partitioned databases, using these techniques alone, is not sufficient. To remove the effect of inserted fictitious transactions, the data owner needs to count support of itemsets in fictitious transactions. In the scenario of vertically partitioned databases, it is not feasible to perform the computations using the methods described in [4] by the data owners.

IV.   EXISTING SYSTEM

4.1   Overview

The work done in [5] is studied. The system consists of at least two data owners and a third party server or cloud. The private database owned by data owners are encrypted before they export the databases to the server. The data owners assign the responsibility of discovering frequent itemsets and association rules to the server. The server receives the databases from data owners and joins them before starting mining. Then the server run a classic data mining algorithm and sends the result to the data owners.

To encipher the Transaction Database (TDB), all items in the database are encrypted using substitution cipher. A method called frequency analysis where the frequency of ciphertext units are analyzed, has been used to crack some encryption methods such as substitution cipher. This attack is possible here also to find the ciphertext of each data item if adversary knows the real frequency of items. For example, suppose shirt and shoes are the topmost frequent items in a transaction database. If an adversary knows this, he can understand that the top two cipher items having maximum frequencies in the encrypted database are ciphers of shirt and shoes, respectively. To prevent the frequency analysis attack, fictitious

transactions are inserted into the database before encryption using k-anonymity method [4]. A Transaction ID (TID) is used to uniquely identify a transaction in a TDB. A customer identification number and date of purchase is used as TID. For the confidentiality of TID, the hash value of TID is stored in the encrypted database instead of storing the original TID.

4.2   Working

There is a private database owned by every data owner. The data owners are willing to collaboratively mine association rules from their databases. A third party server is used for the mining tasks. There are two stages in the solution, namely: preprocessing and mining.

In the preprocessing stage, the data owners encrypt their private databases and the encrypted databases are outsourced to the server. Before encrypting the databases, the data owners insert fictitious transactions to the private databases in order to prevent frequency analysis attack. The k-anonymity method explained in [4] is used for generating fictitious transactions. Substitution cipher is used for encrypting the data items in the database. To detect the genuine and fictitious transactions, data owners mark each transaction with a tag called Realness Value (RV). The RV is either 0 or 1, which indicates whether the transaction is fake or genuine, respectively. The realness value is encrypted using the proposed symmetric homomorphic encryption scheme. Because of the fact that the homomorphic encryption used is probabilistic, the encrypted realness value (ERV) will be different even for the same RV.

In the mining stage, the server runs the classic data mining algorithm called Eclat[10] to discover the association rules. The association rule candidates are generated from the encrypted joint database. There may be candidates which are "false positives" because of the presence of added fictitious transactions. In order to detect them, the server verifies the candidates in a privacy-preserving manner. Using homomorphic addition, the Encrypted Support Verifying Result (ESVR) is calculated from the ERVs by the server. Then the results which include candidates and their encrypted support are sending from the server to data owners. The data owners then verify the encrypted support since it contains support of the fictitious items also. The Encrypted Confidence Verifying Result (ECVR) is also computed in similar manner. At last, the encrypted support and the corresponding association rules are decrypted by the data owners.

4.3   Problem Definition

- The added fictitious transactions increase the size of database to more than double

- Hence the memory consumption and time consumption becomes huge compared to that required for plain data

4.3.1   Known Plaintext Attack

In a known plaintext attack, normally the attacker possesses plaintext-ciphertext pairs. In this system, since customer identification number and date of purchase is used as TID which is known to every customer, a customer can be an attacker. He could purchase an item and locate the corresponding transaction in the encrypted database by comparing the hash value of his ID and date with TID. By repeating the same, he can get several plaintext-ciphertext pairs and break the substitution cipher in a worst case of $O(n)$ steps where n is the total number of items in the database.

V.   PROPOSED MODIFICATION

To encrypt the data items, Advanced Encryption Standard (AES) algorithm can be used as a replacement for the vulnerable substitution cipher. The key sizes of AES are 128, 192 or 256 bits. Even if a 128 bit key is used, it provides very strong encryption compared to substitution cipher. For an attacker, a known plaintext attack on AES requires 2^{128} steps for finding the key of encryption.

VI.   ANALYSIS

6.1   Confidentiality of TID

There may be sensitive information in the original TIDs of databases owned by data owners. For the confidentiality of such data, the TIDs in the outsourced databases are replaced by their hash values. Because of the property of pre-image resistance of hash function, the server or an attacker cannot get the original TIDs.

6.2   Computational Complexity

To analyze the computational complexity of the system, graphs are plotted as size of data against time taken for different executions. Fig.1 shows the time taken for encrypting the data when AES and substitution ciphers are used. It is clear from the graph that time taken for encryption while using AES is slightly greater than while using substitution cipher.
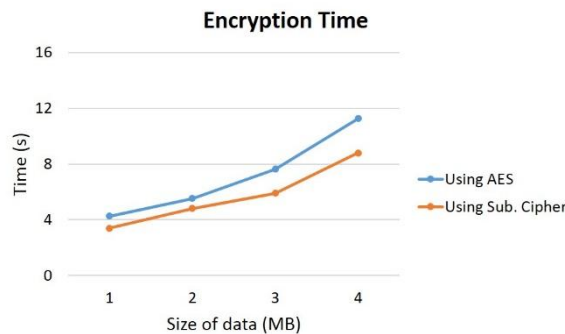

FIGURE 1. Encryption time when AES and substitution ciphers are used

Fig. 2 shows the time taken for decrypting the data when AES and substitution ciphers are used. Since only the data items in the frequent itemsets and association rules have to be decrypted, decryption time is very small compared to encryption time.

FIGURE 2. Decryption time when AES and substitution ciphers are used

Fig.3 shows the variation in running time of the system when the value of k used for achieving k-anonymity in database is increased. The k-anonymity method is used for inserting fictitious transactions and thus the size of database increases according to the value of k. Since the database size increases as value of k increases the running time will also increases. The data extracted from the datasets retail, chainstore and foodmart[13] are used for the experiment.
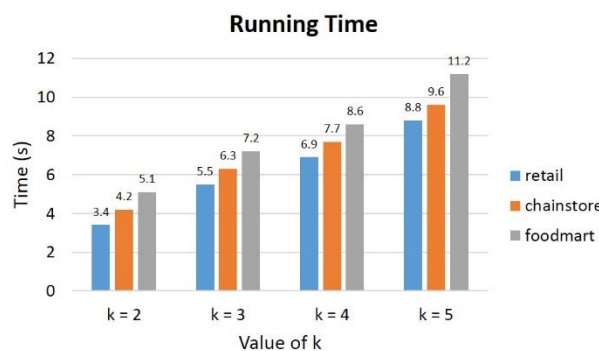

FIGURE 3. Total running time for different datasets

6.3   Communication Overhead and Storage Cost

The data owners communicate with the server for the exchange of encryption parameters as well as outsourcing the data. Other than that there is a mutual understanding among the multiple data owners regarding the selection of keys and

parameters. After the mining process also, the server has to send the results back to the data owners. The quantity of communication rounds is not going to change with any other entities.

The private databases of the data owners are stored at their end and the outsourced database is larger than their private databases because of the added attributes like ERV and fictitious transactions. The server who receives multiple databases from different sources combines them and store the joined database for mining. Thus the storage cost at server side is very large compared to data owners. Other than that, the outsourced database size also depends on the chosen value of k by the data owners.

VII. CONCLUSION

The scenario dealt here is the problem of corporate privacy in the cases where the database for mining tasks are outsourced to a third party. The reason for the need of outsourcing is that sometimes the data owners may not have the expertise or resources for performing the mining tasks internally. In this system, multiple data owners can do the mining tasks collaboratively. The paradigm of data mining as a service helps them to perform such tasks. In the stage before outsourcing the database called pre-processing, the database goes through data item encryption using AES and insertion of fictitious transactions with the help of k-anonymity method to counter the frequency analysis attack. A ciphertext tag approach is used to identify genuine and fictitious transactions which is encrypted using homomorphic encryption. The server who receives the outsourced databases from different data owners combines them and perform the mining task using Eclat algorithm. Homomorphic operations are the key to compute the support values of itemsets. The frequent itemsets are found securely and association rules can be generated from those itemsets. Based on the experiments and findings, though the time taken for encryption shows some increase compared to the existing system, the strength of encryption has increased from $O(n)$ to 2^{128}.

REFERENCES

[1] Agrawal R., Imielinski T. and Swami A. M. (1993), 'Mining association rules between sets of items in large databases', *Proceedings of the 1993 ACM SIGMOD International Conference on Management of Data, Washington*, 207-216.

[2] Agrawal R. and Srikant R. (1994), "Fast algorithms for mining association rules", In Proc. 20th int. conf. very large data bases, VLDB, Vol. 1215, 487-499.

[3] Brijs T., Swinnen G., Vanhoof, K. and Wets G. (1999),"Using association rules for product assortment decisions: A case study", In Proceedings of the fifth ACM SIGKDD international conference on Knowledge discovery and data mining. ACM, 254-260.

[4] Giannotti F., Lakshmanan L. V., Monreale A., Pedreschi D. and Wang H. (2013), "Privacy-preserving mining of association rules from outsourced transaction databases", IEEE Systems Journal, 7(3), 385-395.

[5] Li L., Lu R., Choo K. K. R., Datta A. and Shao J. (2016),"Privacy-preserving-outsourced association rule mining on vertically partitioned databases", IEEE Transactions on Information Forensics and Security, 11(8), 1847-1861.

[6] Malik M. B., Ghazi M. A. and Ali R. (2012), "Privacy preserving data mining techniques: current scenario and future prospects", In Computer and Communication Technology (ICCCT), 2012 Third International Conference on IEEE, 26-32.

[7] Rozenberg B. and Gudes E. (2006), "Association rules mining in vertically partitioned databases", Data & Knowledge Engineering, 59(2), 378-396.

[8] Vaidya J. and Clifton C. (2002), "Privacy preserving association rule mining in vertically partitioned data", In Proceedings of the eighth ACM SIGKDD international conference on Knowledge discovery and data mining. ACM, 639-644.

[9] Vaidya J. and Clifton C. (2005), "Secure set intersection cardinality with application to association rule mining", Journal of Computer Security, 13(4), 593-622.

[10] Zaki M. J. (2000), "Scalable algorithms for association mining", IEEE Transactions on Knowledge and Data Engineering, 12(3), 372-390.

[11] Zhong S. (2007),"Privacy-preserving algorithms for distributed mining of frequent itemsets", Information Sciences, 177(2), 490-503.

[12] Han J. and Kamber M. (2006), "Data Mining: Concepts and Techniques", 2nd ed., The Morgan Kaufmann Series in Data Management Systems.

[13] Fournier-Viger P. (2016), "Real-life Datasets in SPMF Format", [Online]. Available: http://www.philippe-fournier-viger.com/spmf/index.php?link=datasets.php

[14] http://searchbusinessanalytics.techtarget.com/definition/association-rules-in-data-mining.